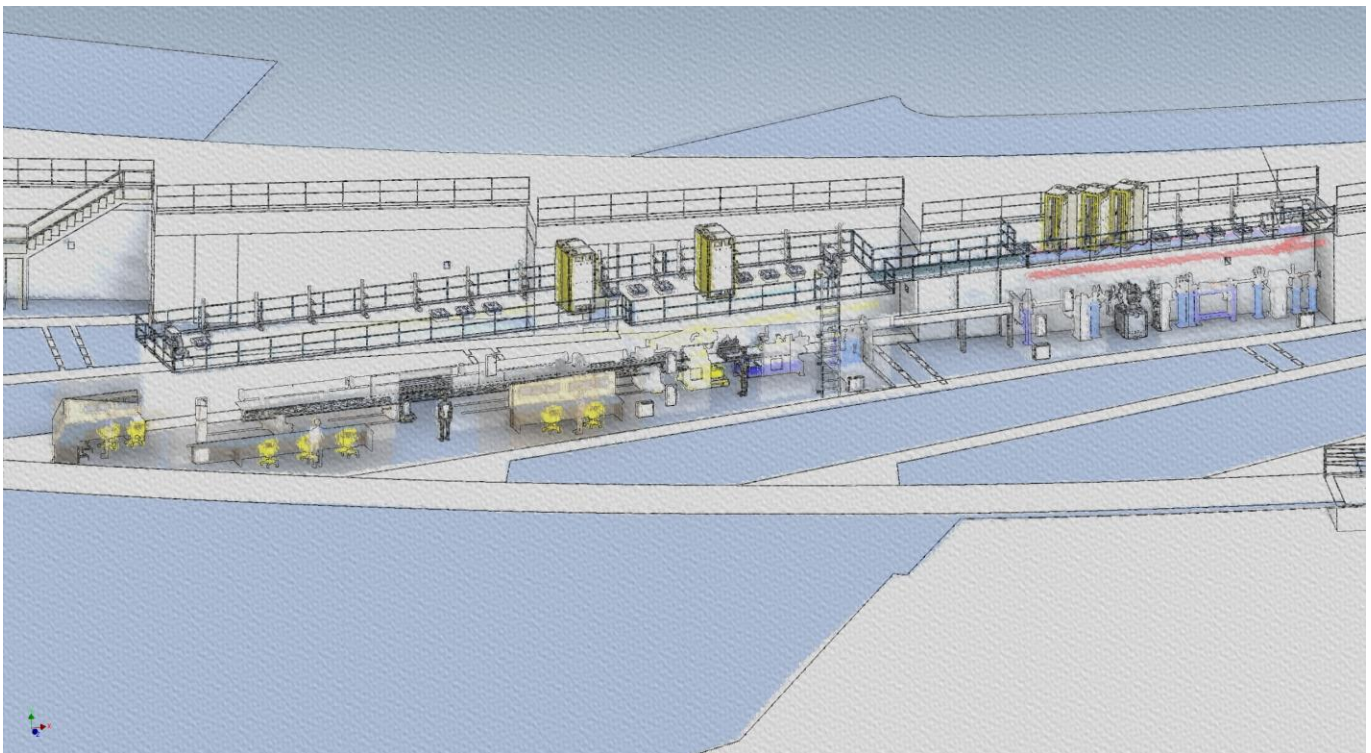


# NSLS-II Project

## PRELIMINARY DESIGN REPORT for the COHERENT HARD X-RAY BEAMLINE AT NSLS-II



final draft October 2010

*Intentionally blank.*

## Authors

**Andrei Fluerasu**, CHX Group Leader  
**Lutz Wiegart**, CHX Beamline Scientist  
**Mary Carlucci Dayton**, CHX Lead Engineer

## Acknowledgements

**Andy Broadbent**, Beamline Manager, Experimental Facilities Division, NSLS-II, BNL  
**Konstantine Kaznatcheev**, Beamline Scientific Support, XFD, NSLS-II, BNL  
**Lonny Berman**, NSLS, BNL  
**Viswanath Ravindranath**, Mechanical Engineer, ASD, NSLS-II, BNL  
**Oleg Chubar**, Beamline Scientific Support, XFD, NSLS-II, BNL  
**Lewis Doom**, Mechanical Engineer, ASD, NSLS-II, BNL  
**Yong Chu**, HXN Group Leader  
**Andrew DeSantis**, ACAD, NSLS-II  
**Ray Conley**, Optics Group, NSLS-II  
**Kenneth Evan-Lutterodt**, NSLS  
**CHX Beamline Advisory Team**

**CHX Beamline Advisory Team**

## Approvals and Reviewers

### Compiled by

Andrei Fluerasu, CHX Beamline Group Leader

Signature

Date

### Approved

Qun Shen, XFD Director, NSLS-II

### Reviewers

Robert Leheny, BAT Spokesperson,

signing on behalf of the BAT

Andy Broadbent, Beamlines Manager

Nicholas Gmür, ESH Coordinator, NSLS-II

Sushil Sharma,

Mechanical Engineering Group Leader, NSLS-II

_____	_____
_____	_____
_____	_____
_____	_____
_____	_____
_____	_____

## Document Updates

The Preliminary Design Report for the Coherent Hard X-ray (CHX) beamline at NSLS-II is a controlled document, revised under change control.

Version No.	Date	Changes made
0	09/14/10	Initial draft
1	09/24/10	Version 1, uploaded on NSLS-II sharepoint site
3	09/30/10	Version 3, uploaded on NSLS-II sharepoint,
4	10/01/10	Version 4, uploaded on NSLS-II sharepoint, submitted to BAT
5	10/10/10	Version 5 submitted to review committee
6	12/06/10	Version 6 minor corrections in spec tables and some typos removed

*Intentionally blank.*

## Contents

1. INTRODUCTION	1
SCIENTIFIC REQUIREMENTS.....	1
<i>Glassy Dynamics in Soft Matter</i>	2
<i>Phase Behavior and Dynamics on Liquid and Solid Surfaces</i>	3
<i>New Investigation Methods; Instrumental Developments</i>	3
COHERENT HARD X-RAY BEAMLINE TEAM.....	3
<i>Beamline Scientific and Engineering team</i>	3
<i>NSLS-II Management, Scientific and Engineering Support:</i>	4
<i>Beamline Advisory Team (BAT)</i>	4
2. BEAMLINE LAYOUT	5
OVERVIEW.....	5
SOURCE.....	7
FRONT END.....	11
<i>CHX Front End Components.</i>	11
OPTICAL LAYOUT.....	14
BEAMLINE PERFORMANCE.....	16
BEAMLINE ELEMENTS.....	18
HIGH HEATLOAD AND BEAM CONDITIONING OPTICS.....	18
<i>Differential Pump with Fixed Aperture</i>	18
<i>Horizontal White Beam Mirror</i>	20
<i>White Beamstop</i>	23
<i>High Heat-load Secondary Slits</i>	24
<i>Double Crystal (pseudo channel-cut) Monochromator</i>	24
<i>Double Multilayer Monochromator</i>	27
MONOCHROMATIC AND PINK BEAM OPTICS.....	30
<i>Precision Slits</i>	30
<i>CRL Transfocator</i>	30
VACUUM.....	31
RAY TRACING.....	31
3. END STATION INSTRUMENTATION	32
OVERVIEW.....	32
BEAM CONDITIONING OPTICS.....	32
<i>Exit Window and Endstation Vacuum</i>	32
FIRST OPTICS STAND.....	33
<i>Fast Shutter</i>	33
<i>Attenuators</i>	34
OPTICS TABLE.....	34
<i>Precision Slits</i>	35
<i>Local Focusing Optics</i>	35
<i>Local Mirror</i>	36
<i>Beam Defining and Guard Slits</i>	37
<i>Beam Positioning Monitor and Diagnostics</i>	38
DIFFRACTOMETER.....	38
SAXS TABLE.....	39
SAMPLE ENVIRONMENTS.....	40
<i>On-axis Microscope</i>	41
<i>Cryo-Furnace</i>	41
<i>Microfluidic Flowcell environments</i>	42
<i>Liquid Surface Chamber</i>	42
DETECTORS.....	42

4	INFRASTRUCTURE FOR BEAMLINE AND USER SUPPORT	44
	BEAMLINE CONTROL AND DATA MANAGEMENT .....	44
	<i>Controls Hardware</i>	44
	<i>Motion Control System</i>	44
	<i>GUIs and Data Acquisition</i>	45
	<i>Fast 2d Detectors: Data Readout and Storage</i>	46
	<i>Scientific Computing Requirements</i>	46
	General Data Visualization Software	46
	CHX Specific Software	46
	HUTCHES.....	47
	<i>First Optical Enclosure (FOE)</i>	48
	<i>Experimental Endstation Enclosure (EESE)</i>	48
	<i>Personnel Protection System (PPS)</i>	49
	<i>User Space</i>	49
	<i>Sample Preparation Laboratory</i>	49
	<i>Storage Space</i>	49
	ENVIRONMENTAL.....	49
	SURVEYING REQUIREMENTS.....	50
4.	SPECIAL BEAMLINE REQUIREMENTS	51
	<i>Special Requirements for Utilities</i>	51
	<i>Special Requirements to the Conventional Facilities Division</i>	51
	<i>Requirements to the Accelerator Systems Division</i>	51
	APPENDIX 1: SCHEDULE	52
	APPENDIX 2: REFERENCE DRAWINGS	53

## Acronyms

APD	Avalanche Photon Diode
Be	Beryllium
CDI	Coherent Diffraction Imaging
CDR	Conceptual Design Report
CRL	Compound Refractive Lens
DCM	Double Crystal Monochromator
DMM	Double Multilayer Monochromator
DW	Damping Wiggler
EIGER	<b>Extremely High Frame Rate</b> Detector
EH	Experimental Hutch
FE	Front End
FEA	Finite Element Analysis
FOE	First Optical Enclosure
FWHM	Full Width at Half Minimum
GI-SAXS	Grazing Incidence Small Angle X-ray Scattering
HM	Horizontal Mirror
IVU20	In-Vacuum Undulator, 20 mm period
KL	Kinoform lens
LOI	Letter of Intent
ML	Multi Layers
OH	Optics Hutch
PDR	Preliminary Design Report
SAXS	Small Angle X-ray Scattering
SNR	Signal-to-Noise Ratio
SVS	Speckle Visibility Spectroscopy
UHV	Ultra High Vacuum
VIPIC	Vertically Integrating Pixel Imaging Chip
WAXS	Wide Angle X-ray Scattering
XPCS	X-ray Photon Correlation Spectroscopy

# 1. INTRODUCTION

## Scientific Requirements

The Coherent Hard X-ray (CHX) beamline at NSLS-II will be dedicated to studies of nanometer-scale dynamics in materials using X-ray Photon Correlation Spectroscopy (XPCS), and to other experimental methods enabled by bright, coherent, X-ray beams. XPCS is based on measuring time correlation functions of the speckle fluctuations that occur when a coherent X-ray beam is scattered from a disordered sample. It can be used to measure equilibrium dynamics via the “usual” single-speckle intensity-intensity autocorrelation functions  $g^{(2)}(q, t)$ . If combined with 2D area detectors and a multispeckle technique, it can also be used to measure non-stationary, non-equilibrium dynamics via two-time correlation functions  $g^{(2)}(q, t_1, t_2)$ . Higher order correlation functions  $g^{(n)}(q, t)$  can be used to characterize heterogeneities in the dynamical properties.

The key quantity that enables XPCS experiments is the source brightness. This determines the flux of coherent X-ray photons and ultimately the signal-to-noise ratio (SNR) of the measured correlation functions. The transversely coherent X-ray flux is approximately,

$$I = \frac{B\lambda^2}{4}, \quad (1)$$

with the SNR proportional to the coherent intensity  $I$ .

The XPCS technique was first demonstrated in pioneering experiments that become possible at NSLS (M. Sutton et al., *Nature* **352**, 608, 1991; S. Dierker et al., *Phys. Rev. Lett.* **75**, 449, 1995) and later “moved” to brighter 3<sup>rd</sup> generation Synchrotron sources such as ESRF and APS. With the unprecedented brilliance of the NSLS-II storage ring exceeding  $10^{21}$  photons/s/mrad<sup>2</sup>/mm<sup>2</sup>/0.1 % bw for a photon energy near  $E \sim 8$  keV (more than one order of magnitude higher than that of the Advanced Photon Source), the CHX beamline will allow studies of dynamics on time scales that can be  $\sim 10^2 = 100$  times faster and on shorter length scales than was ever possible before (see Figure 1). The experiments will be performed in a variety of scattering geometries such as small angle scattering (SAXS), wide angle scattering (WAXS) or grazing incidence small angle scattering (GI-SAXS). With specific sample environments which will be hosted on a versatile diffractometer, the CHX instrument will provide the required flexibility and will be ideally suited to efficiently adapt to all these situations.

There are several classes of XPCS experiments that will probe a combination of length- and time-scales that are fundamentally important, and which are very difficult or impossible to measure at other (less bright) facilities or by using other techniques. These include, but are not limited to:

- Glassy materials, driven and out-of-equilibrium systems
- Colloids, polymers, and nanostructured complex fluids
- Biological systems such as proteins in solution and biomembranes
- Dynamics at fluid surfaces and interfaces
- Molecular dynamics and metallic and orientational glasses; dynamics at solid surfaces

In addition, the XPCS LOI document, “A Coherent Hard X-ray Beamline for XPCS and Microbeam SAXS at NSLS-II” identifies a possible additional scientific application in  $\mu$ -beam SAXS studies on the kinetics of biological processes (e.g. protein and RNA folding, protein crystallization and explorations of solvent conditions). While in the near future it is likely that such experiments will be performed better at dedicated instruments, the CHX beamline will have the technical capabilities to be tuned for  $\mu$ -beam SAXS studies without a major disruption of its main XPCS scientific program. It is our belief that allowing the use of a limited amount of beamtime (e.g. a maximum of 5-10%) for complementary studies like m-beam SAXS, pinhole Ultra Small Angle Scattering (USAX), etc. could ultimately be beneficial for the XPCS scientific program by bringing possible new applications onto the CHX experimental floor.

The CHX research program is described in detail in the XPCS LOI document, and will not be included here in its integrality. The scientific program will be pursued through active collaborations between the user community, the BAT team and the CHX group. A subset of the proposed area of research, which will likely lie at the core of the in-house research program in the CHX group is briefly described below. These “in-house” studies will require instrumental developments, new sample environments, etc. and will undoubtedly become available and useful to the extended user community. Ultimately, such an approach enables new applications and results that otherwise would not be within reach.

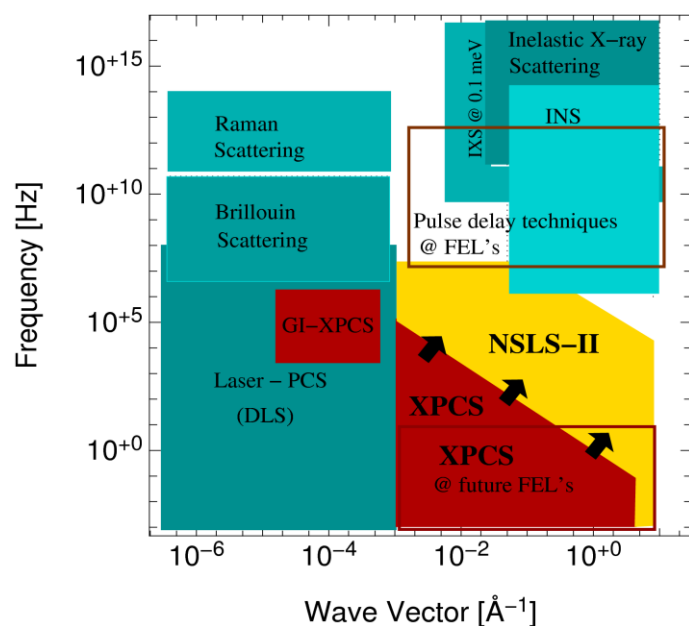


Figure 1. Wave vector – frequency phase-space currently occupied by XPCS at 3rd generation light sources. The goal of the CHX beamline at NLSL-II is to extend this region toward faster time scales and shorter length scales (gold). With its unprecedented brilliance, NLSL-II result could approach (if not match) the faster time scales accessible with neutron spin-echo and close the gap that currently exists in the phase space. This dynamic range will also fall in the gap left open by the future FELs between “classic” XPCS experiments using the high average brilliance of these sources, but being limited by their pulsed structure, and pulse delay techniques being limited by practical considerations such as the size of delay lines. This will make NLSL-II a truly unique instrument for XPCS.

### Glassy Dynamics in Soft Matter

Understanding the underlying mechanism by which model systems such as highly interactive colloidal suspensions arrest to non-equilibrium states and form glasses and/or gels is a fundamental problem in condensed matter physics. As the system approaches the glass transition, the dynamics start slowing down without an obvious reason in the structural (static) properties of the system. At the same time different relaxation modes become increasingly separated in time - e.g. fast modes associated with the motion of individual constituents hindered by neighboring particles and slow modes associated with the motion of groups (cages) of particles. Understanding the glass (or gel) transition is a problem of tremendous fundamental interest in soft matter physics. Solving it will also help us in better understanding phenomena like protein aggregation, which are responsible, for instance, for the cataract formation in the human eye lens or for the neuronal cell death associated with Alzheimer's disease. With their relatively slow dynamical relaxation modes occurring on molecular length scales, glassy systems are well suited for XPCS and very recent results obtained at existing 3<sup>rd</sup> generation light sources (mainly ID10, ESRF and 8ID, APS) have provided an invaluable insight into the mechanisms associated with the slow relaxation modes. At NLSL-II it will become possible to extend the dynamic range by several decades, hence measure also the fast relaxation modes. The tremendous increase in brilliance and special sample handling techniques (e.g., using microfluidic techniques to avoid beam damage and achieve new functionalities – A. Fluerasu et al., *J. Synch. Rad.* **15**, 378, 2008) may also enable, for the first time, studies of dynamics in biological systems such as protein aggregation in a solution.

A second key advantage for the study of glassy dynamics at NLSL-II will be associated with the study of dynamical spatial or temporal heterogeneities. With the high brilliance source, it will be possible to achieve smaller beam sizes to probe smaller volumes or to go beyond analyzing the intensity fluctuations via the second order correlation functions  $g^{(2)}(q, t)$  and measure “fluctuations of intensity fluctuations” via higher order correlation functions  $g^{(n)}(q, t)$ . Such studies have been limited thus far, mainly because the even more stringent requirements they put on the source, i.e. the signal-to-noise ratio (SNR). The SNR is proportional to the square of the source brilliance  $B^2$  for 4<sup>th</sup> order correlation functions  $g^{(4)}(q, t)$ , while only proportional to  $B$  in  $g^{(2)}(q, t)$ .

## Phase Behavior and Dynamics on Liquid and Solid Surfaces

The structure, phase behavior and dynamical properties of liquid and solid interfaces can be studied using a grazing-incidence scattering geometry. Current research includes biological films at liquid-vapor interfaces, bio-membranes, etc. The CHX beamline will enable studies on faster time and smaller length scales than possible today and will facilitate studies of the interplay between surface induced order and surface dynamics in systems such as alkanes undergoing surface freezing.

## New Investigation Methods; Instrumental Developments

The continuous optimization of the CHX instrument by pushing the signal-to-noise level for XPCS experiments to a maximum is, and will remain, a central activity in the CHX group. At the same time, a vigorous research program aiming at developing new investigation tools will hopefully help “pushing the boundaries” of the phase space shown in (see Figure 1). An example of such a development is that of X-ray Speckle Visibility Spectroscopy (XSVS). This method allows the direct measurement of nanometer-scale dynamics in materials by analyzing a single “speckle pattern”. The main idea, which follows the development of *speckle visibility spectroscopy* recently proposed for visible light (P.K. Dixon and D.J. Durian, *Phys. Rev. Lett.* **90**, 184302, 2003), is that the speckle contrast depends on the characteristic time scales of fluctuations in the sample, hence it is possible to resolve the dynamics over a wide range of length scales by analyzing the speckle visibility across a *single* diffraction pattern obtained with a 2D area detector. XSVS will be ideally suited to study dynamics at the high brilliance CHX beamline. As XSVS does not require a continuous time series but only single speckle patterns (with the acquisition time determined by the software trigger of the detector or by a fast shutter), it will offer the possibility to access shorter time scales, beyond the corresponding maximum frame rate of the detector. Since it only requires single images – i.e. “snapshots” – it will offer a unique way of measuring the “instantaneous” dynamics in complex systems with heterogeneous and/or intermittent behavior. In addition, it will also help avoiding beam damage in many soft matter or biological systems as the total required dose will be significantly reduced. Finally, XSVS may allow adopting a “flash approach” in measuring, for instance, the dynamics in a protein crystal. A speckle pattern can be obtained from a single pulse of intense coherent X-rays before causing irreversible damage in the sample.

## Coherent Hard X-ray Beamline Team

In this section, an overview of the CHX team (as of Fall 2010) is given, as well as a brief description of the scientific and instrumentation interests of the NSLS-II Beamline Scientists, the management and engineering support and members of the Beamline Advisory Team (BAT).

### Beamline Scientific and Engineering team

**Andrei Fluerasu**, Associate Physicist, NSLS-II, CHX Group Leader

*Dynamics in non-equilibrium and driven systems – e.g., gels and glasses under flow/shear; Applications of XPCS,  $\mu$ -beam SAXS in biophysics; Speckle Visibility Spectroscopy; Beamline optics and coherence preservation; Pushing the signal-to-noise ratio in XPCS, CDI by optimizing the beamline layout; X-ray detectors; Controls and data acquisition; Statistical analysis of speckle-based methods; Beamline design and operation*

**Lutz Wiegart**, Assistant Physicist, NSLS-II

*Structure and dynamics at liquid surfaces and interfaces; CDI in biological systems; Bulk dynamics associated with self-assembly of organic nanotubes; Solution scattering; Sample environments; Experimental setups adapted to coherent x-ray scattering; Beamline optics and instrumental design; Beamline operation; Controls*

**Mary Carlucci-Dayton**, Mech. Engineer, Lead Engineer of the CHX beamline, NSLS-II

*Extensive experience in design and maintenance of beamline components at NSLS; design of automatic robotic sample changers for macromolecular crystallography (MX) beamlines; Interests in high precision and high stability mechanical components, design of complex sample environments adapted for coherent X-ray scattering, design of wavefront-preserving focusing devices (transfocator-type) based on one-dimensional refractive elements.*

**Lonny Berman**, Physicist, NSLS (MOU)

*Macromolecular and protein crystallography; Applications of coherence for imaging and studies of dynamics; Beamline optics and beamline design; Coherence preservation by beamline optics; Restoring the coherent wavefront with adaptive optics; Vast experience in beamline instrumentation, beamline design and operation.*

### **NSLS-II Management, Scientific and Engineering Support:**

**Qun Shen**, Director, Experimental Facilities Division, NSLS-II, BNL

**Andy Broadbent**, Beamline Manager, Experimental Facilities Division, NSLS-II, BNL

**Oleg Chubar**, Beamline Scientific Support, XFD, NSLS-II, BNL

**Konstantine Kaznatcheev**, Beamline Scientific Support, XFD, NSLS-II, BNL

**Viswanath Ravindranath**, Mechanical Engineer, ASD, NSLS-II, BNL

**Lewis Doom**, Mechanical Engineer, ASD, NSLS-II, BNL

**Sushil Sharma**, Group Leader, Mechanical Engineering, ASD, NSLS-II, BNL

### **Beamline Advisory Team (BAT)**

The Beamline Advisory Team is not only formed by world experts in XPCS but also by scientists who invented and pioneered this technique. The scientific and technical interest of all the BAT members cover a wide range of topics in condensed matter physics, biophysics, instrumental design, and the development at world-class facilities.

**Robert Leheny**, Associate Professor, Physics Department, John Hopkins Univ. (*BAT spokesperson*)

**Karl Ludwig**, Professor, Physics Department, Boston University

**Laurence Lurio**, Associate Professor, Physics Department, Northern Illinois University

**Simon Mochrie**, Professor, Physics Department, Yale University

**Lois Pollack**, Associate Professor, Applied Physics Department, Cornell University

**Aymeric Robert**, XCS Instrument Scientist, LUSI/LCLS, SLAC

**Alec Sandy**, Physicist, Group Leader, 8-ID, APS, ANL

**Oleg Shpyrko**, Assistant Professor, Physics Department, University of California San Diego

**Mark Sutton**, Professor, Physics Department, McGill University

## 2. BEAMLINE LAYOUT

### Overview

The optical and mechanical design of the CHX instrument is simple and robust and puts an emphasis on three key elements:

- Wavefront and brightness preservation by carefully designing and engineering key optical elements, reducing the number of windows, mirrors, etc. to an absolute minimum
- maximizing the useful signal by using the entire available coherent flux (via focusing optics)
- maximizing the mechanical stability of the instrument (e.g. by reducing the degrees of freedom for beamline optics to a required minimum)

The 3 D model of the CHX beamline can be seen in Figure 2. A 20 mm period in-vacuum undulator (IVU20) source and a “standard” Front-End (FE) configuration provide the maximum beam brightness, which is the most important quantity determining the intensity of a coherent beam. In order to minimize wavefront perturbations introduced by any optical element, the beamline will have the possibility of windowless operation. The First Optics Enclose (FOE) vacuum will be separated from the FE “machine” vacuum by a differential pumping system, placed immediately downstream of the ratchet wall.

The coherence of a photon beam has two components: transverse or lateral coherence and longitudinal or temporal coherence. For a synchrotron source of X-rays, with an approximately Gaussian intensity distribution at a distance  $z$  away from the source, the transverse one-sigma coherence lengths  $\xi$  in the horizontal (x) or vertical (y) direction is given by the Van Cittert-Zernike theorem,

$$\xi = \frac{\lambda z}{4\pi\sigma} \quad (2)$$

Here  $\lambda$  is the X-ray wavelength, and  $\sigma$  is the one-sigma source size (horizontal or vertical). For a working energy of  $E=10$  keV, where  $\sigma_h \sim 34 \mu\text{m}$  and  $\sigma_v \sim 8 \mu\text{m}$ , and near the location of the ratchet wall ( $z=25.5$  m) this leads to FWHM ( $=2.35\xi$ ) coherence lengths of  $21 \mu\text{m}$  (horizontal),  $185 \mu\text{m}$  (vertical) and corresponding angular sizes of  $0.83 \mu\text{rad}$  and  $7.3 \mu\text{rad}$  respectively.

Due to the small size of the coherent beam, it is helpful to limit the maximum size of the synchrotron beam. This allows to reduce the unnecessary heat load on the beamline optics and also to achieve a better separation between the X-ray and bremsstrahlung radiation fans further downstream. As a consequence, the maximum size of the beam is limited via a fixed water-cooled Glidcop beam-defining aperture near the ratchet wall which serves the double purpose of providing the high impedance vacuum section required by the differential pumping scheme. The size of the fixed aperture is  $0.15 \times 0.15 \text{ mrad}^2$  which corresponds to  $\sim 3.9 \times 3.9 \text{ mm}^2$ . Since the fixed aperture is much larger than the coherence size of the beam, it will not affect in any negative way the beamline performance in its main purpose, which is studies of dynamics via coherent X-ray diffraction.

The  $\sim 12$  m long FOE hosts the main optical elements – horizontally deflecting mirror, white beam slits, a double crystal monochromator (DCM) and a double multilayer monochromator (DMM) for pink beam operations, monochromatic beam secondary slits, and a monochromatic beam transfocator device based on one dimensional Be Compound Refractive Lenses (CRL). - together with auxiliary equipment such as beam diagnostic tools, bremsstrahlung and X-ray beam stops and collimators, beam transport elements, etc.

The CHX experimental station (ES) will be hosted in a 27 m long monochromatic beam enclosure, featuring a versatile sample diffractometer located near  $z=48$  m from the source and a 15 m long SAXS table. Just upstream of the sample location a  $\sim 2$ -3 m long local optics table will host additional beam conditioning elements such as Si Kinoform Lenses (KL) for vertical and horizontal focusing, beam deflecting mirror, beam position monitor, slits, etc.

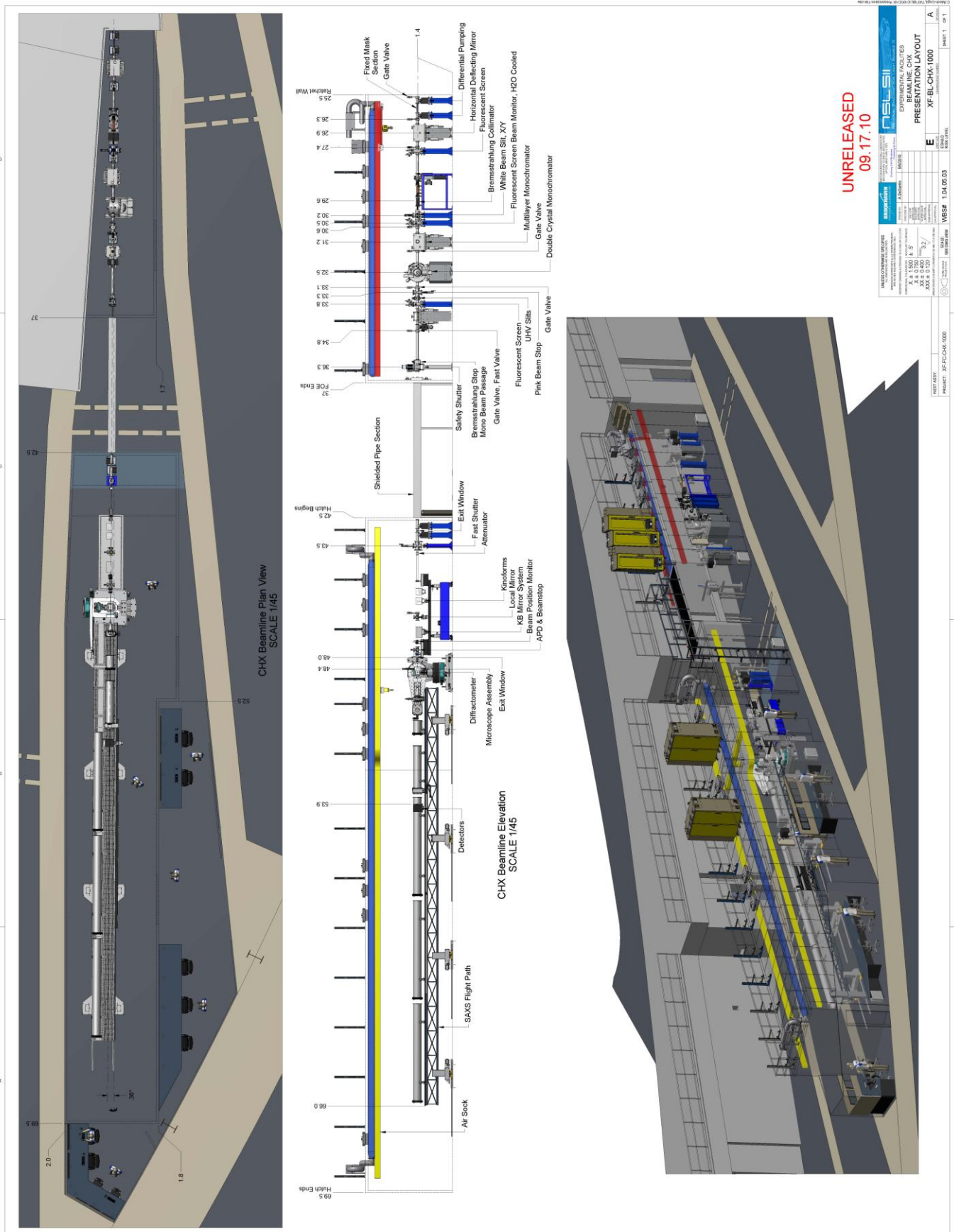


Figure 2 CHX beamline 3D model

The ES will operate under high vacuum (HV) condition, separated from the optics Ultra High vacuum (UHV) upstream by a thin Si<sub>3</sub>N<sub>4</sub> window placed as the first optical element in the hutch. A fast shutter and a filter selector device will be placed on a stand-alone support between the exit window and the local optics, in order to minimize the effect of possible mechanical vibrations.

The canonical beam size for XPCS work at the CHX beamline will be ~10-20 μm (FWHM, both H and V) for XPCS-SAXS experiments or ~1-2 μm (FWHM, both V and H) for either wide-angle (WAXS) XPCS experiments or XPCS-SAXS. With the flexible focusing scheme briefly described here based on refractive optics (CRLs and KLs) it is possible to achieve this beam sizes for a selection of energies such as 6, 8, 10, 12, and 15 keV.

With a beam size  $d$  (determined by the exact focusing scheme), the speckle size at the detector location, a distance  $z_{sd}$  downstream of the sample is given by,

$$s = \frac{\lambda z_{sd}}{d} \quad (3)$$

With  $z_{sd}=15$  m and  $d=10$  μm, in a standard XPCS-SAXS operation mode, the speckle size is  $s\sim 232$  μm and can even be oversampled with a 2D area detector with pixels of 100 μm or smaller. In most situations, it is advantageous for XPCS to relax the requirements for transverse coherence to gain flux, and an overall higher signal-to-noise (SNR) ratio. With a beam size of 20 μm, to corresponding speckles at  $z_{sd}=15$  m will be  $s\sim 116$  μm. Typical wide-angle XPCS experiments will work with much smaller detector distances, e.g.  $z_{sd}=1.5$  m and beam sizes of a couple of microns. The speckle size for  $d=2$  μm and  $z_{sd}=1.5$  m is also  $s\sim 116$  μm.

The ES enclosure extends on the experimental floor to  $z=69.5$  m and needs to be placed on one of the extended floor space spots (up to  $z=72$  m). The current provisional placement of the CHX beamline on the ID-5 straight section meets this requirement.

## Source

The most important source parameter for the CHX instrument is its brightness which is directly proportional to the transversely coherent flux (equation 1). For this reason, the CHX beamline will use a 3 m long IVU20 insertion device on a low- $\beta$  straight section which yields the highest possible brilliance at NSLS-II (see Figure 3). The IVU20 specifications can be seen in Table 1. The beamline will cover an energy range from 6keV to 15keV and will work most typically on the 5<sup>th</sup> or 7<sup>th</sup> harmonic of the IVU20 but also on the 3<sup>rd</sup>, for lower energies, or the 9<sup>th</sup> harmonic for the higher energy end of the covered spectrum. For most working energies, the brilliance of the CHX source will exceed the 10<sup>21</sup> ph/s/0.1%BW/mm<sup>2</sup>/mrad<sup>2</sup> level, at least one order of magnitude higher than APS or ESRF. This unprecedented increase in source brightness is due to the very small emittance of the storage ring achieved with several damping wigglers (DW).

The fully-damped horizontal emittance value of 0.5 nm rad is assumed in all the parameters calculated by the NSLS-II Accelerator Systems Division (ASD) and reported here. This is the performance value for the NSLS-II storage ring when operating with a full complement of eight 7m damping wigglers. The initial emittance value will be greater than this value, owing to operation with fewer damping wigglers. The one-sigma electron beam size –  $\sigma_{\text{electron}}$  – of the NSLS-II undulator is shown in Table 2 (source size and divergence in horizontal and vertical direction).

The diffraction-limited, “natural” photon beam size  $\sigma_{\text{photon}}$  is given by

$$\sigma_{\text{photon}} = \frac{1}{4\pi} \sqrt{2L\lambda} . \quad (4)$$

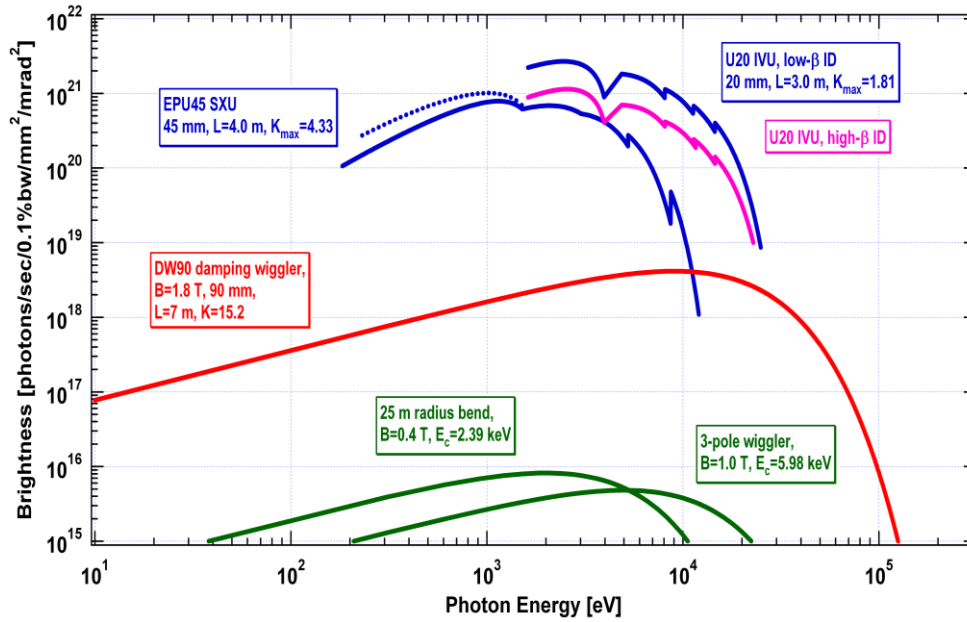


Figure 3 Brightness vs. photon energy for the baseline radiation sources at NLSL-II.  
 Ring parameters: 3.0 GeV,  $I=0.5$  A,  $\epsilon_h=0.5$  nm,  $\epsilon_v=0.008$  nm, energy spread=0.001;  $\beta_h=2.02$  m,  $\beta_v=1.06$

Table 1 Basic Parameters of NLSL-II U20 IVU on a Low-Beta Straight Section (Storage Ring Operating at 3 GeV and 500 mA).

U20	
Type	IVU
Photon energy range [keV]	Hard X-ray (1.9–20)
Type of straight section	Low- $\beta$
Period length, $\lambda_u$ [mm]	20
Total device length [m]	3.0
Number of periods	148
Minimum magnetic gap [mm]	5
Peak magnetic field strength in linear mode, B [T]	1.03
$K_{eff}^{*1}$	1.83
Maximum total power [kW]	8.1
On-axis power density [kW/mrad <sup>2</sup> ]	66
Fan angle <sup>*2</sup> (mrad H)	0.85/1.43
Fan angle <sup>*2</sup> (mrad V)	0.81/1.28

<sup>\*1</sup>  $K = 0.934$  B[T]  $\lambda_u$ [cm]; effective K values listed

<sup>\*2</sup> the fan angles of the radiation quoted here are as seen at 16m from the source, and take into account the effects of source length. The two values quoted are for the points where the power density falls to values that are 1% and 0.1% of the central value. Designs of the XBPM and fixed mask entrance shall take into account these fringe power loads

This is the size of a diffraction-limited photon beam for a zero emittance (and therefore zero size) electron beam. One measure of the effective photon beam size,  $\sigma_{eff}$ , is given by the quadrature sum of the electron ( $\sigma_{electron}$ ) and photon ( $\sigma_{photon}$ ) contributions:

$$\sigma_{eff} = \sqrt{\sigma_{electron}^2 + \sigma_{photon}^2} \quad (5)$$

Table 2. Electron Beam Size and Divergence at the Center of a Low-Beta Straight Section of the NSLS-II Storage Ring.

Type of source	Low- $\beta$ straight section (6.6m)
$\sigma_h$ [ $\mu\text{m}$ ]	31.8
$\sigma_h'$ [ $\mu\text{rad}$ ]	15.7
$\sigma_v$ [ $\mu\text{m}$ ]	2.9
$\sigma_v'$ [ $\mu\text{rad}$ ]	2.8

Similarly, the diffraction-limited, “natural” photon beam angular divergence  $\sigma'_{photon}$  is given by

$$\sigma'_{photon} = \sqrt{\frac{\lambda}{2L}}, \quad (6)$$

and the effective photon beam angular divergence  $\sigma'_{eff}$  is again given by the quadrature sum of the electron ( $\sigma'_{electron}$ ) and photon ( $\sigma'_{photon}$ ) contributions:

$$\sigma'_{eff} = \sqrt{\sigma'^2_{electron} + \sigma'^2_{photon}}. \quad (7)$$

The effective photon beam size and angular divergence for the low- $\beta$  IVU20 source are shown in Figure 5. Solid lines show the the source parameters at undulator resonance energy. The dotted curves show the source parameter for energies slightly below the resonance energy, which yield more flux. The results are also summarized in Table 3 for a series of discrete energies which will constitute the default operation modes at the CHX beamline. An important parameter is the source coherence. This can be quantified by the phase space volume occupied by the emitted photons, which is the product of the linear and angular size  $\sigma_{h,v}\sigma'_{h,v}$  (in either horizontal or vertical directions). For a single Gaussian coherent mode  $\sigma\sigma'=\lambda/4\pi$ . In general a partially coherent beam is characterized by  $\sigma\sigma'\geq\lambda/4\pi$ , which is directly related to Heisenberg’s uncertainty principle stating that the position and angular orientation of a single photon cannot be quantified simultaneously arbitrarily well. The number of coherent modes in each direction  $\sigma\sigma'/(\lambda/4\pi)$  is also given in Table 3. It is important to remember that, as a consequence of Liouville’s theorem, the phase space volume  $\sigma\sigma'$  is conserved during beam propagation, focusing, diffraction. In other words, the beam coherence cannot be increased (for instance by focusing) but only decreased by imperfect optics. The beam coherence can only be increased by an aperture, or in other words, by “throwing away” the incoherent part of the beam. In general, a slit can be used to “tune” the phase space volume of a beam to

$$\sigma \cdot \sigma' = M \frac{\lambda}{4\pi}, \quad (8)$$

where  $M>1$  is the number of “coherent modes” present in the beam.

To avoid unnecessarily increasing the heat load on the beamline optics, the CHX instrument will restrict the beam size to only a part of the beam, corresponding to relatively small number of transverse coherence modes. This will be defined with the high heat load primary slits located in the FE at about 20 m from the source. An approximate transverse coherence lengths ( $\xi_x$  – horizontal and  $\xi_y$  – vertical) calculated from equation 2 is given in Table 4 for different operation energies.

The spectral output of the IVU20 low- $\beta$  source for  $k=1.51$ , corresponding to the optimal setting for work at 10 keV (5<sup>th</sup> harmonic of the undulator) is shown in Figure 4. The flux was calculated through a relatively small aperture of  $0.03 \times 0.03 \text{ mrad}^2$  which corresponds to  $\sim 35(V) \times 100(H)$  coherence modes (equation 8), hence is still much larger than ever needed for XPCS.

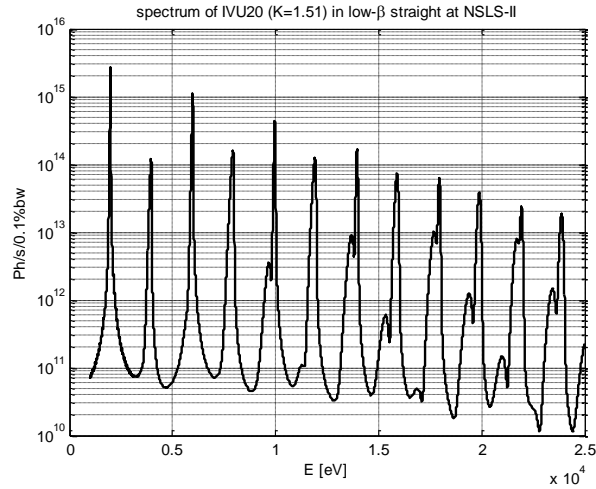


Figure 4 Spectral flux of IVU20 in low- $\beta$  straight section at NLSL-II ( $K=1.51$ ) through  $0.03 \times 0.03 \text{ mrad}^2$  aperture at 25.9m

The filling modes and bunch uniformity will be of a particular importance for the CHX beamline. It is estimated that, in order to have clean baseline for the correlation functions that will enable measurements of sub-microsecond dynamics, the NLSL-II storage ring should provide a high current (500 mA) quasi-DC source with at least 4/5 of the buckets filled and the remaining, ion clearing buckets uniformly distributed across the ring. We estimate that a bunch-to-bunch uniformity better of 1% will lead to a structure in the correlation function safely below the noise level, while a 10% variation would be detectable in data with good statistics (hence, will require correction). More details about various synchrotron filling modes are given in Section 4 – Special beamline requirements.

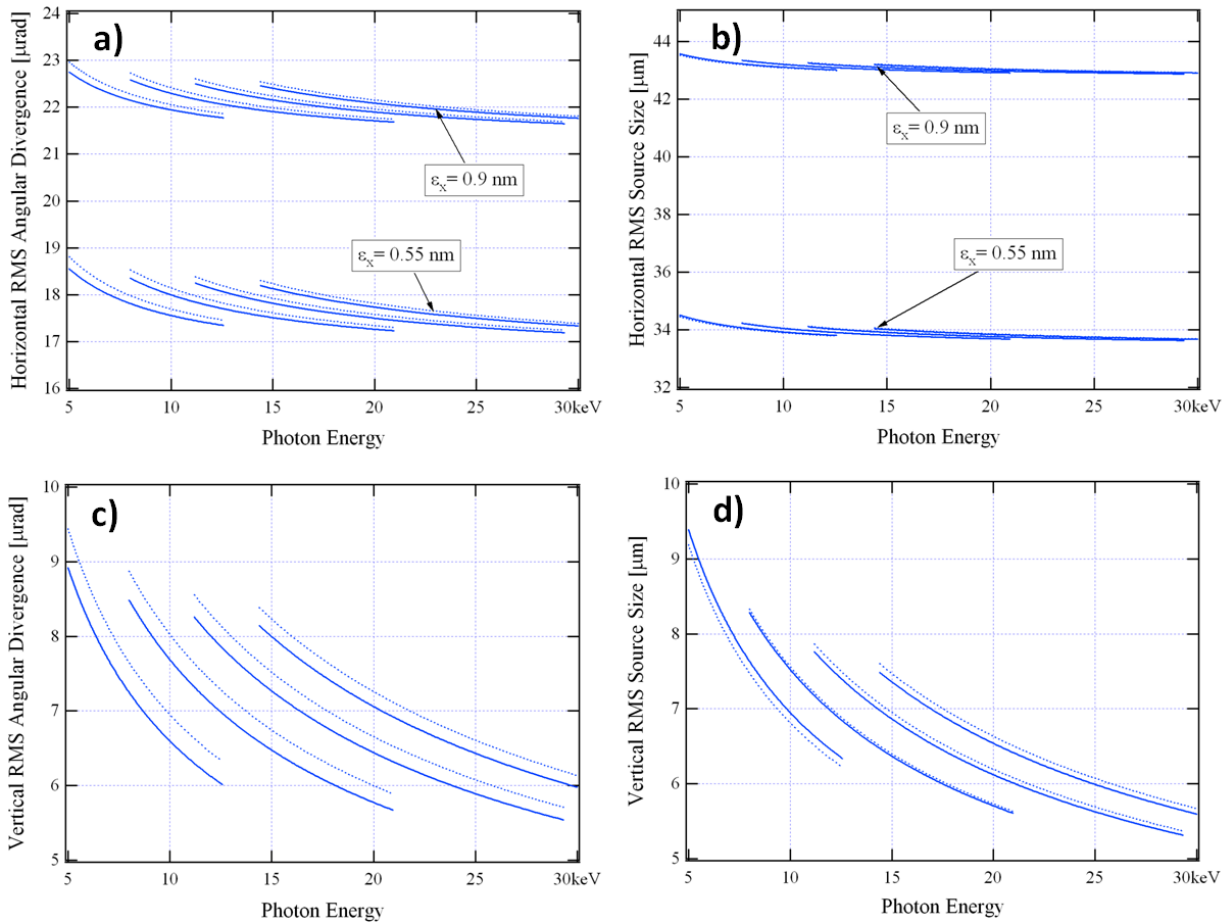


Figure 5 Vertical and horizontal RMS photon source size and angular divergence for the low-beta IVU20 source (courtesy of Yong Chu and Oleg Chubar)

## Preliminary Design Report for the Coherent Hard X-ray (CHX) Beamline at NSLS-II

Table 3. Horizontal “one-sigma” photon beam source size  $\sigma_h$ -linear and  $\sigma_h'$ -angular, vertical source size  $\sigma_v$ ,  $\sigma_v'$ ; and phase space volume -  $\sigma_h\sigma_h'$ ,  $\sigma_v\sigma_v'$ , in units of phase space of a single Gaussian coherent mode  $\lambda/4\pi$ , for different energies.

E (keV)	6	8	10	12	16
$\sigma_h$ ( $\mu\text{m}$ )	34.3	34.2	34.1	34.2	34.2
$\sigma_h'$ ( $\mu\text{rad}$ )	18.3	18.3	18.0	18.2	18.2
$\sigma_v$ ( $\mu\text{m}$ )	8.8	8.0	7.5	7.6	7.4
$\sigma_v'$ ( $\mu\text{rad}$ )	8.5	8.2	7.7	8.1	8.0
$\sigma_h\sigma_h'/(\lambda/4\pi)$	38.2	50.7	62.2	75.7	94.6
$\sigma_v\sigma_v'/(\lambda/4\pi)$	4.5	5.3	5.8	7.5	9.0

Table 4. Vertical and horizontal coherence length  $\xi_y$ ,  $\xi_x$  ( $2 \times \text{FWHM} = 2 \times 2.35\sigma$ ) for different energies, at the primary slits location.

E (keV)	6	8	10	12	16
$\lambda$ (Å)	2.06	1.55	1.24	1.03	0.77
$\xi_y$ ( $\mu\text{m}$ )	447.3	335.5	268.4	223.6	154.2
$\xi_x$ ( $\mu\text{m}$ )	44.7	33.55	26.8	22.4	17.6

## Front End

The CHX beamline will use a standard NSLS-II front end configuration (see Figure 4). The key element in addition to the beam position monitors that will provide information about the transverse and angular position of the photon beam, a fixed aperture and a number of collimators, will be a set of X-Y high heat load slits with 1  $\mu\text{m}$  precision/accuracy. These slits, also shown in the lower inset of Figure 6, are based on the design provided by the Mechanical Engineering Group in the Accelerator System Division (ASD), and are made out of a water cooled GlidCop body with stainless steel adapters and flanges. The beam will be defined by a set of tungsten corners (e.g., top, right with the first unit and bottom, left with the second unit). Each unit will be mounted on a motorized X-Y stage. The slit design (e.g. angle of the tapered profile in the GlidCop bodies and shape/geometry of the beam-defining Tungsten corners) has been optimized to cope with the high power load associated with white beam operation. They are a critical element in the beamline layout since by absorbing several kW of incident power, the flux transmitted to the downstream optics will be greatly reduced. For instance, with the slits set to a “standard” 500  $\mu\text{m}$  (vertical) and 100  $\mu\text{m}$  (horizontal) which is still larger than the coherence length at any wavelength (see Table 3), and an estimated peak power of  $\sim 90 \text{ W/mm}^2$  in the central cone of the IVU20 undulator (which is quite uniform over this reduced spatial range), the total power incident on the next optic element, in this case a horizontally deflecting flat mirror is only on the order of 9 W.

### CHX Front End Components.

We give here a description of the FE components following the beam direction adapted from a document provided by Lewis Doom from the ASD division. The Front End 3D model is shown in Figure 5.

#### Photon Shutter (BMPS)

The BMPS is designed to protect the SGV from BM radiation before the upstream straight is fitted with an insertion device and a complete front end.

#### Slow Gate Valve (SGV)

The Slow Gate valve is included to isolate the machine and FE, but will not withstand white beam from IDs or BM radiation. The SGV is controlled and monitored by storage ring vacuum PLC using a voting scheme with inputs from vacuum sensors at both sides of the valves and position of BMPS.

#### Beam Position Monitor 1 (XBPM1)

The XBPMs shall be designed to work with the insertion devices specified.

Material	Water-cooled mountings and Tungsten blades
Power protection	A pre-mask may be included if design considerations dictate
Motorized	Yes to allow centering of the device around the beam.

The XBPMs shall be mounted on X/Y stages with the following specifications;

Position stability	High stability: $\Delta x, \Delta y = 1 \mu\text{m}$ or better over any 8-hour period Low stability: $\Delta x, \Delta y = 2 \mu\text{m}$ or better over any 8-hour period
Speed	No requirement
Position resolution	x and y = $0.1 \mu\text{m}$ (expected value from calculations); $\ll 1\text{micron}$ (guaranteed).

The X/Y stage for the XBPM and the X/Y slits (see description below) are expected to be the same design, including the stand, where possible.

**Beam Position Monitor 2 (XBPM2)**

This device and X/Y stages shall be identical to XBPM1, however the blades shall be relocated to avoid masking effects.

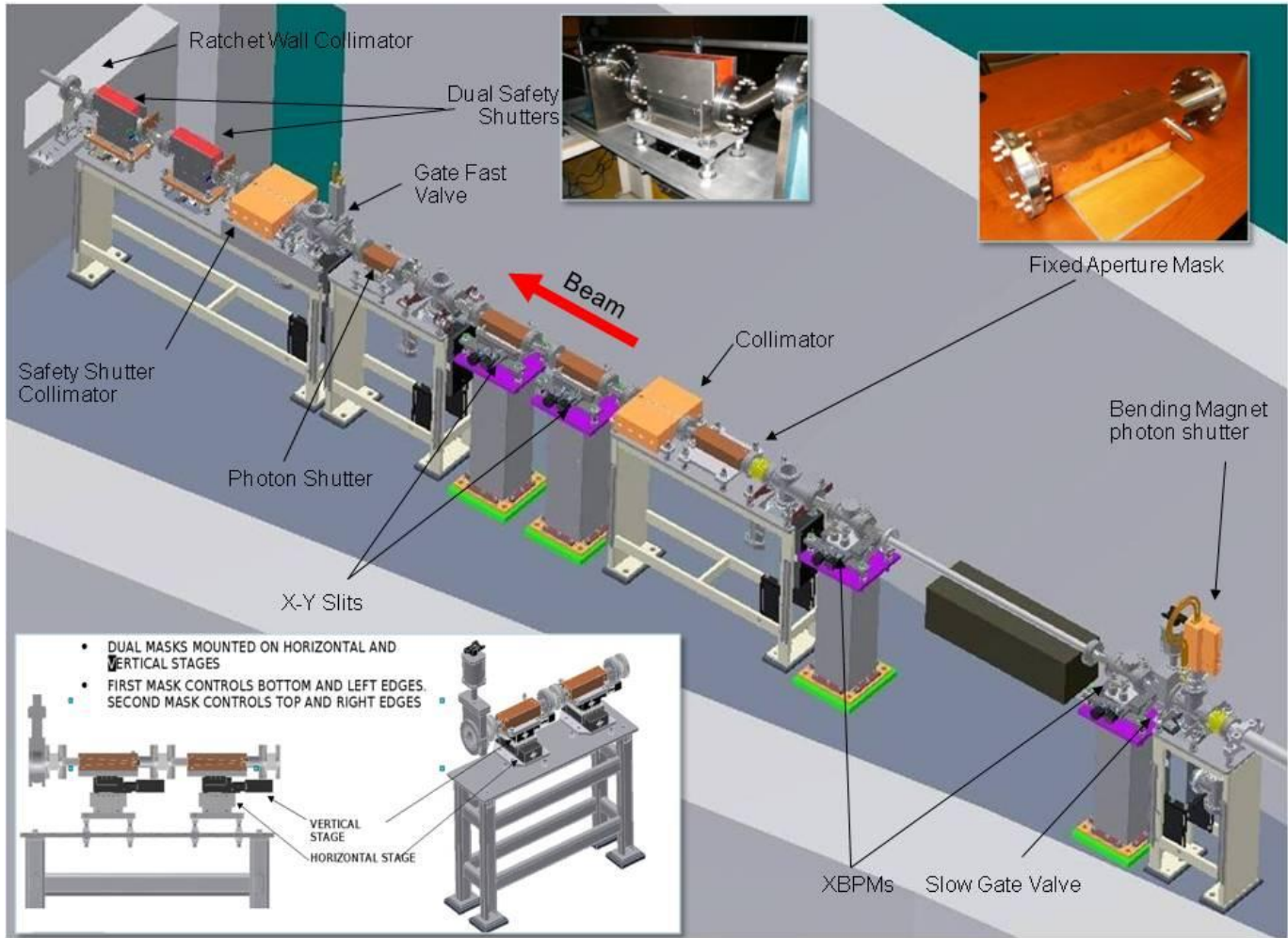


Figure 6. Front End configuration. The lower inset shows the high heat load XY precision primary slits.

### Fixed Aperture Mask (FAPM)

The fixed aperture mask shall provide radiation fans to the FOE as defined in the table above. No tolerance shall be added to the mask for positioning; however a manufacturing tolerance of +/-0.2mm for the aperture (at the downstream end of the mask) shall be included in the downstream fan definition.

For the IVU (and CPMU, if applicable) beamlines, it is permissible for the mask aperture to have corner radii equivalent to half the aperture height, as shown below.



### Bremsstrahlung Collimator (BC1)

The Bremsstrahlung collimator restricts the Bremsstrahlung radiation fan exiting the shield wall. This should be as tight to the beam as is reasonable without undue mechanical tolerances or alignment difficulty.

#### X-Y Slits

The X-Y slits shall be of the SPring8 dual “L” type design, connected with bellows to allow full adjustment of all four “blades” via two X-Y stages. The specifications are as follows;

Material	Water-cooled Glidcop with Tungsten blocks
Power protection	A pre-mask may be included if design considerations dictate
maximum opening angle	Sufficient to allow full FAPM fan to continue to the FOE without clipping.
Motorized	Yes to allow selection of any part of the FAPM fan. The same X/Y stage shall be used for the XBPMs.
Aperture stability	High stability: $\Delta x, \Delta y = 1.5 \mu\text{m}$ or better over any 8-hour period Low stability: $\Delta x, \Delta y = 4 \mu\text{m}$ or better over any 8-hour period

The aperture stability specification is governed by differential movement between the two X/Y slit units; the specification will be met with the low stability X/Y stages. For the high stability stages some form of additional coupling between stands may be required to constrain any differential movement.

#### Photon Shutter

The photon shutter is required to stop full white beam, for IDs this is expected to be water cooled Glidcop at a grazing incidence angle.

#### Fast Valve (FV)

The fast valve is to shut within a few milliseconds once triggered by FV sensors located in the FE and beamline whenever there is a sudden increase of pressure of a few decades. The stored beam has to be dumped prior to FV closing and the cause then investigated and mitigated

### Bremsstrahlung Collimator (BC2)

Bremsstrahlung collimators 1 and 2, and ratchet wall collimator should be made as tight as possible using out-of-vacuum lead designs or in-vacuum Tungsten if needed. The original specification of 3 mm on either side (i.e 9.5 mm for the fixed mask and 15.5 mm for BC2) is too loose for most beamlines.

#### Safety Shutter

The safety shutter is actually a pair of shutters, required for redundancy, air actuated with independent redundant and diverse position sensing.

#### Ratchet Wall Collimator

See note above for BC2.

#### Gate valve downstream of Ratchet Wall

This slow gate valve, pneumatically actuated, with position sensing switches will be monitored and controlled by the SR vacuum PLC using vacuum sensors in the FE and beamlines. This valve cannot be removed after commissioning. This gate valve must be protected from any exposure to beam.

#### Motion Controls

The front end components requiring motion control include the XBPMs (2 units, X/Y axes for each) and the slits (4 axes – 2 for each unit).

#### Vacuum controls

The FE vacuum control is part of storage ring vacuum control through EPICS and SR vacuum PLC. EPICS provides the menu driven on-line control and logging of all vacuum devices, while the PLC provides the control logics for various vacuum devices and interface to EPS PLC for machine protection.

## Optical Layout

The optical scheme presented here is simple and robust. The transverse coherence length of the beam can be adjusted via a flexible focusing scheme to an optimal spot size in both the vertical and horizontal directions. The longitudinal coherence of the beam can also be tuned by the choice of different crystals in double-bounce monochromator or a wider bandpass set of multilayer (ML) optics. A schematic representation of the CHX optics is shown in Figure 7.

The working energy range at the CHX beamline should be as large as possible, in order to offer a good flexibility in designing different experiments. A lower working energy will maximize the coherent flux which is given by equation 1. However, higher energies will help to reduce beam damage, allow experiments with thicker samples, allow working near or above several potentially useful edges (Mn, Fe, Co, Ni, Cu ...) etc. The proposed energy range for the CHX beamline is 6-15 keV. It follows that, for a photon energy of e.g.  $E=8\text{keV}$ , and at a distance  $L=48\text{ m}$  from the source, near the current sample location in the CHX layout, the FWHM transverse coherence lengths (equation 2) in the horizontal and vertical directions are  $\xi_x=40\ \mu\text{m}$  and respectively  $\zeta_z=347.8\ \mu\text{m}$ . In addition, in basically all XPCS experiments it is advantageous to relax somehow the coherence requirements by working with more than one coherent mode. It is thus clear that the coherent or partially coherent spot size is too large to enable speckle detection. A useful beam size is rather on the order of 1-3  $\mu\text{m}$  for a wide-angle experiment or 10-20  $\mu\text{m}$  for a small-angle experiment. These estimates assume a detector pixel size of 80-100  $\mu\text{m}$  and a maximum detector distance of  $R=15\text{ m}$  in SAXS or  $R=1.5\text{ m}$  in WAXS (limited by practical and/or technological constraints). As a consequence, in order to match the transverse coherence length with the desired spot size, focusing is needed in both vertical and horizontal directions. This can be achieved in numerous ways. In our design, a transfocator focusing instrument consisting in a combination of one-dimensional Beryllium Compound Refractive Lenses (CRL) for vertical focusing is placed downstream of the monochromator, at 33.8 m from the source. The required horizontal focusing is achieved with Si kinoform focusing lenses (also 1-dimensional) placed in a lens selector focusing device at  $z\sim 45\text{ m}$ , in the ES. The focusing and beam-defining scheme is schematically shown in Figure 8. For clarity, the flat mirror and the monochromator have been omitted and only the focusing devices (represented here as thin lenses) are shown. The degree of coherence of the beam incident on the sample can be tuned by limiting the angular size of either the primary or the secondary source with any of the secondary slits SS1 – SS3, which will determine the angular size of the spot on the sample –  $\rho'$ . With the linear size of the spot  $\rho$  determined by the geometrical demagnification, the degree of coherence can be tuned to the desired number of coherent modes  $M=\lambda/(4\pi\rho\rho')$  (see also equation 8).

The speckle size  $S$  is given by equation 3. The sample-detector distance in a XPCS-SAXS experiment can be as large as 15 m, but can also be easily changed to any other shorter distances. With coherent beam of  $\sim 23 \times 23\ \mu\text{m}^2$ , the speckle size 15 m downstream, at the detector location is of  $\sim 93\ \mu\text{m}$ . This can be resolved with either the VIPIC detector, currently under development (D. P. Siddons et al., *unpublished*) with its pixel size of  $\sim 80\ \mu\text{m}$  or the Eiger detector currently under development by Dectris Inc. with a pixel size of  $\sim 75\ \mu\text{m}$ .

In addition to the transverse coherence, XPCS requires also partial longitudinal coherence (S. Mochrie, *unpublished*) The longitudinal coherence length of the beam is given by its monochromaticity  $\Lambda=\lambda(E/\Delta E)$ , where  $E$  is the photon energy, and  $\Delta E$  is the full-width-at-half-maximum (FWHM) of the energy spectrum. Partial longitudinal coherence requires that the optical path length difference ( $\delta$ ) between X-rays scattered from different parts of the sample should not be more than a few times  $\Lambda$ . In transmission geometry, there are two contributions to  $\delta$ . The first one, which arises because of a non-zero width ( $D$ ) of the illuminated portion of the sample within the scattering plane, is

$$\delta_D = 2D \frac{Q}{k} \sqrt{1 - \frac{Q^2}{k^2}}. \quad (9)$$

The second comes from the non-zero sample thickness ( $W$ ) and is

$$\delta_W = 2W \frac{Q^2}{k^2}. \quad (10)$$

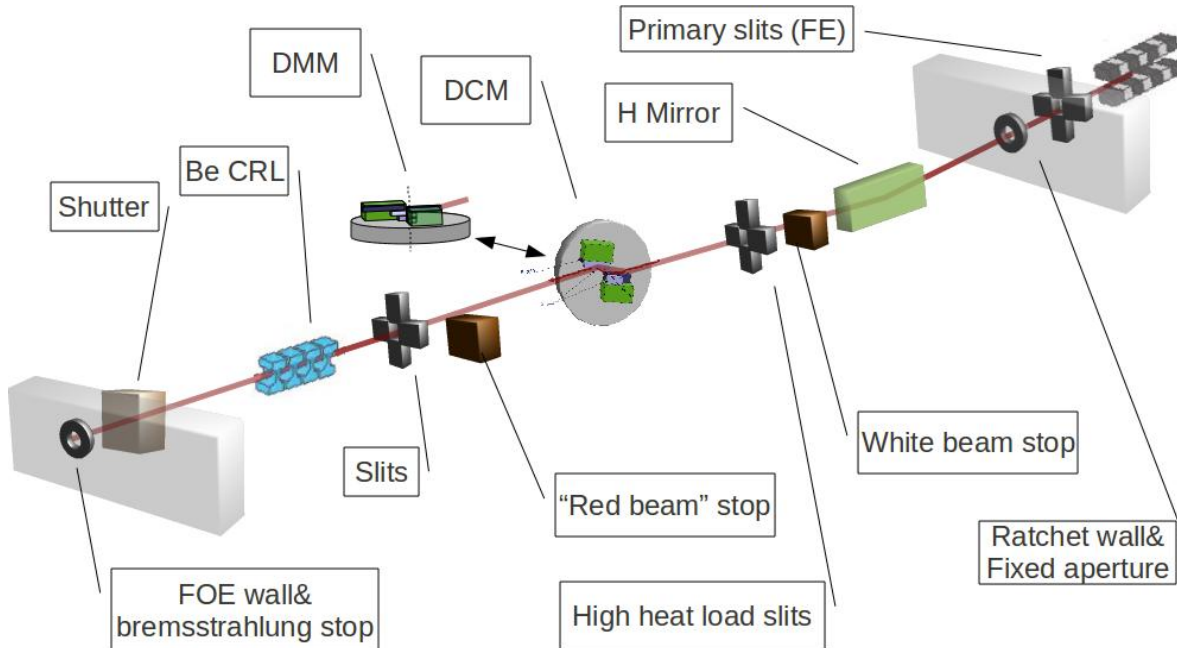


Figure 7. Schematic representation of the CHX optics. A horizontally deflecting fixed incidence angle mirror provides the required separation between the bremsstrahlung and X-ray fans. The mirror is followed by a white beam stop and a set of high heat load water cooled slits. A small gap and small offset vertical DCM or a horizontal DMM provide the choice between monochromatic or pink beam operation. The high precision monochromatic beam slits following downstream of the DCM/DMM allow selecting a beam with the desired degree of coherence. Finally, a Be CRL transfocator unit is used to focus down the beam to the desired spot size on the sample.

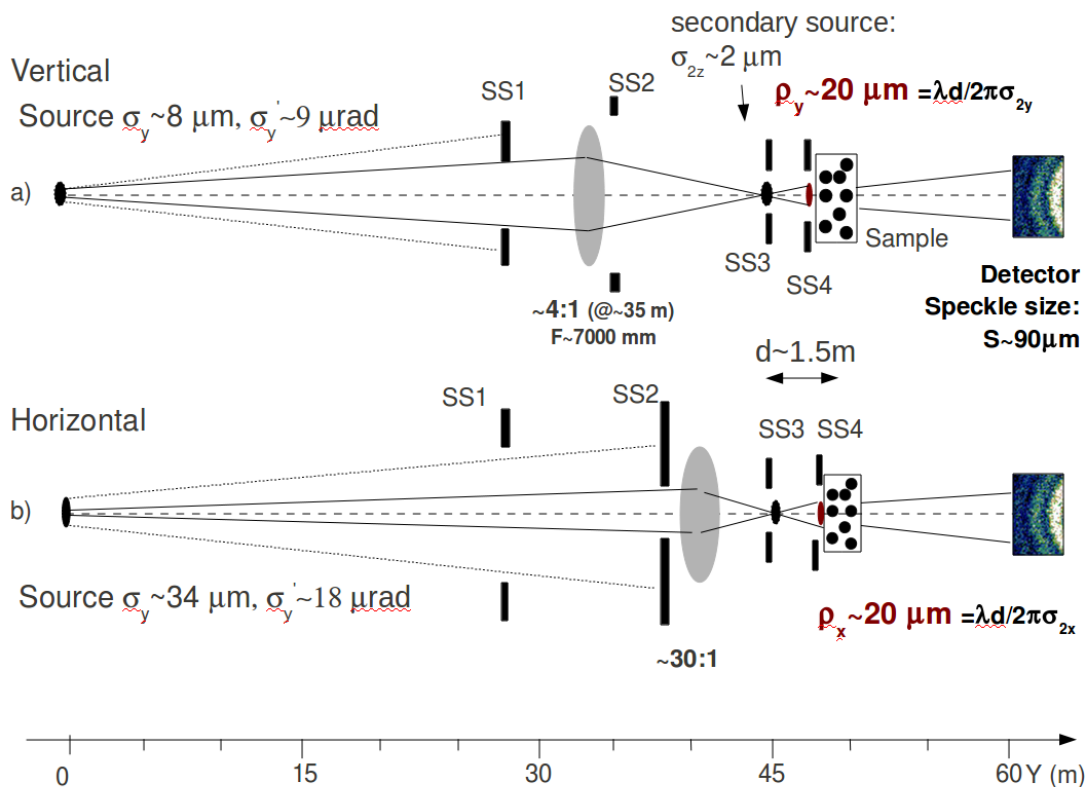


Figure 8. Optical layout for XPCS in a SAXS geometry. Only the focusing optics - Be CRL around  $z=34$  m for vertical focusing and Si kinoform lenses around  $z=45$  m for horizontal focusing - are shown in this diagram. A symmetric coherent beam size of  $\sim 20 \times 20 \mu\text{m}^2$  (FWHM) can be achieved for different operating energies.

Usually,  $\delta_W$  is small for typical values of  $W$  and may be neglected. By contrast,  $\delta_L$  becomes comparable to  $\Lambda$  as  $Q$  reaches a maximum acceptable value. For a Si(111) monochromatic beam with  $E/\Delta E \approx 10^4$ , and a “typical” XPCS-SAXS transverse beam size  $D \approx 20 \mu\text{m}$  the maximum value of  $Q$  is about  $1.5 \text{ nm}^{-1}$ . As this is higher than needed in most SAXS experiments, many of them can be performed using a “pink” beam with  $E/\Delta E \approx 400$ , which limits the  $Q$  range to below  $Q_{\text{max}} \approx 0.1 \text{ nm}^{-1}$ . From this analysis it is clear that longitudinal coherence requirements are more stringent in XPCS-WAXS. With the same Si(111) crystal and a beam size  $D \approx 1 \mu\text{m}$ , the maximum value of  $Q$  becomes  $Q_{\text{max}} \approx 3.2 \text{ \AA}^{-1}$ . This also shows that a higher crystal cut with a smaller bandwidth will be beneficial for many WAXS experiments. The design of the CHX double crystal monochromator will allow the choice of several Si crystals – e.g. Si(111) and Si(220).

## Beamline performance

The CHX beamline operation and performance is evaluated using advanced wavefront propagation methods, the so-called SRW code, developed by O. Chubar (O. Chubar et al., Proc. SPIE Int. Soc. Opt. Eng. 4769, 145, 2002). The method has the unique advantage of predicting not only quantities like flux, spot size, etc. like other methods (e.g. ray tracing) do, but also the intrinsic coherence properties of the beam. Moreover, the effect those optics imperfections have on the coherent wavefront can also be evaluated in ways that are inaccessible to other methods.

The optical layout presented above was implemented in the SRW software (K. Kaznatcheev, L. Wiegart, M. Carlucci-Dayton, O. Chubar, and A. Flueraşu, *in progress* 2010). A double-slit Young experiment was used as a “sample” to probe the coherence of the beam. Some of the preliminary results of the simulations are summarized in Figure 9. A relatively symmetric partially coherent spot at the sample of  $\sim 10 \times 10 \mu\text{m}^2$  (FWHM) is obtained, and this results in the double-slit interference pattern on the detector shown in Figure 9 b. The speckle visibility in this case is on the order of 50%, resulting in a contrast of the intensity-intensity correlation functions in an XPCS experiment of  $\beta \sim 0.5^2 = 0.25$ .

The (partially) coherent flux obtained from these calculations, taking into account the efficiency of the Be CRLs was  $\sim 6 \times 10^{11}$  ph/s, which is nearly two orders of magnitude higher than that available today at instruments dedicated to XPCS.

These simulations will be completed in the near future by considering a representative number of situations in terms of operation energy, spot size, scattering geometry, etc. The effect of imperfection on beamline optics will also be evaluated. These calculations will allow establishing optimal requirements for the beamline optics figure errors in terms of coherent wavefront preservation.

Several such experimental and theoretical studies are in progress and will be briefly described here. The first one focuses on the wavefront disturbance by in-house grown synthetic multilayers. Several measurements were carried on at the ESRF ID6 beamline in collaboration with A. Snigirev et al. on the coherent wavefront preserving properties of in-house grown multilayers. The experiments measured diffraction patterns introduced on purpose by inserting well defined and calibrated objects such as a 100 mm diameter Boron fiber. The same reference interference pattern were imaged with or without the optics being tested (see Figure 10).

Similar experiments were performed in April 2010 at the APS, 32-ID beamline (A. Flueraşu, L. Wiegart, Y. Chu, L. Berman et al.) on a large variety of optical components such as filters, windows, in-house grown multilayers, Be CRLs. The results which are being analysed and interpreted during this phase of the project will undoubtedly provide extremely useful information for the detailed design of wavefront preserving beamline optics.

The numerical simulations and theoretical interpretation of these results using the SRW are a critical component of this “unofficial” research program and the CHX team is determined to pursue this effort in collaboration with O. Chubar, K. Kaznatcheev et al.

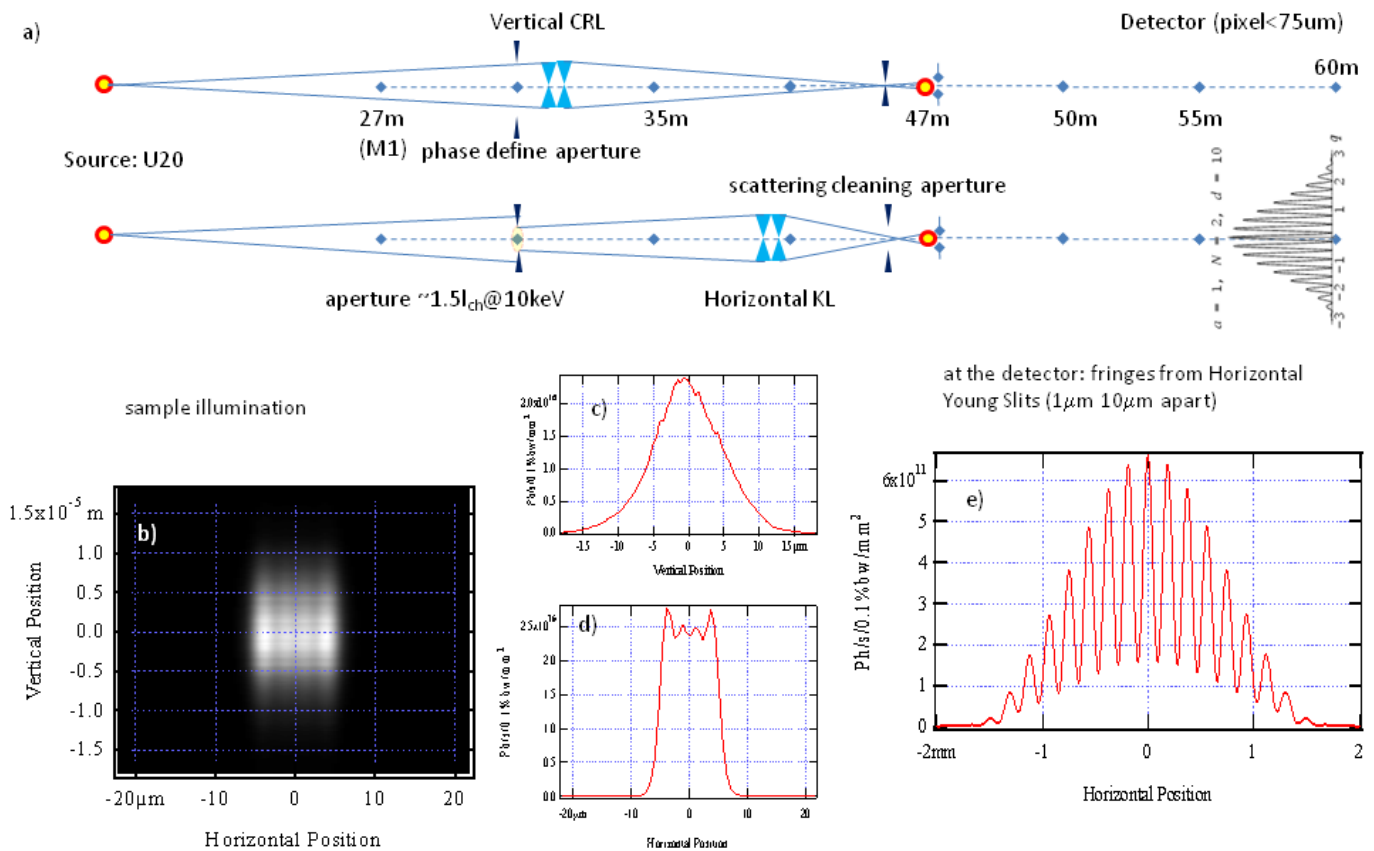


Figure 9. SRW simulations of the CHX performance for XPCS-SAXS operation at 10 keV. a) schematic optical layout (see also Figure 8) with refractive focusing lenses in both vertical and horizontal directions and double-slit Young experiment as the “sample” (1 μm slits that are 10 μm apart); b)-d) sample illumination – a ~10x10 μm<sup>2</sup> spot (FWHM) is achieved here; e) interference fringes from horizontal Young slits in the far field, at the detector location.

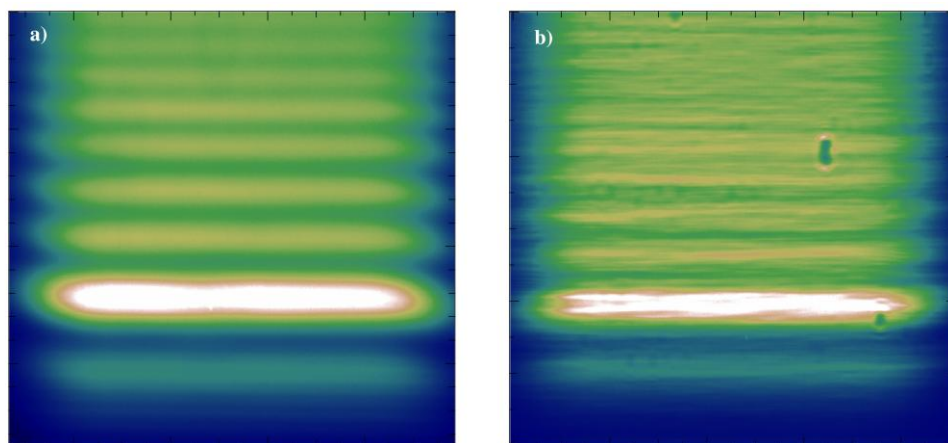
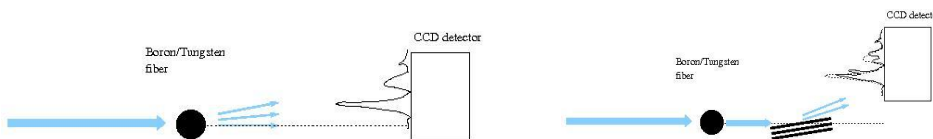


Figure 10. Experimental results (A. Fluerașu, R. Conley, O. Chubar, A. Snigirev et al., *in preparation*) on wavefront preservation by synthetic multilayer; a) the interference pattern resulting for a 100 μm horizontal Boron fiber introduced in a partial coherent (vertical) wavefront are imaged in the far field by a high resolution CCD detector; b) same interference pattern, but reflected before the detector through the 1<sup>st</sup> Bragg reflection of a synthetic multilayer



## Beamline elements

All the major beamline elements, including vacuum parts and beam diagnostics are given in the table below with their distance from the source, utility requirements and vacuum section. The exact location of the elements will certainly change as the design will be pursued in collaboration with our vendors, but the overall layout is not expected to change significantly.

### High Heatload and Beam Conditioning Optics

This section provides a detailed description of the major high heat load and beam conditioning optics elements listed in the FOE section of Table 5, following their location along the beamline downstream of the front end ratchet wall. All instruments, beam transport and diagnostic elements, materials, motors, encoders etc. up to (and including) a first vacuum-tight Silicon Nitride window placed at the beginning of the experimental hutch shall be UHV compatible and designed to work at a base pressure not exceeding  $5 \times 10^{-10} - 10^{-9}$  mbar. The vacuum and utility requirements for the beamline optics sections will be given in more details at the end of this section.

#### Differential Pump with Fixed Aperture

The use of beryllium or other types of solid windows to isolate the machine vacuum from the beamline can perturb the coherent wavefront in uncontrolled fashion and should be avoided at the CHX beamline. For this reason, we will use a differential pumping scheme offering an uninterrupted line of sight between the Front End and the beamline optics (FOE). This is achieved by using a high impedance vacuum connection placed in-between two independent vacuum ion pumps. The whole differential pumping assembly is placed right after the Front End ratchet wall around  $z=26$  m from the source. Since the scientific applications at the CHX beamline require only the coherent part of the beam, the connecting aperture will also serve at a fixed beam aperture. Its design will be similar with that of the individual block of the L-shaped white beam primary slits. The power will be dissipated across a large area obtained by a water-cooled tapered aperture (see Figure 11).

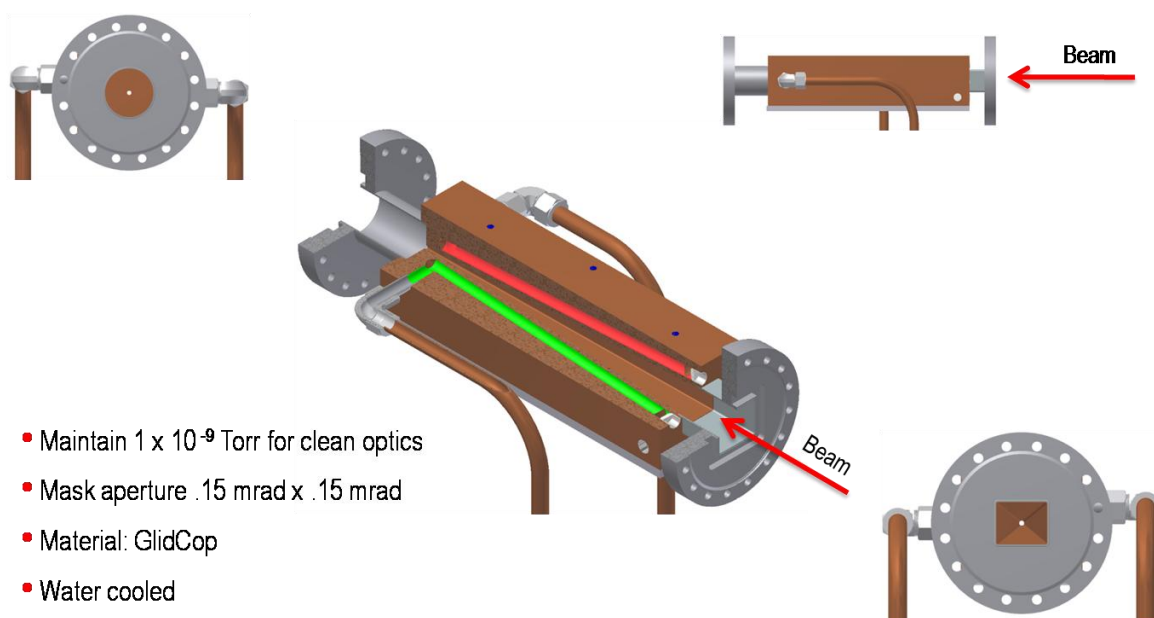


Figure 11.3D representation of a fixed aperture which will be a part of the differential pumping system. The maximum beam size will be limited to  $0.15 \times 0.15$  mrad.

# Preliminary Design Report for the Coherent Hard X-ray (CHX) Beamline at NSLS-II

Table 5. Beamline elements starting with the high heat load primary slits in the Front End and following the beamline layout downstream to the sample location. For the major optical elements, we indicate also the approximate overall length of the vacuum tank in brackets in the second column – distance from the source.

Element	distance from source [m] <sup>1</sup>	comp. N <sub>2</sub>	comp. Air	DI-H <sub>2</sub> O	chilled H <sub>2</sub> O	Liq. N <sub>2</sub>	cylinder gas	Vac section
<b>Front End</b>								
primary slits	~20.5 (~ 1 m)			✓				0
<b>FOE</b>								
gate valve	25.50		✓					0/1
ion pump	25.65							1
diff pumping mask	25.96			✓				1
ion pump	26.26							1
gate valve	26.43		✓					1/2
horizontal mirror	27.00 (0.72m)			✓				2
gate valve	27.56		✓					2/3
fl screen (cooled)	27.70		✓	✓				3
ion pump	28.80							3
white bst. w aperture	29.30			✓				3
Brem. collimator	29.60							3
Slit	30.30			✓				3
fluorescent screen	30.50		✓					3
gate valve	30.77		✓					3/4
DMM	31.35 (0.72m)			✓				4
gate valve	31.73		✓					4/5
DCM	32.60 (0.85m)							5
gate valve	33.20		✓					5/6
red bst	33.40			✓				6
Slit	33.60							6
fluorescent screen	33.88		✓					6
CRLs	34.40 (0.64m)			✓				6
ion pump	34.80							6
fast valve	34.94		✓					6/7
Bremsstrahlungsstop	36.10			✓				7
photon shutter	36.40							7
gate valve	36.55		✓					7/8
<b>Transfer pipe</b>								
<b>EESE</b>								
ion pump	42.80							8
fast valve sensor	42.72							8
Window	42.98							8/9
ion pump	43.16							9
fast shutter	43.60							9
Attenuators	43.90		✓					9
Slit	45.00							9
kinoform (h)	45.35 (0.27m)							9
kinoform (v)	45.72 (0.27m)							9
gate valve	46.30		✓					9/10
Mirror	46.47							10
QBPM	47.44		✓					10
Slit	47.52							10
pin diode	47.80		✓					10
Slit	48.50							10
sample position	48.70	✓	✓		✓	✓	✓	10

The maximum beam size will be limited by this aperture to 0.15 x 0.15 mrad (or about 3.9 x 3.9 mm). This is still considerably larger than the coherent beam size and will not compromise in any way the CHX beamline performance. The aperture will be placed on manually adjustable XY stages and surveyed in place during beamline commissioning.

In standard operation it is expected, that the FOE vacuum ( $10^{-10}$ - $10^{-9}$  mbar) will be comparable, or sometimes even better, than the Front End vacuum. However, for commissioning purposes, and taking advantage of the small fixed mask aperture, the differential pump will be designed to allow safe operation at pressures as high as  $10^{-7}$  mbar with the machine vacuum at  $10^{-10}$  mbar.

In addition, a removable water-cooled window will be designed to be used during beamline commissioning.

### Horizontal White Beam Mirror

CHX requires a high stability white beam mirror with exceptionally small slope errors, so that even the strain from mounting the mirrors can have an impact on the performance of the beamline. Therefore we consider the mirrors and their mounts as a single entity, which needs to meet the specification given in the Table 6.

The substrate dimensions and coating layout can be seen in Figure 12. The exact mounting and cooling scheme will be provided by the vendor. Our finite element analysis (FEA) suggests that indirect water side-cooling provides the best results. However, discussions with vendors about other cooling mechanisms, if they will increase stability, reduce slope-errors or vibration-levels, are encouraged. In particular, given the low power adsorbed by the mirror, the option of using flexible brads for the thermal connexion between the mirror mount and the heat sink shall be thoroughly investigated.

The FEA analysis on the CHX mirror performed by V. Ravindranath is summarized in Figure 13 and Table 7. Owing to the low power density that is achieved with the mirror under grazing incidence, the slope errors can be very low even with straightforward indirect water cooling. A side-cooling geometry optimizes the cooling efficiency and allows for simple and natural and stress free mechanical mounting.

The mirror and its holder will require a cooled grazing incidence mask to protect the leading edge of the Si crystals and any mechanics that might become exposed to the white beam. The mask will be water cooled to safely absorb the full power in the central cone. The heat adsorbing edge of this “disaster mask” will be coated with a fluorescent film. A simple digital camera and a viewing port will allow visually monitoring the beam, which will help the alignment procedure.

The mirrors shall be fitted with one or more UHV compatible PT100 platinum resistance thermometer attached to the substrate and to the white-beam mask to monitor the temperature.

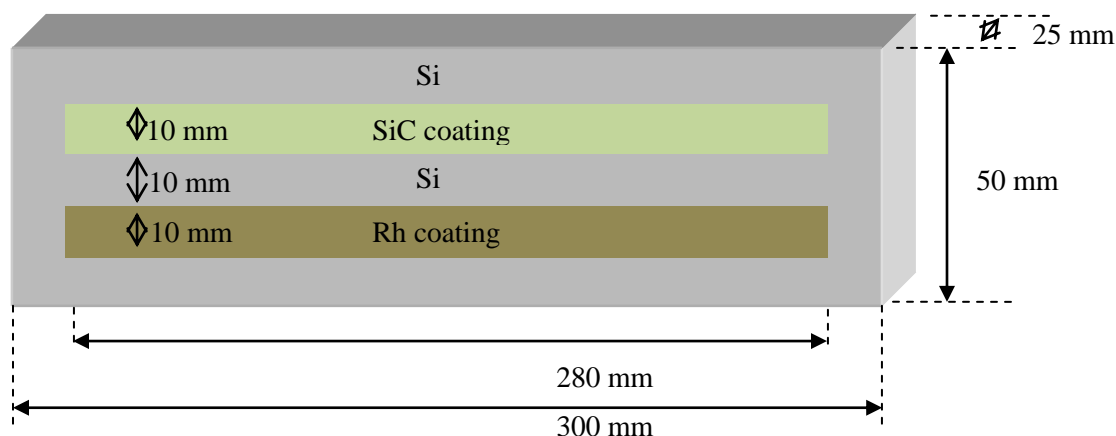


Figure 12: Proposed Substrate layout for the mirror

Preliminary Design Report for the Coherent Hard X-ray (CHX) Beamline at NSLS-II

The total length of the mirror vessel should be kept below 60 cm. The overall height of the vessel is less important, but we assume it will scale in a “normal” fashion with its overall length. Beam height is 140 cm. The axis orientation of the mirror are defined in Figure 14.

Table 6. Specifications for the CHX white beam mirror.

Substrate material	Silicon (Single Crystal)
Substrate area <sup>1</sup>	300 mm long x 50 mm wide
Active area	280 mm x 30 mm
Orientation	Horizontally deflecting (inboard)
Incidence angle	3.14159 mrad ( $\pi$ mrad)
Nominal shape	Flat
Bender	No; Optional bender could be quoted by vendor if not detrimental to stability
Residual radius	>50 km in both tangential and sagittal directions (flat)
Tangential slope error <sup>2</sup> (rms)	<0.3 $\mu$ rad
Sagittal slope error (rms) – along individual lines	<0.6 $\mu$ rad
Cumulative sagittal slope errors (including any twisting or sag)	<1 $\mu$ rad
Coatings	3 stripes each ~ 10 mm wide: bare Si, Pt-coated (500 Å), Rh-coated (500 Å); 10 mm wide stripes; density >95% of material bulk density
Roughness of coatings	<3 Å

<sup>1</sup> Total substrate area can be slightly increased by vendor if more room around the active area is needed for handling

<sup>2</sup> To be achieved with the mounted mirror over the active area

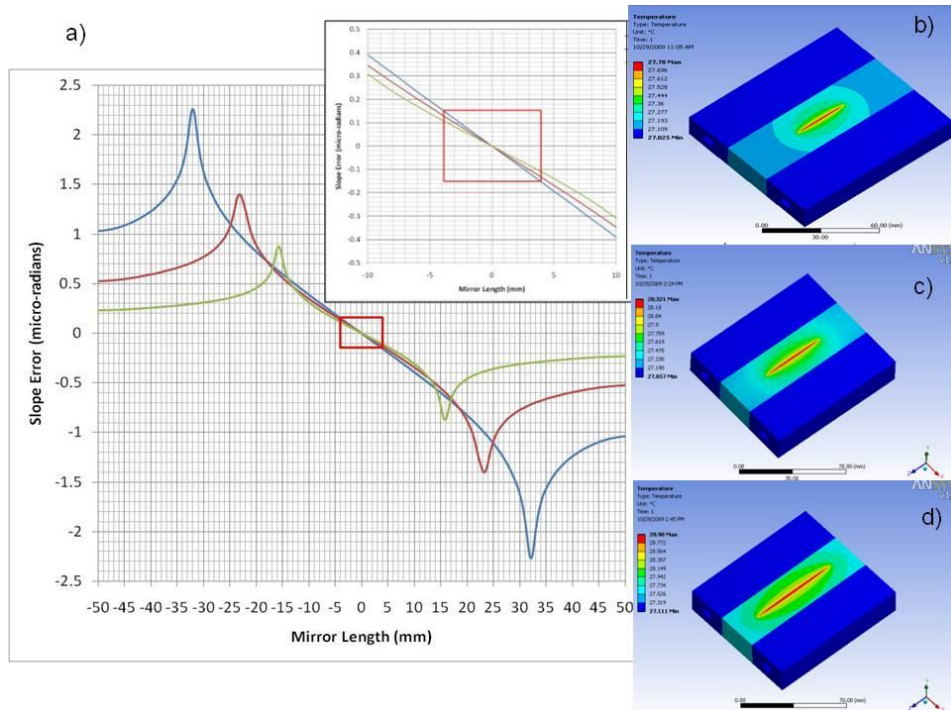


Figure 13: Summary of FEA results on the CHX side water cooled white beam mirror;

a) Slope errors corresponding to a “worse case” scenario in terms of heat load ( $k=1.8$ ); the inset shows a detail around the center of the heat bump focusing on the slope errors in the coherent part of the beam (red box). The temperature and slope error profiles were calculated for three different beam sizes:  
 b) 0.5 mm(V) x 0.1 mm(H) -green lines in a),  
 c) 0.75 mm(V)x0.15 mm(H) – red lines in a)  
 d) 1mm(V)x0.2 mm(H) – blue lines in a)  
 (See also Table 7)

Table 7. Summary of FEA results for the CHX white beam mirror.

Beam Size	$\Delta T_{\max}$ (°C)	$T_{\max}$ (°C)	Slope Error (nad)
0.5mm(v) by 0.1mm(h)	0.8	27.8	100
0.75mm(v) by 0.15(h)mm	1.3	28.3	130
1 mm(v) by 0.2(h) mm	1.97	28.97	150
Full beam (0.15 x 0.15 mrad)		39	

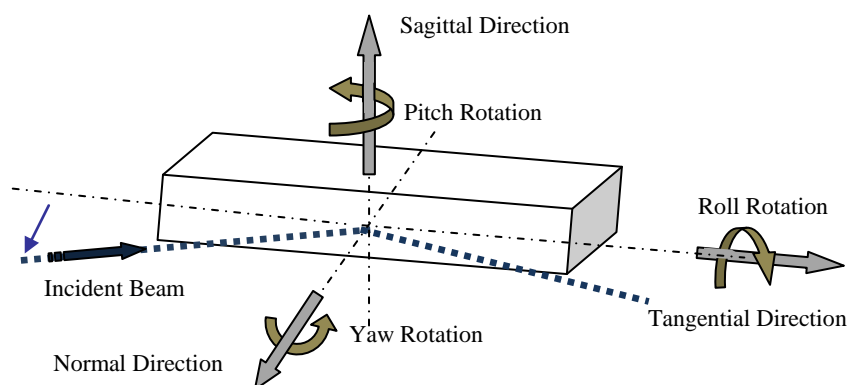


Figure 14. Axis orientation of the inboard deflecting horizontal mirror

In order to maximize the mechanical stability, the mirror is designed to work in a fixed geometry with a constant incidence angle of 0.18 deg. However, a minimal set of degrees of freedom with limited travel ranges will be required in order to align the mirror relative to the photon beam, or to adjust for small beam instabilities. The supplier shall provide all motors, limit-switches and encoders, which are required for this purpose. The different degrees of freedom shall be decoupled and are described below.

**Pitch adjustment**

Due to single bounce and fixed angle geometry of the beamline, the pitch adjustment is the most critical degree of freedom. The angle needs to be deflected at a fixed angle of 0.36 deg (=2x0.18 deg) through a fixed aperture of 2 x 2 mm<sup>2</sup> placed 1.3 m downstream of the mirror (see description of white beam stop below). The total travel range is small as the mirror has to cover the range from 0 to 0.18 deg. A slightly higher maximum travel range of approximately +/-0.23 deg would take into account possible misalignment of the beam and/or surveying errors. A flexure assembly with a neutral position centred on the nominal 0.18 deg incidence angle is preferred over less stable ball bearing assemblies. The small travel range can likely be covered with a fine adjustment piezo actuator capable of operating in a closed-loop control. We prefer a design, where the pitch rotation axis is close to the centre of the mirror surface. The specs for the mirror pitch motion are given in Table 8 together with that for the other degrees of freedom.

**Roll adjustment**

The roll adjustment is not very sensitive, but it is required to compensate for the roll error introduced by the coating exchange mechanism. It is preferred if the rotation axis of the roll adjustment is close to the centre of the mirror surface.

**Yaw adjustment**

A manual yaw adjustment is preferred over a motorised solution if it increases the stability and is only required during the initial commissioning of the beamline.

**Sagittal adjustment (stripe selector)**

To change between the different mirror coatings a vertical translation is required. The accuracy of this motion is less important than its impact on the stability and the pitch misalignment it can induce. These effects must be minimized.

### Normal adjustment (normal to mirror surface)

This adjustment is required to align the photon-beam onto the centre of the mirror and to fully retract the mirror from the beam for alignment purposes. It's possible impact on the stability and the pitch misalignment of the mirror surface is critical and should be minimized

All motorised axes are to be equipped with encoders and switches in order to ensure that (i) positional feedback to the control system is provided, and (ii) ALL possible collisions between moving parts are prevented. In particular, it must not be possible to damage the optical surface of the mirror and mechanical hard-limits shall be provided to prevent this.

The mirror systems shall meet the best vibration specifications that are reasonably achievable. In particular, pitch stability and the stability against vibrations along the normal direction are critical. Vibrations of these axes should be kept at a minimum (see Table 8 )

Table 8. Specification of the mirror alignment system.

Motion	Parameter	Specification
Pitch	Drive	Motorized; Encoder & limits switches to be fitted
	Range	-2 to +6 mrad
	Nominal Angle	3.1415 mrad
	Resolution	<50nrad; State what can be achieved as best effort.
	Repeatability	<200nrad; State what can be achieved as best effort.
	angular stability	<50 nrad (rms)
	8hr stability	<1 $\mu$ rad
	Rotation axis	on the mirror surface
Roll	Drive	Possibly manual with possibility of locking in place.
	Range	-10 to +10mrad
	Resolution	< 5 $\mu$ rad
	Repeatability	< 5 $\mu$ rad
	Rotation axis	Coincident with mirror surface
Yaw	Drive	Possibly manual, if required at all
	Range	-10 mrad to +10 mrad
	Resolution	< 20 $\mu$ rad
	Repeatability	< 100 $\mu$ rad
Sagittal-Translation (Coating exchange)	Drive	Motorised Encoder & limit switches to be fitted.
	Range	Approx. 30mm
	Resolution	<10 $\mu$ m
	Repeatability	<100 $\mu$ m
	Parasitic pitch misalignment	<100 $\mu$ rad between strips <250 $\mu$ rad total State what can be achieved as best effort.
Normal-Translation (normal to mirror surface)	Drive	Motorised Encoder & limit switches to be fitted.
	Range	From -2mm to +2mm
	Resolution	<1 $\mu$ m
	Repeatability	<5 $\mu$ m
	Stability	<1 $\mu$ m
	Parasitic pitch misalignment	<100 $\mu$ rad State what can be achieved as best effort.
Tangential-Translation (along the beamline axis)	Drive	Not required

A Compton shield is preferred to protect mechanical components from undue radiation heating. This component shall protect the upstream of the mirror surface and shall be water-cooled through adequate feed-throughs from the NSLS-II chilled water supply.

### White Beamstop

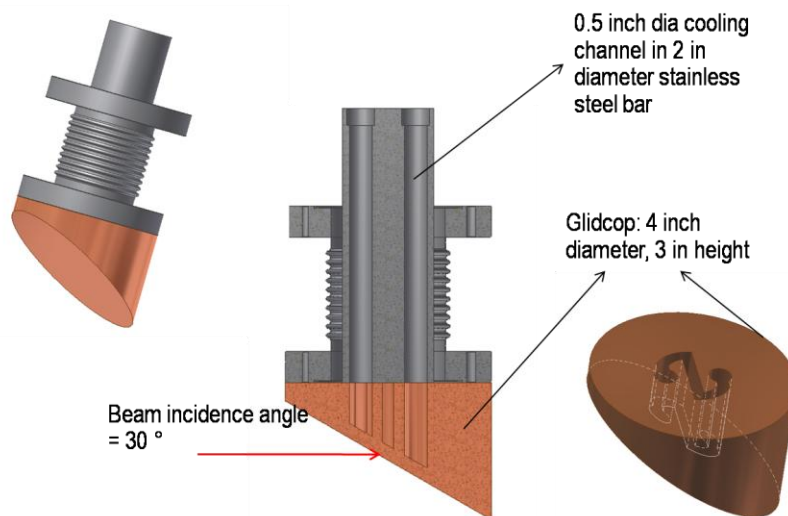
A water-cooled white Glidcop beamstop will be placed at ~2.3 m downstream. This in-house beamstop design (see Figure 15) will feature a small aperture for the beam deflected by the mirror (not yet included in the design). The white beam is designed to handle the full power density of the white beam. However, in normal operation the

primary slits will limit the white beam to a transverse size smaller than the cross section of the horizontal mirror and hence the white beamstop will actually not be exposed. As a consequence the specifications are more “relaxed” than for other white beam components like slits or fixed apertures. The temperature of critical Glidcop components will be kept below 300°C which limits the thermal stress to values below the yield to plastic deformation (<330-350 MPa for Glidcop). The temperature of all other components of the beamstop will be limited to 400°C, which ensures a thermal fatigue life larger than 10000 duty cycles. Under normal operation the beamstop will not be exposed to the beam.

The final white beam stop design will feature a 2x2 mm<sup>2</sup> aperture ~14.4 mm off-axis (inboard) – for the pink beam deflected by the mirror at an angle of 6.28 mrad. The white beam stop, equipped with XY translations (manual or motorized), will be surveyed in place during the beamline commissions and locked in place.

Figure 15: Conceptual design of a water-cooled Glidcop white beam beamstop. The final design will feature a 2x2 mm<sup>2</sup> aperture for the beam deflected at 6.28 mrad by the horizontal white beam mirror.

courtesy of V Ravindranath and S. Sharma



### High Heat-load Secondary Slits

The High Heat Load UHV-compatible slits are used in the FOE to define the beam incident on the DMM or DCM. Due to the relatively small beam size transmitted through the differential pumping aperture and over the horizontal mirror, the maximum aperture of the slits does not need to exceed  $\geq 10 \times 10 \text{ mm}^2$ . The full aperture of the slits should be scannable and blades must be able to travel past each other without interference (overlapping/zero beam). The slit blades can be made of e.g. tungsten or tantalum and special attention should be drawn to a good surface polishing to minimize parasitic scattering. The blades of the slits should be electrically isolated so that the stray current can be used to obtain information about the beam position.

The slits have to cope with a heat load of up to 66.3 W/mrad<sup>2</sup> (power density in the central cone of the IVU20 source) and will therefore have to be water cooled. The vibrations of the slit blades potentially introduced by the cooling should be well below the accuracy of the blade movements. Both slit units have to be vacuum compatible to 10<sup>-9</sup>mbar.

Table 9. Specification for white beam slits

Position stability	High stability: $\Delta x, \Delta y = 1 \mu\text{m}$ or better over any period up to 8-hour
Max aperture	$> 10 \times 10 \text{ mm}^2$
Min aperture	0 (w possibility to overlap blades)
Speed	No particular requirement; as fast as reasonable achievable w/o compromising resolution
Position resolution	x and y = 0.1 $\mu\text{m}$ or $\ll 1 \mu\text{m}$ .

### Double Crystal (pseudo channel-cut) Monochromator

In order to allow measurements of fluctuations in the sample on wide ranges of time and length scales, CHX requires an exceptional stability of the monochromator. For this reason a small gap “pseudo channel-cut” design of the “crystal cage”, with a minimal set of degrees of freedom will be chosen. The design will emphasize exceptional

relative stability between the two crystals and of the whole device, and compromise on some of the functionalities required in more “standard” devices (e.g. monochromatic beam offset will not be kept constant).

The crystal gage will be hosted in a standard “main assembly” of the DCM consisting in a support structure, a vacuum chamber, and a high precision and stability stage providing the main rotary motion of the crystal

The mechanically accessible angular range covered by the primary rotation stage must be from  $-1^\circ$  to  $40^\circ$  (incident angle of beam on first crystal), with  $0^\circ$  being used primarily for alignment purposes. The expected operational range is from  $7^\circ$  to  $33^\circ$ . The primary rotation must have  $1 \mu\text{rad}$  steps or smaller at an accuracy of  $2 \mu\text{rad}$  or better. Throughout this operational range, the radial runout of the rotation axis must be less than 25 microns under full loading condition (with all mechanical components, crystal holders, and crystals included). Because the primary rotation stage has to carry the weight of the crystals and all their mechanical components, the rotary axle should be supported at least at 2 points and must be fitted with precision bearings of high loading capacity. Also, the driving motor must produce sufficient torque and holding force to overcome all tensions and forces created by the coolant transport lines, electrical cables, and the rotary feedthrough seal.

A schematic representation of the crystal cage can be seen in Figure 16. The main horizontal “X” translation of the DCM housing will allow selecting one of the two possible pair of crystals – Si(111) or Si(220). The crystals are dimensions are 40 mm length x 20 mm width x 20 mm thick (The first Si111 crystal only needs to be 20 mm long). The two crystal surfaces are separated by a 2.5 mm gap. The main rotary stage of the DCM housing selects the energy. The 2<sup>nd</sup> crystal mount is equipped with flexure adjustments of pitch and roll to compensate for difference in heat load. The flexures will be driven by precision stepper motors for “rough” adjustment, and piezo actuators for the fine-tuning of the crystal position.

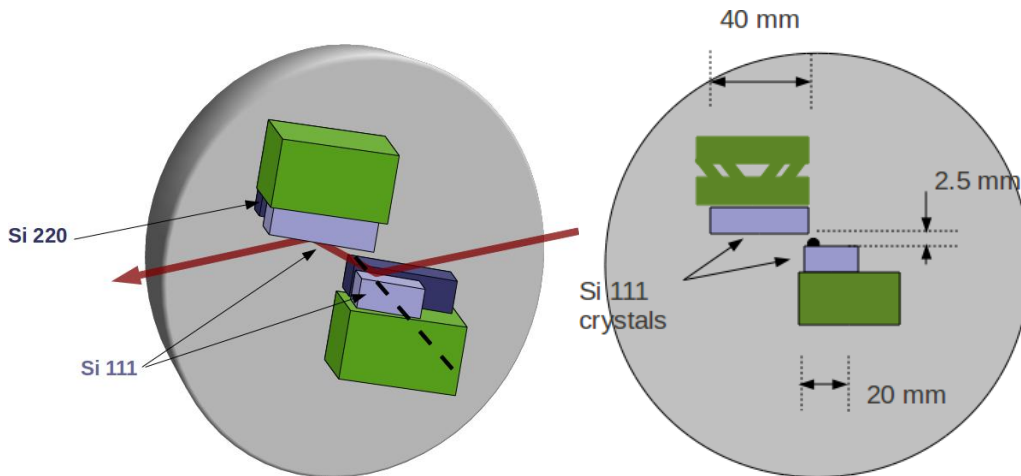


Figure 16: 3D representation and side view of the “pseudo channel-cut” DCM. The crystal cage, mounted on the main rotary stage providing the pitch alignment, will host two pair of crystals – Si(111) and Si(220). The pitch and roll of the second crystal can be adjusted via flexure mounts to compensate for differences in heatload.

This pseudo channel-cut design will provide exceptional mechanical stability of the crystal cage. A schematic diagram of the DCM operation with calculated rotation angles and vertical beam offset is show in Figure 17 for three energies (6,10 and 16 keV) spanning the whole CHX energy range and for each of the two sets of crystals. The beam offset will change between 4.71 and 4.96 mm with the Si111 crystals and between 4.18 and 4.89 mm with the Si220 crystals. These offsets will be followed by the all the downstream optics, including focusing elements, sample position, etc as described in the Monochromatic and Pink Beam Optics and End station instrumentation sections further below.

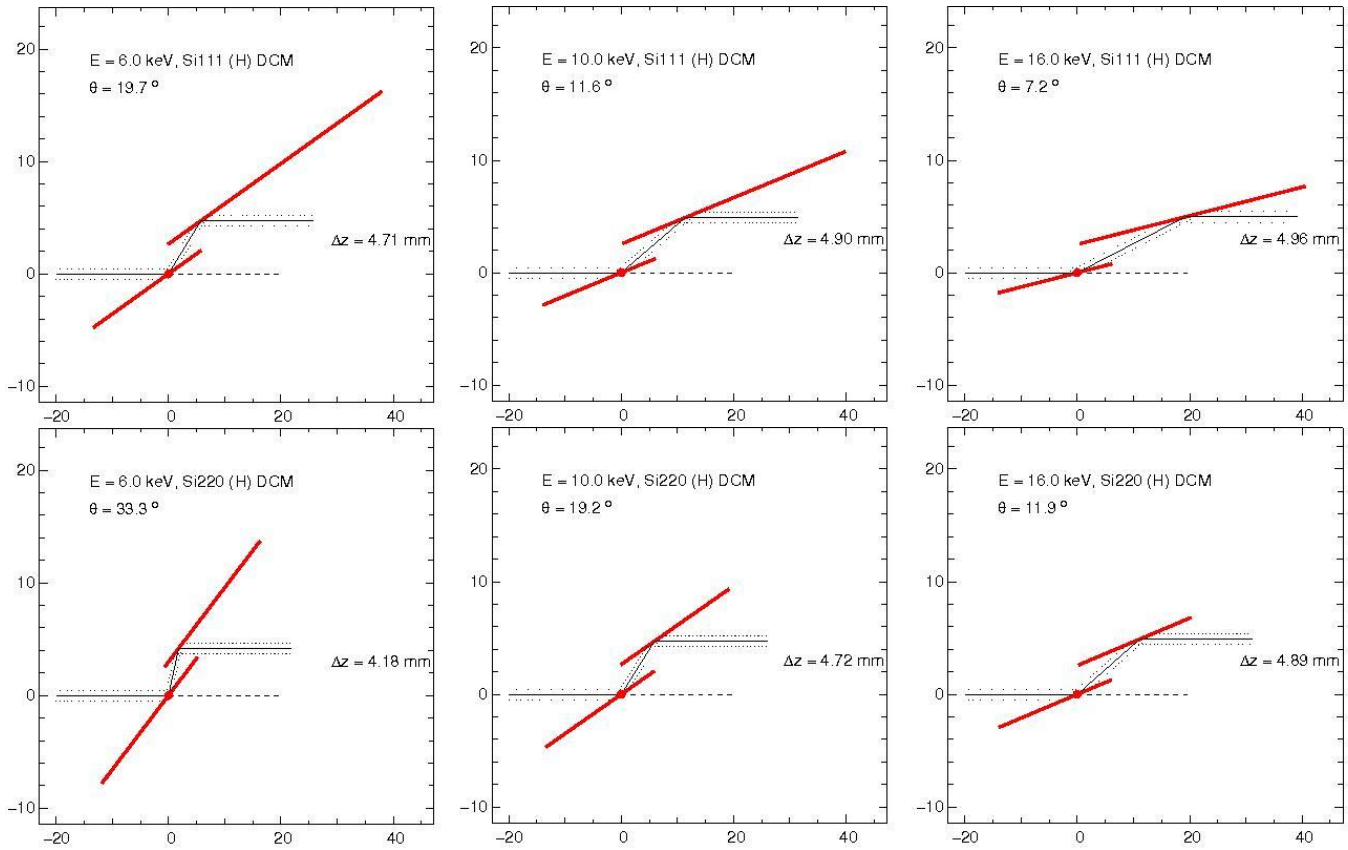


Figure 17: Schematic representation of the DCM crystal cage with operation angle and calculated beam vertical offset for three different energies. The monochromator will provide a choice (via a horizontal translation) between a pair of Si111 crystals (upper row) and a pair of Si220 crystals (lower row)

Overall the DCM system is expected to be a rather compact system and occupy no more than  $\sim 0.90$  m in the direction along the beam  $\pm 0.50$  (in-board and outboard) transverse to the beam, and less than  $\sim 1.80$  m in total height. The incident beam is at a height of 1.400 m from the experimental floor, the exit beam will be offset by 4-5 mm upwards depending on the working energy (see Figure 17)

At least two motorized degrees of freedom must be provided within the support structure: one linear axis of vertical translation and one linear axis of horizontal translation transverse to the beam. Each motorized vertical translation unit of the support is required to have  $\sim 2$  cm of travel range with 1 micron steps and accuracy. It is assumed that the vertical translation system will provide also the possibility of a coarse alignment of the roll and yaw of the main rotary stage. The horizontal translation stage requires a  $\sim 5$  cm travel range with 10 microns steps and 100 microns accuracy. If this will improve stability during operation, a clamping mechanism for each axis shall be provided to rigidly lock the structure at any accessible position. The short term and long-term stability of the support structure are of paramount importance and the design needs to focus on this requirement.

The vacuum chamber shall be fixed to the main support structure through rigid links. It is expected that all the degrees of freedom for the crystal cage will be hosted in-vacuum. The only possible exception is the main rotary stage, if preferred by the vendor, and if placing it outside vacuum does not compromise the stability of the whole assembly.

The main specifications for the crystal pseudo channel-cut DCM are summarized in Table 10.

Table 10 Specifications for the DCM motions

Motion	Parameter	Specification
Bragg angle (i.e. rotation of the crystal cage)	Range	-1° to 40°; expected “standard” operation range 7° to 33°, 0° is for alignments purposes
	Resolution	<1 μrad
	repeatability	<2 μrad
Vertical translation (of the whole assembly)	drive	Stepper motor; encoded; preferably in-vacuum; high stability ball-bearing rotation stage
	Range	~2 cm
	Resolution	10 μm
Note: will also provide pitch and roll alignment for the whole DCM assembly via independent motion of the jacks	Repeatability	20 μm
	drive	possibly manual; other wise 3-4 stepper motors (jacks) preferably encoded;
Horizontal translation (X) of the whole DCM – provides selection between different crystals	Range	~5 cm
	Resolution & repeatability	~10 μm
	Drive	Stepper motor; encoded
Pitch of 2 <sup>nd</sup> crystal – flexure coupling	Range	±1 °
	Resolution & repeatability	<2 μrad
	Drive	In-vacuum stepper motor, encoded;
Coarse motion	Range	200 μrad
	Resolution	<50 nrad
	Repeatability	<100 nrad
Fine motion	Drive	In-vacuum piezo; flexure
	range	±1 °
	Resolution & repeatability	<2 μrad
Fine roll of 2 <sup>nd</sup> crystal – flexure coupling	Drive	In-vacuum stepper; encoded;
	range	±1 °
	Resolution & repeatability	<2 μrad

### Double Multilayer Monochromator

The fine monochromatic resolution obtained with a crystal monochromator is sometimes unnecessary in XPCS experiments working in a small-angle (SAXS) scattering geometry. For such experiment, broader bandwidth diffractive optics such as multilayers (ML) provide a good practical means to obtain an important gain in beam intensity, with excellent harmonic acceptance/rejection efficiency

As a consequence the CHX beamline baseline scope will include pink beam operation with a horizontally bouncing Double Multilayer Monochromator (DMM). The horizontal geometry is chosen to reduce the wavefront disturbances that figure errors would introduce otherwise (see Figure 10). The DMM will be hosted in a vacuum chamber similar with that of the DCM. Due to the small range of angular motion required (less than 2 deg) a high stiffness flexure coupling driven by a piezo assisted by a stepper motor is preferred for the main rotary stage.

The optics cage will provide a flexure-based pitch adjustment for the second multilayer. The multilayers will be grown in-house by the NSLS-II Optics Group (R. Conley et al.). The structure of choice, which is currently being tested in different experiments, is a WSi<sub>2</sub>/Si multilayer with a d-spacing of 38 Å. Two MLs, each 160 mm long and a 2 mm gap will be held by the optics cage. A schematic representation of our conceptual design is shown in Figure 18. The optics cage, with calculated operating angles of this conceptual design for different working energies is shown in Figure 19. The DMM specifications are given in Table 12.

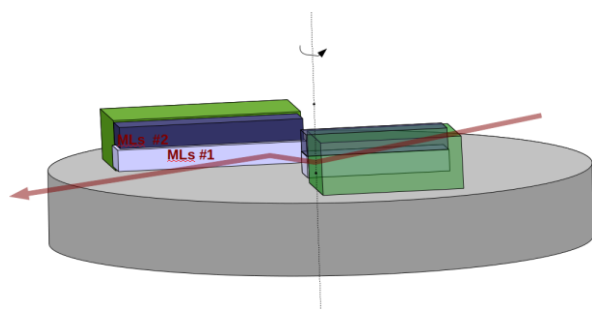


Figure 18: 3D schematic model of the DMM pink beam monochromator with up to two pairs of multilayer structures.

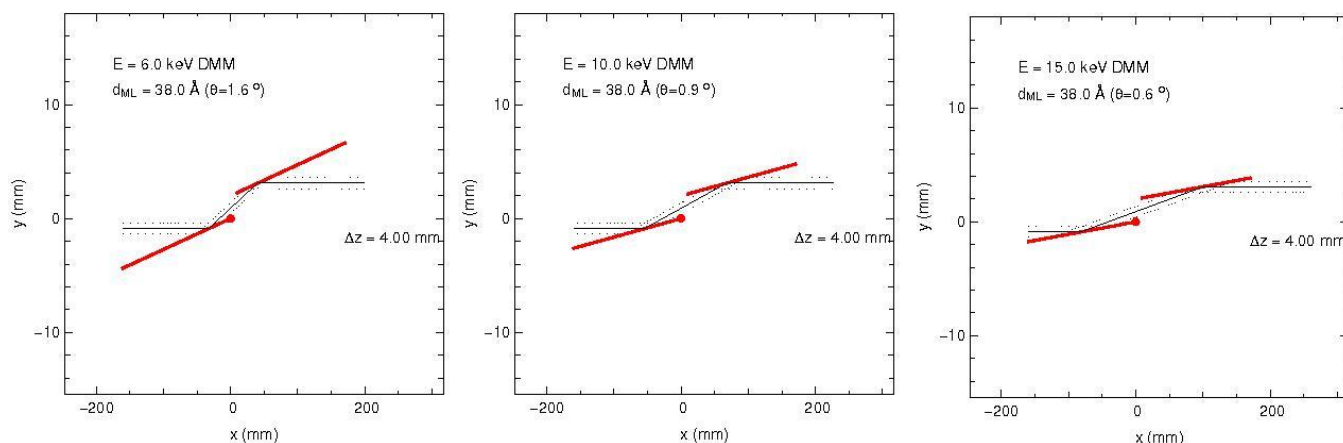


Figure 19: Schematic representation of the DMM pink beam monochromator multilayer cage with operation angle and calculated beam vertical offset for three different energies.

The harmonic selection “efficiency” of the proposed optical layout for pink beam operation at 8 keV is shown in Table 11. The calculations are done for the total transmitted intensity at the peak of the odd undulator harmonics of a system consisting in the horizontally deflecting Si or SiC mirror, and the DMM. For the rejection of the first undulator harmonic, a 100  $\mu\text{m}$  diamond filter was added in the system. Our SRW coherent wavefront propagation numerical simulations will tell if this filter is indeed needed, or if the Be CRLs placed just downstream of the DMM and optimized for focusing at different (higher) energies can fulfill this harmonic rejection role (albeit at a price in terms of heatload).

Table 11 Harmonic acceptance/rejection efficiency for work with a 8keV pink beam obtained from the 5th undulator harmonic ( $k=1.83$ ). The system consisting in: i) white beam (fixed angle) mirror; ii) multilayer monochromator; iii) 100  $\mu\text{m}$  diamond exit window.

U20 Harmonic #	#1	#3	#5	#7	#9
E [keV]	1.6	4.8	8	11.2	14.4
R - ML reflectivity	0.7	7.5e-3	0.81	3.8e-4	2.7e-4
T (100 $\mu\text{m}$ diamond)	1e-5	0.62	0.90	0.96	0.98
Mirror reflectivity $R_m$	0.94	0.96	0.96	0.13	2.5e-2
Total efficiency $R^2TR_m$	4.61E-06	3.35E-05	<b>0.57</b>	1.80E-08	1.79E-09

The full spectrum obtained after the DCM is shown in Figure 20. Here the harmonic selection/rejection efficiencies were finely adjusted and optimized by “de-tuning” the DMM from the perfect Bragg condition.

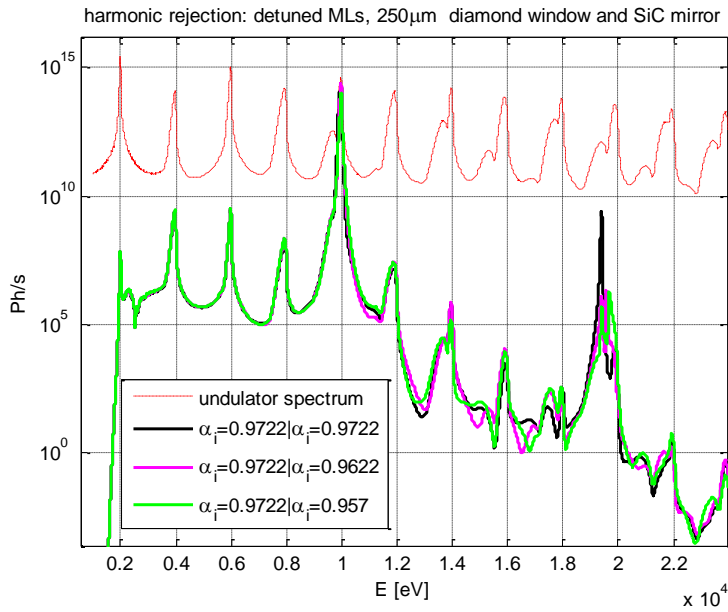


Figure 20: Harmonic selection with for pink beam operation with DMM for two operating energies: 8keV ( $k=1.83$ , 5<sup>th</sup> harmonic) and 10 keV ( $k=1.51$ , 7<sup>th</sup> harmonic)

Table 12 Specifications for the DMM motions

Motion	Parameter	Specification
Bragg angle (i.e. rotation of the ML cage)	Range	$-1^\circ$ to $2.4^\circ$ ; expected “standard” operation range $0.9^\circ$ to $2.1^\circ$ , $0^\circ$ is for alignments purposes
Preferably flexure coupling	Resolution	$<1 \mu\text{rad}$
	repeatability	$<2 \mu\text{rad}$
	drive	Stepper motor; encoded; preferably in-vacuum;
Vertical translation (of the whole assembly)	Range	$\sim 5 \text{ cm}$
	Resolution	$10 \mu\text{m}$
Could allow the choice between different sets of ML	Repeatability	$20 \mu\text{m}$
	drive	3-4 stepper motors (jacks), preferably encoded, out of vacuum
Note: will also provide pitch and roll alignment for the whole DMM assembly via independent motion of the jacks	Resolution & repeatability	$\sim 1 \mu\text{m}$
	Drive	Stepper motor, out of vacuum, encoded
	Resolution & repeatability	$\sim 1 \mu\text{m}$
Horizontal translation (X) of the whole DCM – provides selection between different crystals	Range	$\sim 5\text{-}10 \text{ mm}$
	Drive	Stepper motor, out of vacuum, encoded
Pitch of 2 <sup>nd</sup> crystal (flexure coupling)	Range	$\pm 1^\circ$
	Resolution	$<2 \mu\text{rad}$
	repeatability	$<4 \mu\text{rad}$
	Drive	In-vacuum stepper motor, encoded;
Fine motion	Range	$200 \mu\text{rad}$
	Resolution	$<50 \text{ nrad}$
	Repeatability	$<100 \text{ nrad}$
	Drive	In-vacuum piezo;
Roll of 2 <sup>nd</sup> crystal (flexure coupling)	Range	$\pm 1^\circ$
	Resolution	$<2 \mu\text{rad}$
	Repeatability	$<4 \mu\text{rad}$
	Drive	In-vacuum stepper motor, encoded;

## Monochromatic and Pink Beam Optics

### Precision Slits

This set of UHV-compatible precision slits have all the specifications similar with those for the High Heat-load Secondary Slits (see description above). The heat load on the second slit unit will be lower than on the High Heat-load Secondary Slits and it is expected that they will not require cooling. However, FEA will be performed to determine precisely whether cooling will be required or not for these slits. These slits will be used to define a coherent beam incident on the focusing Be CRL lenses described below. As a consequence the slit blades will be highly polished and optimized to minimize parasitic scattering. More advanced options of “scatterless” hybrid metal-single-crystal slits (Y. Li et al., *J. Appl. Cryst.*, **41**, 1134-1139, 2008) or partially transmitting crystal slits (E. Dufresne, S. Dierker, Z. Yin, L. Berman, *J. Synchrotron Rad.* **16**, 358-367, 2009) will also be explored.

### CRL Transfocator

With the unprecedented low emittance of the NSLS-II source, the transverse coherence lengths of the X-ray beam are larger than at any other 3<sup>rd</sup> generation SR facility. In order to match this with resolution requirements and other practical or experimental constraints, the possibility of focusing the beam is one of the most important capabilities of the CHX instrument.

At the same time, the beamline has important requirements for ultra-high stability, and minimal wavefront disturbance of the beam. For this reason, more “tolerant” refractive optics is preferred over reflective optics for focusing in both vertical and horizontal directions. As refractive optics are chromatic elements, the focusing units are designed to provide operation options for a series of discrete energies, e.g. 6, 8, 10, 12, and 15 keV.

A “transfocator” type of device offering the possibility to insert a different number of similar or even identical lenses in the beam is the CHX device of choice for low demagnification focusing. Due to the asymmetric shape of the beam, the horizontal and vertical focusing will need to be decoupled. For this reason the design uses one-dimensional Be Compound Refractive Lenses (CRL) that have very recently started to become available (B. Lengeler et al., *private communication*). The transfocator is placed in monochromatic/pink beam at  $z \sim 34.5$  m from the source and will provide a coherent spot of  $\sim 20 \times 20 \mu\text{m}^2$  (FWHM) at the sample location.

A scheme for vertical focusing using up to 16 one-dimensional Be CRLs with a 0.5 mm radius at the apex is summarized in Table 13. In all cases the secondary source created by the lenses gives a vertical coherence length at the sample on the order of 20  $\mu\text{m}$  (FWHM). This is somewhat tunable by changing the number of lenses. However, to obtain much smaller spots sizes, on the micron scale, another focusing unit with one-dimensional kinoform lenses will be placed closer to the sample to provide the required higher demagnification ratio. This system, is described further below in the End station instrumentation section.

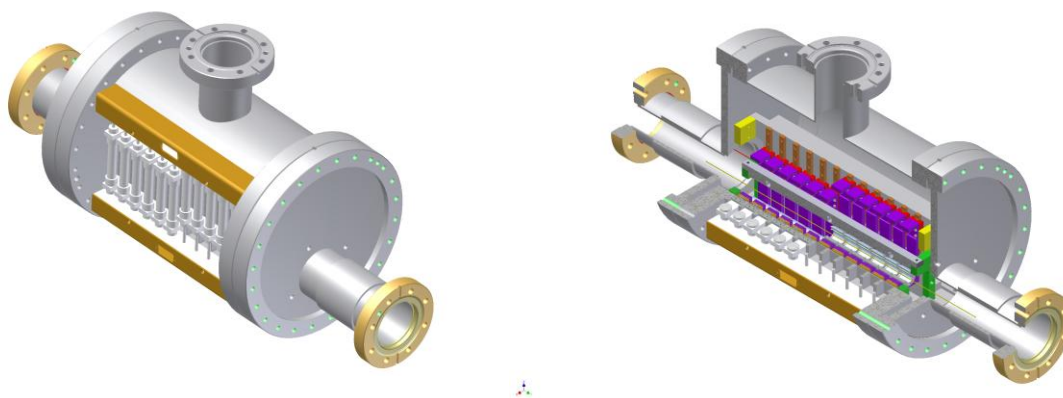


Figure 21: 3D model of a transfocator unit with Be CRLs designed at Petra-III (courtesy of Yong Chu, Petra-III)

Table 13 Transfocator device for vertical focusing based on 1-dimensional 0.5 mm Be CRL lenses

E (keV)	6	8	10	12	16
N lenses	3	4	9	14	22
Efficiency <sup>1</sup>	0.83	0.90	0.88	0.88	0.875
FWHM coherent spot at the sample (μm)	25.5	18.1	24.2	20.4	23.3

<sup>1</sup> calculated for a highly coherent beam with  $\sigma\sigma'=\lambda/2\pi$ ; the efficiency drops to ~0.8 or slightly below for larger radiation fans

The motorized degrees of freedom required for the alignment of the Transfocator(s) are specified in Table 14.

Table 14 Specifications for the motorized axes of the transfocator unit.

Axis	motorized	encoder	resolution	bi-directional repeatability	Stability	travel range
X	Y	y	<0.2μm	<.2μm	<0.1μm	± 10mm
Y	Y	y	<0.2μm	<0.2μm	<0.1μm	± 15mm
pitch/θ*	Y	y	<0.001°	<0.002°	<0.00005°	± 5°
yaw/φ*	Y	y	<0.001°	<0.002°	<0.00005°	± 5°
roll/χ*	Y	y	<0.001°	<0.002°	<0.00005°	± 5°

\* possible in-vacuum motion

### Vacuum

We anticipate that detailed vacuum requirements will be specified in the very near future for the entire NSLS-II facility. At this stage, inspired by the specs from other facilities, we are specifying here a set of probable vacuum requirements for the entire FOE. The pressure must be less than  $5 \times 10^{-8}$  Torr, preferably  $10^{-9}$  Torr with all the mechanical parts, crystal mounting stages, and in-vacuum motors installed. The leak rate must be less than  $1 \times 10^{-9}$  Torr-l/sec. Residual gas analysis must be done, and the total pressure from masses above 38 must be less than  $5 \times 10^{-10}$  Torr. A residual gas sensor will be placed just downstream of the differential pumping system. The beamline will be allowed to operate only if all the vacuum requirements are met.

### Ray Tracing

The bremsstrahlung ray tracings for the horizontal and vertical directions are shown in Figure 37 and Figure 38 in appendix 2: reference drawings . One collimator placed at  $z=29.6$  m will ensure that bremsstrahlung radiation cannot propagate to the experimental hutch which will be shielded for monochromatic/pink beam. A tungsten bremsstrahlung stop with a  $15 \times 15$  mm<sup>2</sup> aperture for the monochromatic or pink beam will be placed at the end of the FOE (Figure 22). The synchrotron radiation ray tracings are shown in both horizontal and vertical directions for the monochromatic beam obtained with the DCM or the pink beam obtained with the DMM (see Figure 39-Figure 42 in appendix 2: reference drawings)

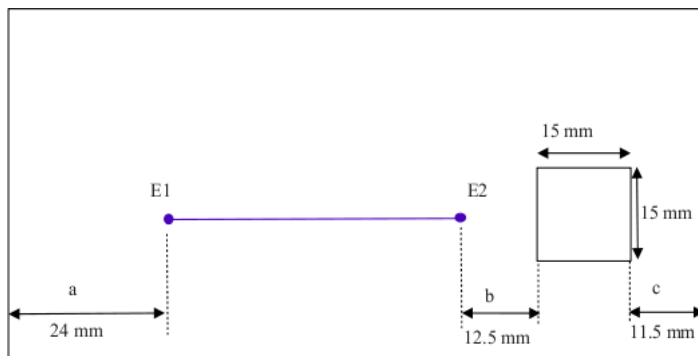


Figure 22: Tungsten bremsstrahlung stop with aperture for the monochromatic/pink beam

### 3. END STATION INSTRUMENTATION

#### Overview

While offering optimized setups for SAXS and WAXS experiments, the CHX end station will also allow for XCPS studies in SAXS and GISAXS geometries accompanied by (static) WAXS or GIXD measurements. This combination is of particular interest for studies of soft condensed matter systems like e.g. thin organic films or thermotropic gels of self-assembled organic nanotubes. These systems are characterized by an intimate relationship between structure and dynamics, where often the larger scale dynamics is determined by the microstructure. The endstation will feature an optics table for some beam defining optics, a versatile diffractometer providing both horizontal and vertical scattering geometries and a SAXS table with adjustable flight tube length (up to 15m) and a multi-detector bench (see Figure 23). The different elements of the endstation will be described in the following.

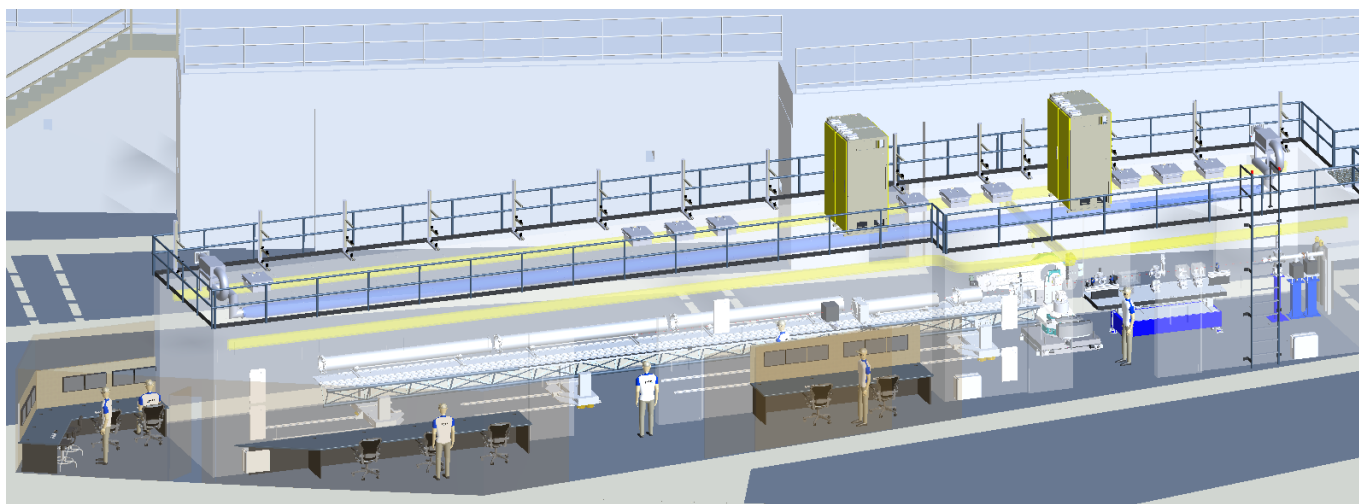


Figure 23. Overview of the CHX endstation

#### Beam Conditioning Optics

##### Exit Window and Endstation Vacuum

The first two elements in the CHX endstation will be a fast valve sensor and a window which separates the UHV in the optics hutch ( $\sim 1 \times 10^{-9}$  mbar) from the HV ( $1 \times 10^{-6}$  mbar) section of the local optics. The elements of the local optics which are likely to stay in place in all possible beamline configurations (e.g. fast shutter, attenuator) will be interfaced by conflate flanges, while the part which requires a higher flexibility will be interfaced by quick flanges and viton o-rings. The local optics will be pumped initially with a turbo and roughing pump and then switch over to vibration free ion pumps. In order to disturb the coherence of the beam as little as possible, the window will be likely a thin silicon nitrate membrane. Alternatives are a highly polished beryllium or a single crystal diamond window. The window may be motorized to move in the x and y-direction to facilitate a change of the irradiated spot on the window, which might be necessary from time to time if the window gets gradually damaged by the intense X-ray beam (particularly in pink beam operation). However, it is currently assumed that the heat load on this window is sufficiently low, so that no additional cooling is required. Despite the gate valve in front of the window, which can be closed as a means of protection during changes of the local optics, which require breaking the vacuum, it is anticipated that this window might break occasionally. For this reason, a fast valve sensor is located just upstream of the window, which detects a rise in pressure and shuts the fast valve located downstream of the focusing optics in the FOE so that the vacuum of the optical elements in the beamline would be preserved in the case of an incident. Currently, the fast valve is assumed to close within 10ms of the pressure rise at the sensor. With a shock wave velocity of 440m/s and a distance of about 8m between the fast valve sensor and the fast valve, this would be fast enough to have the fast valve closed before the shock wave arrives. Contrary to the fast valve located

in the front end, triggering of the fast valve in the FOE will not dump the beam in the storage ring. Because the local fast valve has only to withstand the monochromatic/pink beam, it is assumed that the valve can withstand this at least for 4-5s without damage. Within this time the safety shutter in the front end and the gate valves in the FOE, which are interlocked via the EPS, will be closed.

### First Optics Stand

The first optics stand in the CHX endstation will support equipment that can potentially create vibrations, like e.g. pneumatic attenuators or a mechanical shutter closing and opening at a high frequency. It will furthermore support an ion pump and a pumping port for a turbo-pump. By separating these elements from the beam defining local optics located on the optics table (see Figure 25), an improved stability of these critical optical elements is anticipated. The top of the stand will feature translations and rotations to follow the offsets from the DCM and DMM and to align the fast shutter (see Figure 24) with the X-ray beam. Special vacuum bellows will be used to connect the last element on the stand with the first element on the optics table, in order to minimize the transmitted vibrations

### Fast Shutter

The fast shutter will mainly be used to protect the sample from the X-ray beam between acquisition and thus to limit beam damage. Fast detectors for XPCS will be (arrays) of APDs or 2d pixel detectors, which can both read out the data while being exposed to the beam. The shutter speed does thus not need to approach the timescales of the fastest dynamics probed at CHX. A rather standard millisecond shutter (e.g. Azsol) with opening times of a few milliseconds will be sufficient. For faster time series, the shutter will stay open during the acquisition of the images (series mode), instead of closing between individual frames. A typical design employs a blade which is moving around a pivot point, accelerated by an electromagnet. For a blade length of 25mm, 1mm thickness and an angle of 4.6° in closed position, the effective thickness of the shutter blade for the absorption of the beam becomes 12mm, sufficient to block any beam within the energy range of the CHX beamline. A low jitter of the shutter opening time would allow a very good synchronization of the shutter with the acquisition, thus maximizing the sample protection. However, the jitter of the shutter will not affect the accuracy of the exposure time of an image, as this is defined by the detector itself. The opening and closing time of the shutter depend on how well the beam is aligned with the shutter blade. In order to align the beam parallel with the blade and center it in the shutter opening, motorized pitch and Y axis below the shutter mount (possible on the top of the supporting stand) are required. In addition, a motorized horizontal X-translation is also needed. In general the XY motorized axes will allow following accurately the DCM/DMM offsets with the shutter. The shutter needs to be vacuum compatible to  $1 \times 10^{-6}$  mbar.

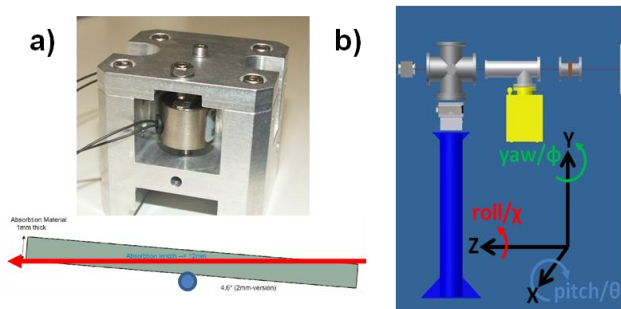


Figure 24. a) fast shutter, blade design (Azsol). b) first optics stand.

Table 15. Specifications for the motorized axes for the fast shutter and attenuators

Axis	motorized	Encoder	Resolution	bi-directional repeatability	Stability	travel range
X	Y	Y	<10µm	<10µm	<1µm	± 25mm
Y	Y	Y	<1µm	<2µm	<1µm	± 10mm
pitch/θ	Y	Y	<0.002°	<0.01°	<0.002°	± 5°

## Attenuators

The attenuators will consist of a set of pneumatic actuators which insert metal foils of a certain thickness into the beam. The foils should be combinable in a way that the beam can be attenuated in steps of about half an order of magnitude. The choice of the metal should avoid absorption edges in the energy range from 6 to 16keV to avoid strongly non-linear behavior of the attenuators as a function of energy. It should be possible to remove all attenuators from the beam and at maximum attenuation the beam should be totally blocked, both in monochromatic and pink beam mode. The actuators should have limits to provide a feedback about their actual position. The attenuator system needs to be vacuum compatible to  $1 \times 10^{-6}$  mbar or better.

## Optics Table

The optics table in the experimental station is reserved for local beam conditioning optics like focusing elements, a mirror to tilt the beam down for grazing incidence studies on liquid surfaces, high precision slits to define and clean the beam and beam monitoring and diagnostics. An optics table is chosen here as a support to provide a certain flexibility in the arrangement of local beam conditioning optics, which will not only evolve with time, but might also be experiment specific. In addition, the table would provide also enough space and flexibility to house not only the beam defining optics, but also the sample itself. This would be a convenient option for some possible experiments requiring an extremely high positional stability of the incident beam on the sample, e.g. ptychography. Moreover, the optics table will allow to follow the X-ray beam offsets induced by the DCM and DMM and which will change with energy. Rather than moving all the individual elements on the table to compensate for these offsets, a movement of the entire table will preserve the relative alignment of the optical elements and thus facilitate and quicken the realignment procedure upon a change in energy or the switching between monochromatic and pink beam. The table should therefore have motorized adjustments in the support of the table top. The offsets from the monochromators are in the vertical and horizontal directions, respectively. In the ideal case, changing the energy or switching between monochromatic and pink beam would not introduce a deviation in the angular direction of the beam and thus a table with two degrees of freedom (2DOF) would be sufficient, assuming that the table will be well surveyed in place. However, in case the tweaking of the second crystal/monolayer changes with e.g. energy, it would become very handy to be able to compensate with the table for angular changes as well. Thus a table with all six degrees of freedom (6DOF) will be the better option. First evaluation of prices indicates an additional cost of less than 10% for the additional degrees of freedom. It needs to be evaluated though, whether the 2DOF table would have some advantages in terms of stability over a 6DOF version. The table will likely achieve pitch and roll via the movement of jacks serving as the 'legs' of the table. bi-directional repeatability of such jacks of  $<4\mu\text{m}$  is achievable, which for legs being 2m apart results in a rotation with  $<0.0003^\circ$  repeatability, good enough even for the alignment of the kinoform lenses. The specifications of the motorized axis for a 6DOF table are summarized in Table 16. The table will be 3000mm long and 600-900mm wide. The width of the table will limit the clock-wise rotation of the  $\delta$ -arm of the diffractometer, so further design studies will be necessary to find the best compromise between available table surface and diffractometer movement. The overhang of the table surface might be used to accommodate the counter weight of the diffractometer  $\delta$ -arm (see Figure 25). Therefore the design of the optics table should take into account the design of the diffractometer. The height of the table should allow enough clearing for the stacks of motions underneath the individual optical elements. A table height of 900-1000mm is currently anticipated. The surface of the table will be breadboard to provide a maximum flexibility for mounting elements to it. The load capacity of the table should take into account all possible configurations of local optics and should also be able to accommodate possible future upgrades like e.g. a two-crystal tilt stage for reflectivity on liquids. Analyses of the resonance frequencies of the empty table as well as of the table with different configurations of beam conditioning optics should be performed in order to avoid picking up floor vibrations.

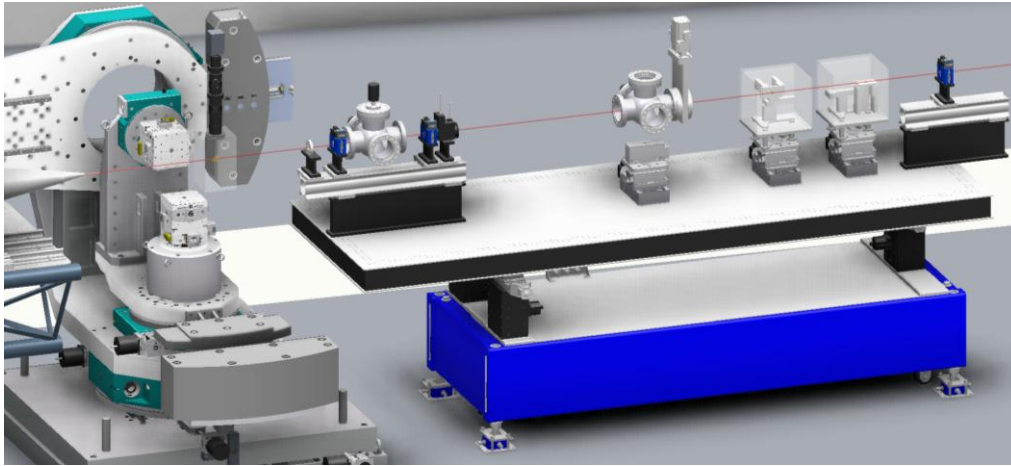


Figure 25. Optical table with local optics and sample diffractometer.

Table 16. Specifications for the motorized axes of the optics table.

Axis	motorized	Encoder	resolution	bi-directional repeatability	travel range
X	y	Y	<0.5 $\mu$ m	<4 $\mu$ m	$\pm$ 25mm
Y	y	Y	<0.5 $\mu$ m	<4 $\mu$ m	$\pm$ 25mm
Z	-	-	-	-	-
pitch/ $\theta$	y	Y	<0.001 $^\circ$	<0.002 $^\circ$	$\pm$ 5 $^\circ$
yaw/ $\phi$	y	Y	<0.001 $^\circ$	<0.002 $^\circ$	$\pm$ 5 $^\circ$
roll/ $\chi$	-	-	-	-	-

### Precision Slits

Precision slits (horizontal and vertical) will be used to define/clean the beam before the kinoform lenses. It is assumed at this stage that the heat load on the slit blades will be in both the monochromatic and the pink beam operation sufficiently low to not require additional cooling. 10 mm aperture size would be sufficient, as the optics table will follow the beam offsets from DCM and DMM and thus the beam will always pass approximately in the center of the slit aperture. The slit blades could be independently motorized or coupled to move as ‘gap’ and ‘center’. The blades should be well polished to avoid unnecessary scattering. As the beam will be still rather large at the slit position, a moderate precision/repeatability of about 1  $\mu$ m will be sufficient. The slits need to be vacuum compatible to  $1 \times 10^{-6}$  mbar or better

### Local Focusing Optics

The local focusing optics in the EH will be used to provide focal spots down to 1 $\mu$ m at the sample. In the current design, this focusing will be achieved by silicon kinoform refractive lenses, which provide 1d focusing in either vertical or horizontal direction. For a maximum flexibility and to achieve a  $1 \times 1 \mu\text{m}^2$  beam at the sample position, two sets of lenses will be combined. Like for the beryllium lenses in the FOE, it is assumed at this stage that the kinoform lenses do not need to be cooled in monochromatic and pink beam. The lenses are chromatic refractive optics, therefore several sets will be needed to cover the energy range of the CHX beamline. Typically, several sets of lenses (see Figure 26 a) are etched in the same silicon chip. The chip is about 10mm wide and the separation between lenses is about 0.5-1mm. It is assumed that one chip will contain enough lenses to cover the desired energy range, however, if needed; several chips could be stacked within a holder. To ease the rough alignment, the lens holder might have a fluorescent coating and the lens chambers might feature correspondingly a view port. The stack of motorized axes which is needed to align the lens is sketched in Figure 26 b. The angular alignment of the lens needs to be precise to about 0.002 $^\circ$  and highly stable. In order to not have the goniometers to force against the vacuum bellows and thereby spoil the precision, they could be moved inside the vacuum chamber. The top translation is used to move the lens into the center of the  $\phi$ -rotation. For the horizontal focusing unit, this translation

will also provide the switching from one lens to another. The x-translation below the vacuum chamber is needed to align the rotation axis of the goniometer with the beam, while the y-translation is needed for height adjustment. Moreover, for the vertical focusing unit the y-translation also provides the lens selection. The precision and travel ranges for the motorized stages for the lens alignment are summarized in Table 17. The lens chambers, mountings and in-vacuum translations/rotations need to be vacuum compatible to  $1 \times 10^{-6}$  mbar or better.

Table 17 Specifications for the motorized axes to align the kinoform lenses.

Axis	motorized	encoder	resolution	bi-directional repeatability	Stability	travel range
X	Y	y	<0.2 $\mu$ m	<.2 $\mu$ m	<0.1 $\mu$ m	$\pm$ 10mm
Y	Y	y	<0.2 $\mu$ m	<0.2 $\mu$ m	<0.1 $\mu$ m	$\pm$ 15mm
pitch/ $\theta^*$	Y	y	<0.001 $^\circ$	<0.002 $^\circ$	<0.00005 $^\circ$	$\pm$ 5 $^\circ$
yaw/ $\phi^*$	Y	y	<0.001 $^\circ$	<0.002 $^\circ$	<0.00005 $^\circ$	$\pm$ 5 $^\circ$
roll/ $\chi^*$	Y	y	<0.001 $^\circ$	<0.002 $^\circ$	<0.00005 $^\circ$	$\pm$ 5 $^\circ$
X1*	Y	y	<0.2 $\mu$ m	<0.2 $\mu$ m	<0.1 $\mu$ m	$\geq \pm$ 6mm

\*1 possibly in-vacuum motion

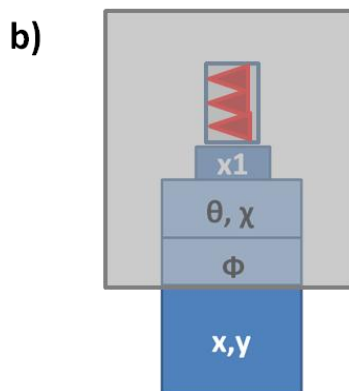
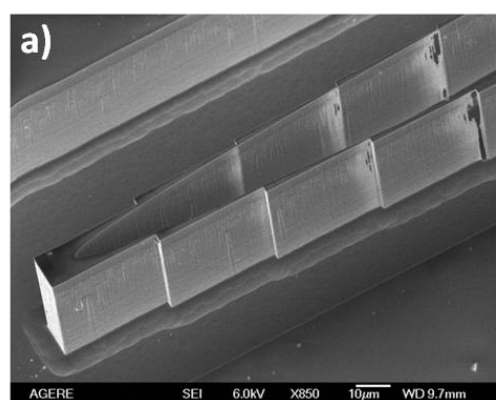


Figure 26.

a) kinoform lens etched into a silicon chip.

b) stack of positioners to align the kinoform lenses for vertical focusing.

## Local Mirror

A mirror located on the optics table (see 0) in the EH will be used to deflect the beam downwards for scattering experiments from liquid surfaces in grazing incidence geometries (GISAXS, GIXD). For other experiments the mirror will be translated out of the beam along the y-direction. The most important subphase in the domain of soft matter systems is water and other organic liquids like oils or solvents with similar electron density. For these liquids, incident angles up to their critical angle of total external reflection ( $\alpha_c$ ) can be easily achieved by a bare silicon mirror (see Figure 27 a). However, if liquid metals (e.g. Hg) are studied, a mirror material like e.g. Pd is needed to approach incident angles close to the critical angle of the liquid metal. The mirror may therefore consist of a bare Si and a Pd stripe. With stripe widths of 15 mm each, the mirror is anticipated to be about 30-40mm wide. A fix aperture on the mirror mounting would give an easy reference for the stripe selection by one transverse scan of the mirror. With a distance of 1m between the mirror and the sample stage, the maximum incident angle of 1.2 $^\circ$  results in a vertical offset of about 20mm at the sample position which needs to be compensated by the corresponding movement of the diffractometer. The length of the mirror is determined by the vertical size of the incident beam and the smallest angle that should be reached on the sample surface. For an incident beam of 16keV with a vertical height of 50 $\mu$ m, the beam footprint on the mirror becomes  $\sim$ 100 mm for 75%  $\alpha_c$  of water, so a mirror length of about 150mm seems to be largely sufficient. The specifications of this mirror in terms of roughness and slope error should be similar to the ones of the horizontal mirror in the FOE. As the vertically deflecting mirror is operated in monochromatic/pink beam, it is assumed to achieve the required performance without additional cooling.

The main axes needed for the mirror alignment (see Figure 27 b) are Y (mirror height), X (stripe selection), pitch (mirror angle) and roll. A misalignment in the yaw of the mirror would affect the effective width of the reflecting

stripe. However, a misalignment of 1mrad reduces the effective stripe width by only 1%, so that a pre-alignment of the mirror is sufficient. A misalignment in the roll of the mirror would result in an unwanted horizontal deflection of the beam, the resulting horizontal offset could become quite large due to the large sample-detector distance. In order to keep the horizontal offset below 0.5 mm for the largest sample-detector distance (15 m), the roll of the mirror needs to be aligned within  $33 \mu\text{rad}$  ( $0.002^\circ$ ). This makes it desirable to have the roll of the mirror motorized. For a mirror width of 40 mm, a misalignment of  $33 \mu\text{rad}$  results in a difference of about  $1.5 \mu\text{m}$ , which would be detectable in a mirror height scan. While the X-translation has very moderate requirements for resolution and repeatability, straightness and wobble of the stage must be small enough to not influence Y, pitch and roll of the mirror. The main mirror axis Y and pitch should be encoded to enable precise and reproducible alignment. The stability requirements for the mirror are the following: 1) the beam shouldn't move by more than a fraction ( $10 \mu\text{m}$ ) of a detector pixel at 15 m downstream from the sample 2) the guard slit is for surface scattering experiments usually aligned within  $1 \mu\text{m}$  and the mirror stability should not spoil this alignment 3) the footprint on the sample surface could be as short as 1mm and shouldn't move by more than 10%. The most stringent ones out of these three requirements is listed as the required stability in Table 18. The mirror chamber, mirror and mountings need to be vacuum compatible to  $1 \times 10^{-6}$  mbar or better.

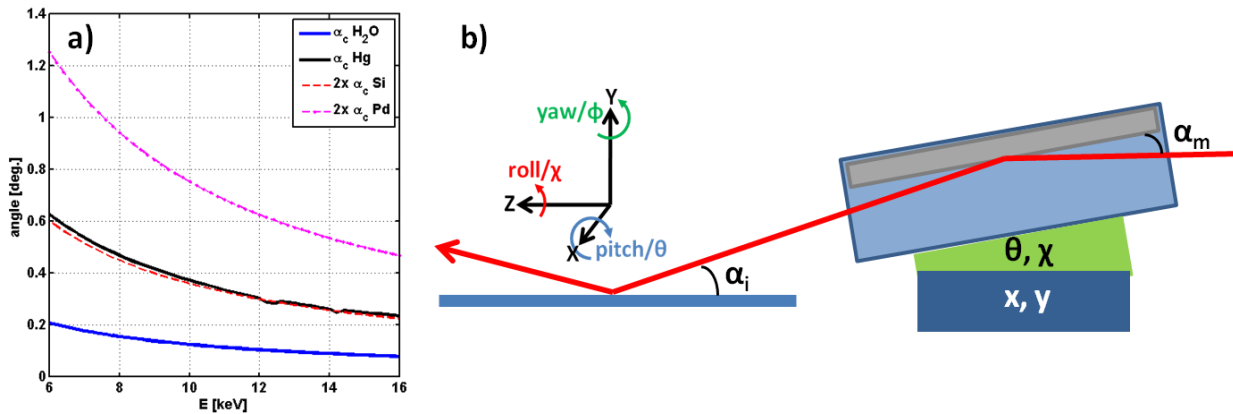


Figure 27. a) critical angle  $\alpha_c$  for total external reflection for water and Hg as well as the maximum incident angle of on the liquid surface achievable with a bare Si and a Pd coated mirror b) geometry and definition of axis for the vertically deflecting mirror, in this geometry  $\alpha_c=2 \alpha_m$  holds.

Table 18. Specifications for the motorized axes of the vertically deflecting mirror.

axis	motorized	encoder	resolution	repeatability	stability	travel range
X	y	o	$<10 \mu\text{m}$	$<10 \mu\text{m}$	$<0.1 \mu\text{m}$	$\pm 25 \text{mm}$
Y	y	y	$<0.1 \mu\text{m}$	$<0.1 \mu\text{m}$	$<0.1 \mu\text{m}$	$\pm 10 \text{mm}$
pitch/ $\theta$	y	y	$<0.0001$	$<0.0001$	$<0.00002$	$\pm 5^\circ$
roll/ $\chi$	y	o	$0.001^\circ$	$0.001^\circ$	$<0.00004^\circ$	$\pm 2^\circ$

### Beam Defining and Guard Slits

The two sets of beam defining slits and guard slits (both horizontal and vertical) have some stringent requirements in terms of precision and repeatability. The first set of slits will be used as beam defining aperture ('pinhole') when the desired beam size /coherence length at the sample position cannot be achieved by focusing optics alone. Highly polished blades are indispensable as stray scattering will be difficult to clean up and will eventually pollute the scattering pattern. The form of the slit blades (e.g. knife edge or roller blade) should be also evaluated in order to achieve the cleanest beam. Special attention should be drawn to a parallel alignment of the opposing slit blades as

to facilitate the guard slit alignment. The beam defining slits will use apertures as small as  $1 \times 1 \mu\text{m}^2$ , so the precision and bi-directional repeatability should be  $<0.2 \mu\text{m}$ . A  $10 \times 10 \text{ mm}^2$  maximum aperture will be sufficient for both beam defining and guard slit. While the beam defining slit could consist of coupled blades (moving as ‘gap’ and ‘offset’), the guard slit must consist of four individually motorized blades to enable the optimization of individual blade positions with respect to the beam. The blades of the guard slits need to be aligned in the minima of the Fraunhofer pattern created by the beam defining slit. In particular for larger beams ( $>20 \times 20 \mu\text{m}^2$ ) the width of the fringes becomes so small that a precise alignment of the guard slit blades requires a high precision ( $<0.1 \mu\text{m}$ ) and high repeatability ( $<0.2 \mu\text{m}$ ). The blades of this slit set will most likely be knife edges. A recent slit design features ‘semi transparent’ slit blades, which could be used for the beam defining slits, in order to mitigate the creation of the Fraunhofer pattern and create a beam with steep flanks instead. However, the effect of these ‘semi-transparent’ slit blades varies with energy and moreover, these blades might act as phase objects and create unwanted features in the far field. The slits will be clamped on a rail (e.g. X95) fixed to the optics table, serving as an ‘optics bench’. This setup enables a very easy adjustment of the distance between beam defining and guard slit and allows moreover to approach the guard slit as close to the sample as possible. Both sets of slits need to be vacuum compatible to  $1 \times 10^{-6}$  mbar or better.

### Beam Positioning Monitor and Diagnostics

A quadrant beam positioning monitor (QBPM) will be mounted just before the beam defining slit to monitor the positional stability of the incoming X-ray beam with a resolution of about  $1 \mu\text{m}$ . The signal rate from this QBPM will be fast enough to detect any instability in the beam due to vibrations of optical elements and could serve as a feedback sensor. However, in normal operation it is assumed that the QBPM will be retracted by a pneumatic actuator so that no scattering foil is hit by the incident beam. After the beam defining slit, a pin diode on a pneumatic actuator can be inserted into the beam to align the local beam conditioning optics such as kinoform lenses, the vertical deflecting mirror, etc. Ideally this pin diode would be calibrated so it would enable to quantify the photon flux after the beam defining slit. The pin diode will be mounted on a beam stop that safely blocks the beam when the diode is inserted in to the beam path, so that sample and downstream detectors are protected during the alignment of optical elements. It should be evaluated if a BPM with a thin high quality diamond window could stay permanently in the beam without spoiling the coherence. Such a device could serve as a monitor counter for the incoming intensity and give permanent feedback of the beam position. Both the QBPM and the pin diode need to have a sufficient dynamic range to cope with the monochromatic and the pink beam intensity and need to be vacuum compatible to  $1 \times 10^{-6}$  mbar or better.

### Diffractometer

The diffractometer will be used for WAXS and GIXD experiments, where large Q-values in reciprocal space need to be accessed. It will provide both vertical and horizontal scattering geometries. While the first one avoids losses at

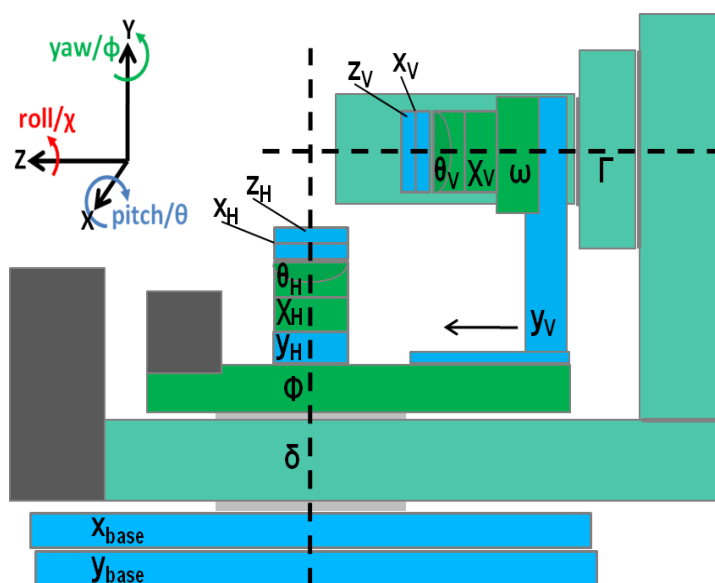


Figure 28. Sketch of the diffractometer with horizontal and vertical scattering geometry

large scattering due to the polarization of the X-ray beam, the latter one is needed for the study of liquid surfaces. The horizontal sample stage of the diffractometer will also be used for SAXS studies, where the detector will be located on the SAXS table (see Figure 29). In order to follow the vertical and horizontal offsets of DCM and DMM and to keep the common center of detector and sample rotations aligned with the X-ray beam, the base of the diffractometer needs x- and y-translations. The detector circle consists of horizontal and vertical rotations to support both scattering geometries. The length of the detector arm will be about 1.5m and should be optimized for a high load capacity to support potentially heavy 2d detectors. The horizontal sample stage can be a high load capacity stage for heavy (e.g. up to  $>50\text{kg}$ ) and bulky sample environments. It will consist of  $\phi$ -rotation, y-translation,  $\chi$ - and  $\theta$ -arc

motions and x,z translations. The vertical sample stage will feature the same translations and arc-motions, with a lower load capacity. The goal would be to use this stage e.g. with a small cryo-furnace. However, the maximum load in the vertical geometry will depend strongly on the length of the lever arm. For the sample stages, a typical precision and repeatability of 0.1 $\mu$ m is envisioned, corresponding to one tenth of the smallest X-ray beam size which will be routinely used at the CHX beamline. For the sample and detector rotations the envisioned precision and repeatability are 0.05 mdeg. Preferably all stages of the diffractometer will feature encoders. A sketch of the diffractometer is shown in Figure 28. The detailed design of the customized solution will be provided by the vendor and it is assumed that this item will be purchased as a turn-key element.

## SAXS Table

The SAXS table will be located downstream of the sample position and support the flight tube, a beamstop box and a multi-detector bench. Its design follows instrument at CHEM-MAT-CARS APS beamline and at the SAXS/WAXS beamline at the Australian synchrotron. The maximum sample-detector distance will be about 15m in order to resolve speckles with a detector pixel size of about 80 $\mu$ m. The base of the table will be made of a steel frame structure on four pairs of legs (see a)). The legs will allow some height adjustment as the difference between the direct and the reflected beam will be up to about 100mm in grazing incidence geometry ( $\alpha_i=0.2^\circ$ ). A mechanical coupling between the individual legs will provide the necessary stability for this movement. The legs of the table will sit on air pads, which enable to move it downstream by 2m so that the diffractometer can operate without restrictions in wide angle experiments. The table will be guided by a rail in the floor in order to preserve its angular alignment with the X-ray beam. Moreover, the air pad will also allow introducing a coarse tilt angle of up to  $\sim 3.8^\circ$  (obtained by translating outboard the downstream end of the 15 m SAXS table by  $\sim 1$  m) so that larger scattering angles become accessible. A second system of floor mounted rails will provide the required guiding for the motion of the SAXS table towards larger scattering vectors. The top of the steel frame will be covered by breadboard to which a rail system will be mounted. Two sets of rails will run parallel to each other. While the first supports the nozzle of the SAXS flightpath, the beamstop box and the detector bench, the second one supports the flight tube sections, which can be manually flipped to overhang the first rail and become part of the flight path. All elements which move on the rails should be lockable at any position. A selection of beam pipe sections of 4m (3x), 2m and 1m which can be joined by flanges will allow flexible flight path length from 1-15m. The accessible Q-range with such a configuration and a 1500x1500 pixel detector (80x80 $\mu$ m<sup>2</sup> pixel size, possible gaps between individual modules are not taken into account) is shown in b). The minimum diameter for the flight tube would be 170mm, however, at least 400mm should be chosen to easily offset the detector (in order to cover a larger Q-range at the cost of sacrificing  $2\pi$  coverage of the scattering pattern) and to have some margin for larger detectors which might become available in the future. The first element in the beam path will be the a box to which the nozzle is attached (see c)). Different nozzles will be fabricated, according to the needs of the individual experiment. These nozzles could interface directly to the vacuum of a sample chamber on the goniometer of the diffractometer. However, due to the large polyimide exit window of the flight path, the vacuum in the flight tube will likely be in the 10<sup>-3</sup>mbar range, insufficient for sample environments like LN<sub>2</sub> cooled sample chambers. Therefore, in the standard configuration the nozzles might start from a silicon nitride membrane as an entrance window to the SAXS flightpath. Because of the fragility of a thin silicon nitrate membrane, this entrance window needs to be small, hence a manual translations to adjust it with the incoming beam will be indispensable. The nozzle box will feature a retractable photodiode or APD, serving as a transmission detector. In addition, a moveable beamstop is needed in the nozzle box to stop the direct beam hitting the flight tube wall when the SAXS table is tilted with respect to the incident beam. The downstream side of the box will interface to the flight tube. A similar box will house a selection of beamstops, which can be inserted and retracted by pneumatic actuators (see d)). The actuators will have limits to provide feedback about their actual position. In addition, these beamstops can be aligned in x- and y-directions. Depending on the size of the beamstops, they could feature photodiodes which would allow monitoring the intensity transmitted through the sample during the measurements. The detector bench will accommodate the fast 2d detector and an APD or APD array. The APD detector will use high precision slits similar to the ones used as pre-detector slits. Both detectors will share a common x-translation, which will also allow switching between the detectors, and individual z-translations. A summary of the translations, their travel range and precision is given in Table 19. In general, the required alignment precision is given by the pixel size of the 2d detector so typically a precision and repeatability in the micrometer range will be sufficient.

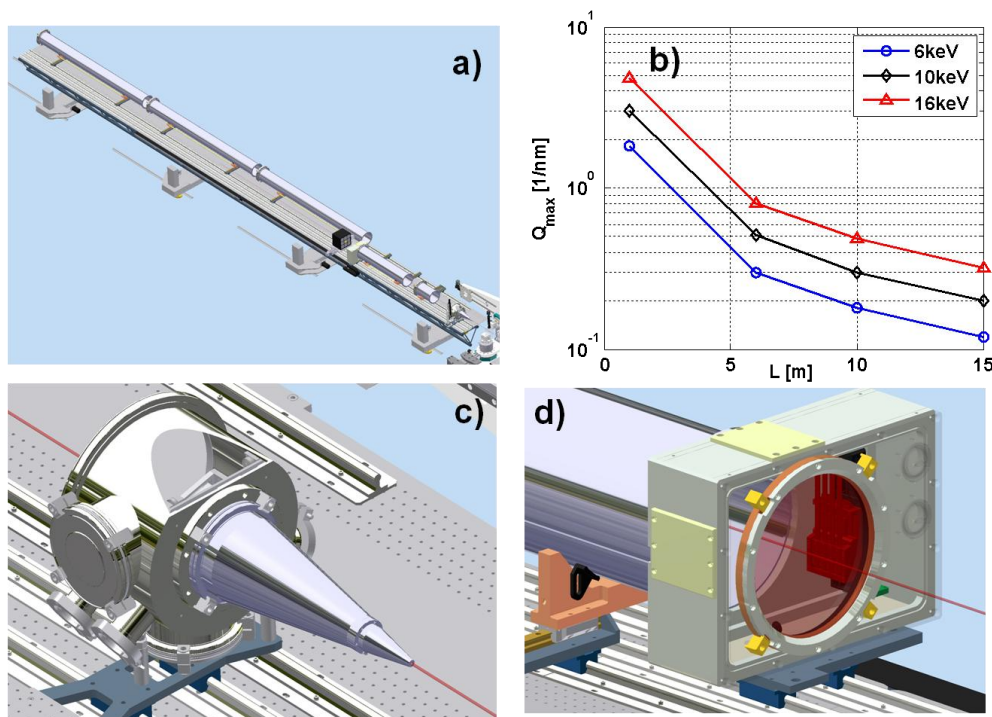


Figure 29. a) SAXS table with sectioned flight path in the CHX endstation. b) maximum Q-range covered ( $2\pi$  coverage) as a function of energy and length of the light path. c) box with beamstop nozzle. d) beamstop box with large exit window.

Table 19. Specification for the motorized stages on the SAXS table. The travel range for each individual beamstop is  $\pm 50\text{mm}$  around the center position, if the entire set of beamstops moves together, the travel range of the corresponding translation needs to be larger.

Axis	Motorized	encoder	resolution	repeatability	travel range
Y SAXS table	Y	o	$<5\mu\text{m}$	$<20\mu\text{m}$	$\pm 50\text{mm}$
X,Y beamstops	Y	o	$<2\mu\text{m}$	$<5\mu\text{m}$	$\pm 50\text{mm}^*$ )
X detector	Y	o	$<1\mu\text{m}$	$<2\mu\text{m}$	$>\pm 200\text{mm}$
Y 2d detector	Y	o	$<1\mu\text{m}$	$<2\mu\text{m}$	$>\pm 60\text{mm}$
Y 0d detector	Y	o	$<0.5\mu\text{m}$	$<1\mu\text{m}$	$>\pm 60\text{mm}$

## Sample Environments

XPCS is a relatively young technique, with applications to a wide field of research, from hard materials to soft matter or biological samples. Experiments are performed in a variety of bulk and surface scattering geometries, and it is therefore impossible to design a generic sample environment for the CHX beamline which would satisfy the needs of virtually all users and experiments. The sample environments described below will provide a selection of possibilities, which is supposed to serve a fairly large user community. This selection is, however, not exhaustive and a continuous development of sample environments and sample handling capabilities will certainly be required at the CHX beamline, an hopefully supported by the operation budget.

### On-axis Microscope

The optical on-axis microscope (OAV) will be designed to be compatible with as many sample environments and experiments as possible. It will be designed to look at the sample position along the direction of the X-ray beam. Therefore, the same spot in the sample which is hit by the X-rays can be optically inspected. A selection of functionality for the sample alignment and data acquisition, which comes with the OAV, is given in section 0. In combination with a fluorescent screen, it will also be an excellent tool for beam diagnostics. The OAV will mount to the vertical or horizontal sample stage of the diffractometer to image the sample mounted on the horizontal or vertical stage, respectively. The advantages of using one of the diffractometer sample stages for the microscope are the excellent stability of the mounting, the proximity to the sample position (enabling the use of optics with shorter focal distance and better resolution) and availability of all motorized axes needed to align the OAV with the beam (x, y, pitch, yaw). The OAV consists of a motorized zoom lens which is mounted to a 45° deflecting mirror with a hole (~Ø 1.5mm) to let the X-ray beam pass onto the sample. Contrary to existing OAVs, the microscope for the CHX beamline should be vacuum compatible. A possible design would consist of a deflecting mirror in a vacuum pipe to which the zoom lens mounts via a viewport (see Figure 30 a). The image will be transmitted by a high resolution Ethernet camera. Apart from the drilled reflecting mirror in a vacuum compatible environment, the OAV can be build from standard components used in machine vision applications. In general, there is a trade-off between the achievable focal distance and the resolution. The focal distance needs to be large enough to accommodate flexible bellows between the OAV and the sample chamber, in order to move the sample independently of the OAV. The preliminary specifications for the OAV feature a focal distance of 86 mm and a resolution of ~1.7µm. Optional, the OAV could be with a corresponding filter and illumination for fluorescent imaging, e.g. for visualizing flow in a micro-channel or identifying labeled bio-tissue in a CDI experiment.

### Cryo-Furnace

A vacuum isolated cryo-furnace based on a LN<sub>2</sub> cold finger will be used to investigate samples like colloidal suspensions in capillaries, deposited films on Si wafers, etc. Different sample holders will be attachable to the cold finger to use the cryo-furnace for a variety of samples. An interface to the OAV (see 0) will enable in-situ visualization of the samples. Internal guard slits formed by metal corners on micro motors will also hold a fluorescent screen for beam diagnostics without the need to remove the sample (see Figure 30 b). The chamber will provide feedthroughs for fiber optics for sample illumination, UV to trigger sample reactions, etc. Nitrogen flow and heater power should be remotely adjustable via the beamline control system. The anticipated temperature range for this sample environment is 100-500K, with a temperature stability of <±0.005K. The design will need to address the requirement of excellent stability, i.e. vibrations from the cold finger should not be transmitted to the sample.

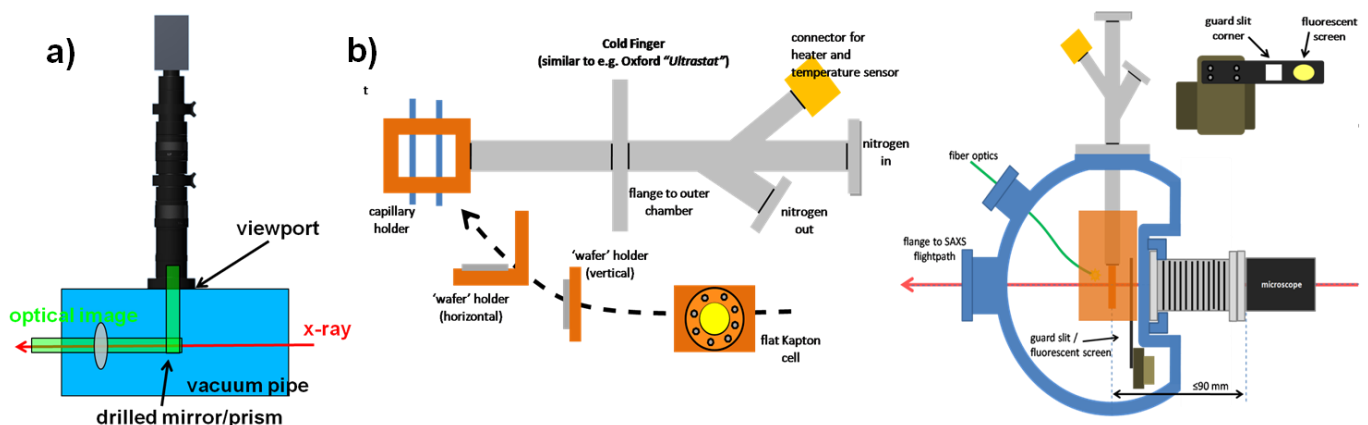


Figure 30. a) vacuum compatible on-axis microscope. b) conceptual design of a temperature controlled chamber for SAXS studies.

### Microfluidic Flowcell environments

One of the most common problems associated with the use of bright x-ray beams is beam-induced radiation damage, and this is likely to become an even more limiting factor at future synchrotron and free-electron laser sources. Flowing the sample during data acquisition is one of the simplest methods allowing the radiation damage to be limited. In addition to distributing the dose over many different scatterers, the method also enables new functionalities such as time-resolved studies. An experimental technique that combines XPCS and continuously flowing samples (A.Fluerasu et al., *New Journal of Phys.* **12** 035023, 2010) was recently developed, and this will allow many experiments that were not possible before. For this reason, a number of microfluidic sample environments will be developed for operation at the CHX beamline (see Figure 31 a).

### Liquid Surface Chamber

For grazing incidence experiments at liquid surfaces, like e.g. studies of dynamics of ordering phenomena, a temperature controlled chamber (chiller and peltier cooler/heater) housing exchangeable trough ( $\varnothing$ 100-150mm) will be available (see Figure 31b). The double chamber will provide a helium atmosphere above the sample in the inner chamber and an insulation vacuum (whenever necessary for high or low temperature studies) between the inner and the outer chamber. Such a sample chamber could cover a temperature range of  $-50$ - $70^{\circ}\text{C}$  with a stability of  $<\pm 0.005\text{K}$ .

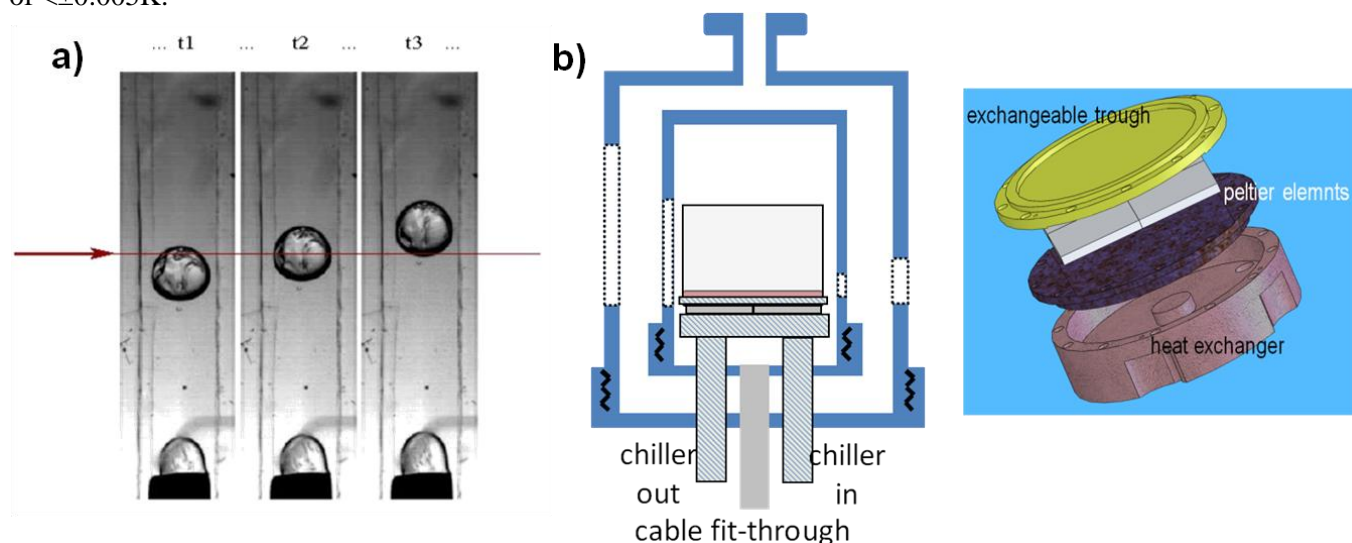


Figure 31. a) Flow cell producing a stream of droplets. b) Conceptual design of a liquid sample chamber.

### Detectors

A fast 2D photon-counting area detector is the single most important piece of equipment that will be required at the CHX beamline. Unfortunately, at least for the moment, there is no commercial instrument meeting the specific requirements for XPCS experiments: 2D pixelated detector (e.g. 1k x1k pixels), fast readout ( $<10\ \mu\text{s}$  full frame), small pixel size ( $<100\ \mu\text{m}$ ), single photon sensitivity. To date, the two best instruments in this category are the Pilatus detector (Dectris) and the Medipix (Medipix Collaboration). The Medipix detector was already successfully used in XPCS experiment and enabled results that would have not been possible otherwise (e.g., Chiara Caronna et al. *Phys. Rev. Lett* **100**, 055702, 2008). Unfortunately, the Medipix is not a commercial device and it is not clear if it will become one. More importantly, even if NSLS-II joined the Medipix project (which would perhaps be something advisable) the current maximum full frame readout rate – 1 kHz – is not sufficient for some of the experiments planned at NSLS-II. The Pilatus Detector has the advantage of being commercially available but for the moment is clearly unsuitable for our purpose, as it is lagging behind in terms of performance for XPCS applications (slow readout speed, large pixel size).

The best alternative for the CHX beamline is a XPCS detector that is currently being developed in a R&D collaboration between the BNL Detector Development Group and Fermi National Laboratory (D.P. Siddons, private

## Preliminary Design Report for the Coherent Hard X-ray (CHX) Beamline at NSLS-II

communication). The so-called Vertically Integrated Pixel Imaging Chip (VIPIC) detector consists in a detector chip bonded to a stack of signal processing "layers" using a "3D integration technology". A first prototype chip, with the main characteristics described in Table 20, is currently being fabricated and will be connected to a data acquisition controller designed in collaboration with the NSLS-II Controls group. The whole system could be ready for a test experiment as early as the first quarter of 2011.

Due to the intrinsically long times required to advance with a chip design and fabrication, a second generation VIPIC detector, the "VIPIC-2" is already being planned. Most importantly, this chip will enhance the time resolution to 10 ns.

It is our firm belief that the development of fast 2d detectors like the VIPIC should be a top priority the NSLS-II facility. Without a suitable detector the CHX beamline will simply not be able to reach its full potential. This idea is also fully supported by the CHX BAT team as is transparent for their most recent report:

*"The availability of a suitable detector remains centrally important if the CHX beamline is to reach its potential. The BAT was encouraged by the report it received from Peter Siddons on his group's efforts in this regard. We advise NSLS-II to take a proactive stance in advocating for continued support for such detector development programs"*

A very interesting option for a fast 2d detector for the CHX beamline is the Eiger system, currently developed at the PSI (Swiss light source). The first modules (256x256 pixels) have been tested successfully at PSI. Dectris will commercialize this detector, like they did with the Pilatus. It is anticipated that first multi-module detectors will be available by 2012 (C. Brönnimann, private communication). The Eiger is a hybrid detector with 75  $\mu\text{m}$  pixel size and variable counter depth that reaches frames rates of up to 24 kHz.

Fast point-like detectors to be used in conjunction with a hardware correlator will still be required for a certain class of experiment for which the dynamics time scales are typically on the order of 1  $\mu\text{s}$  or faster. The clearest example of such class of applications is that of capillary waves at liquid surfaces. The time scales involved in a vast majority of such experiments will likely remain too fast for the next generation of detectors like the "VIPIC" detector. These phenomena will be best studied using a linear array of Avalanche Photon Diode (APD) detectors.

Other detectors of interest that will need to be available at the CHX beamline include:

### CCD Detector

A "standard" CCD detector with small pixel size (<30 $\mu\text{m}$ ) will be used for CDI experiments and/or certain static studies (e.g., SAXS, studies of kinetics via time-resolved SAXS or WAXS, etc.)

Table 20. Main characteristics of the first prototype of the XPCS VIPIC detector

Pixel size	80 $\mu\text{m}$
Number of pixels	64 x 64
Active area	5120 x 5120 $\text{mm}^2$
Chip size	5.5 x 6.3 $\text{mm}^2$
Operation:	Will provide dead timeless readout: each pixels is read sequentially by 2 5-bit counters Noise well below 1 photon level (~100 electrons vs. ~2200 electrons generated by a 8keV photon) Data sparsification will be provided on chip - only the detectors that had a hit will be read. Max readout speed 10 $\mu\text{s}$ , limited by the estimated max count rate ~0.5 photons / pixel / 10 $\mu\text{s}$ . Readout consists in pixel address, time no. of hits (no energy info).

## 4 INFRASTRUCTURE FOR BEAMLINE AND USER SUPPORT

### Beamline Control and Data management

#### Controls Hardware

The backbone of the motion control hardware will be the generic NSLSII 8 axes motion controller currently under evaluation by the controls group. Standardization -wherever possible- to this motion controller has obvious advantages in terms of maintenance and management of spare parts throughout the entire facility. Motors at the CHX beamline will be mainly (2 phase) stepper motors, which will be compatible with the generic motion controller. Vendors will be given an incentive to use the generic motion controller for their systems (e.g. monochromator). The motion controllers are housed in water cooled Racks on FOE and ES and can be fully remotely configured, so that no access to the roof is necessary to install a motor at the beamline. The cable bundle for each axis contains the motor driving signals and power, end/limit/home switches and encoder. Wherever appropriate, the cables from the motion controllers will not directly connect to the equipment, but go through a patch panel (or other form of a fix point) in order not to force on sensitive stages. The motion controllers connect to the controls network by a rack mounted IOC and will likely allow coordinated motions of motors connected to different motor control boxes (via a dedicated link). Water cooled high heat load element will be equipped with water flow and temperature sensors which will directly connect to the equipment protection system (EPS), which can trigger an automatic closure of the safety shutter to prevent damage in the event of a cooling failure. Similar, the cryo-cooler controller of the nitrogen cooled monochromator will not only communicate to the controls system, but alarms will be directly fed into the EPS to avoid damage in the case of a failure. The diffractometer in the ES will feature proximity sensors connected to the corresponding motion controllers, in order to avoid collisions with other equipment. Retractable elements like e.g. fluorescent screens will be driven by pneumatic actuators and should always feature limits so that their actual position can be verified. Optical cameras looking e.g. at fluorescent screens will be preferably Ethernet cameras which could directly connect to the network. The ES will have a patch panel in the proximity of the sample stage, providing 15 axes of motion control, connection to a generic PID controller for sample environments, connections for serial, Ethernet and coax cables which go outside the hutch. The temperature controller will be also housed in a rack on the ES. Detectors like APDs or pin diodes are assumed to have their dedicated electronics, which will be housed in the standard racks and connected to the network via IOCs. The more complex case of fast 2d detectors will be discussed in more details further below in the Fast 2d Detectors: Data Readout and Storage section (Pag. 46). A timing signal, synchronized to the RF system of the storage ring, will be available in a VME crate and can be used to trigger acquisitions on individual bunches. The vacuum elements at the CHX beamline which will be integrated in the controls system are ion pumps, gate valves, and vacuum gauges. Ion pumps and vacuum gauges will be wired to their respective controllers, housed in a vacuum-dedicated rack on the FOE and connect from there via OIC to the network. Alarms from an ion pump controller or vacuum gauge are directly monitored by the EPS, which will trigger closing of safety shutter and gate valves in case of a vacuum failure. The preliminary controls layout for the CHX beamline is shown in Figure 43-  
Figure 46

#### Motion Control System

The choice of a generic control and data acquisition system for the future NSLSII beamlines is currently under evaluation, with the goal to achieve wide standardization and correspondingly excellent support for the beamlines. The CHX beamline would be preferably controlled by a command line based control system (CS) (similar to e.g. SPEC) which can co-exist with GUIs for some specific applications. The general controls, data acquisition and storage layout is sketched in Figure 32. The basic low level device control is done by EPICS. A unification layer on top provides a common configuration tool for all devices (motors, counters, detectors, etc.) and serves as a device pool, where all devices of the beamline are configured. The device pool should also include all relevant counters like e.g. counts from point detectors, integrated intensities of ROIs from 2d detectors, BPM positions, temperatures, vacuum gauges, sample environment parameters. It should be possible from this pool to define sub-sessions in the CS, which contain only the motions and counters relevant for a given experiment. This will greatly facilitate the beamline operation for the users and avoid accidental movement of optical elements or even IDs. The IRMIS database, which will be adapted from the accelerator, could be a good alternative to this unification layer. The

database would not only be able to store all configurations of currently connected equipment as configuration snapshots, but would moreover provide links to configuration files for e.g. temperature controller or motor controller settings, which could be restored manually or using another application which would need to be developed. Moreover, the database would also handle the maintenance planning for installed and on-the-shelf equipment. The layer on top of the unification layer serves as CS, allows the calculation of pseudo-motors and counters, the definition of sequences/scans and high-level user macros (scripting). This approach provides an easy way to define new user macros/sequences as a large number of quite different experiments is anticipated for the CHX beamline, requiring a certain flexibility and easy development of the CS. For instance, certain experiments require a sequence where a number of images is required in a scan, then the sample is removed from the beam and the scan is run again to acquire the background signal. Such sequences are typically refined during the experiment and need thus to be defined at a high-level in the CS. This layer should ideally use iPython as it will allow an easy interface to the data processing/analysis software which is likely to be based on Python. In addition, the mathematical power of *numpy* would be available in the control system, allowing for instance to easily implement even complicated fitting procedures in the alignment scans and data acquisition sequences. The functionality which is expected from the CS comprises (non-complete): absolute and relative movements of multiple motors in both user and dial units; soft limits; predefining groups of motors and saving of their positions to later move all motors back to their saved position; software lock (disabling) of motors; relative and absolute scans of multiple motors; fast shutter control (set shutter time due to finite opening speed, switch between single image and sequence mode, set which detector is triggering the shutter or set it permanently open/closed); integration of attenuators, integration of hardware correlator and sample environment controllers; integration of all detectors and setting of their main parameters; history function, etc.

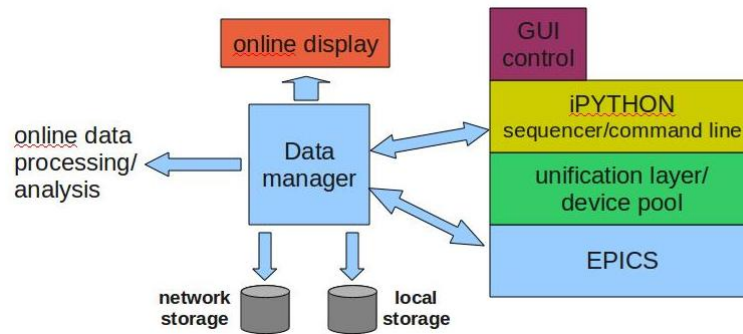


Figure 32. Schematic of the beamline control, data management and data processing.

### GUIs and Data Acquisition

A GUI is in particular envisioned for the on-axis microscope, which will not only allow sample visualization, but also sample alignment and setup of scans. The functionality provided by this GUI comprises: display position of direct beam (with florescent screen); zoom with auto-adjustment of camera gain and exposure for constant illumination; real space measurements in absolute units; display motor range and position; click on object to move it into the beam; graphical selection of scan region; semi-automatic centering of rotation axis ('3-click'); illumination control; snapshot and movie function; auto-focus;... Many of these functional GUI building blocks (so-called 'bricks') have been developed at the ESRF based on Python and are available to other facilities upon request. GUIs can be also used to setup the acquisitions for the various detectors. In this case it is necessary to set detector parameters like e.g. gain; acquisition parameters like exposure time, time between images, number of images; data storage information like path and file names; shutter control parameters like single frame or series mode;... These GUIs should also allow to select files with additional information (like e.g. flat field files) to enable direct saving to pre-processed data files. Ultimately, during the acquisition the information necessary to process the data directly is passed from the CS to the online correlation program (see 0). This metadata would include data path and file names, position of the direct beam (automatically acquired and found via a fast 2d fitting routine), X-ray energy, motor positions... The CS would also provide a link to the detector device for the processing software to monitor the status of the acquisition (e.g. current frame acquired, scan aborted, etc.) The envisioned maximum

frame rates of the (2M) 2d detectors reach 100kHz, thus fast writing of files and accompanying information (like e.g. monitor counts, BPM information, etc.) are a necessity. To allow for a maximum flexibility in the data acquisition, it will be indispensable to have all detectors not only controlled by GUIs, but also integrated in the CS for the use within scans and user macros.

### Fast 2d Detectors: Data Readout and Storage

Fast 2d detectors will be used to follow the dynamics in a sample via a time resolved series of speckle pattern. The high coherent flux of the CHX beamline enables the investigation of faster time scales and correspondingly the detectors and the will be faster and the data rates higher compared to what is in use today. The two fast 2d detector which are under consideration for the CHX beamline are the VIPIC (BNL development lead by P.Siddons) and the Eiger (commercial detector from Dectris). None of these detectors exists today, so the following estimations are based on the best available information. Both detectors will have similar pixel sizes (VIPIC:  $80 \times 80 \mu\text{m}^2$ , Eiger:  $75 \times 75 \mu\text{m}^2$ ) and 2M versions (32 chips of  $256 \times 265$  pixel) are assumed for the following estimation of data rates. For the Eiger detector, the maximal achievable data rate is connected to the adjustable counter depth of the pixels (4bit: 24kHz, 8bit: 10kHz, 12bit: 8kHz) and the data will be read and saved in the conventional way as frames. Contrary, the VIPIC will read events with a 5bit counter depth and time stamp the events, leading to a virtual counter depth of 42bit (21bit pixel location, 16bit time stamp). Data rates will exceed 550 GB/s (VIPIC with 50% event occupancy), thus requiring special strategies for the data transfer from the detector to the data storage. At this rate, a direct transfer of the data from the detector to a hard disk is impossible, so that data buffering using RAM directly in the detector head becomes indispensable. A typical XPCS experiment consists of time series of images (~20000) taken with a certain exposure and interval time. The Eiger detector will provide 2GB of RAM dedicated to each chip ( $256 \times 256$  pixel) sufficient for about 60000 frames. The VIPIC will need at least 120GB of RAM to buffer one series of 20000 frames before transferring it to a RAID system at the beamline via a fast local network. Using special network equipment and parallelization, data transfer and writing rates of 1.5 GB/s have been achieved at the ESRF. It is expected that with the availability of fast flash memory and further parallelization techniques the detector buffers could be flushed in about 10-20s, which determines the dead time between image series. Depending on the availability of a central data storage facility, the local RAID system (20-40TB) will be continuously backed up via the standard network link (10Gb/s) of the beamline to a central storage facility. The detector characteristics and data rates are summarized in the table below.

Table 21 Data size and data transfer requirements for pixilated area detectors

	maximum frame rate	counter depth	data set size *)	maximum data rate	# data sets on 20TB RAID	transfer time/data set from RAID*)
VIPIC	100kHz	42bit	110GB	550GB/s	182	88s
EIGER	24kHz	4bit	21GB	25GB/s	954	17s

## Scientific Computing Requirements

### General Data Visualization Software

Both CS and GUIs will need online and quasi-real time visualization of the currently acquired data. Furthermore, for beamline alignment and diagnostics, visualization software for scans with 1d and 2d detectors will be needed, which could be generic and robust enough to cope with all the detectors and data formats of the various beamlines at NSLSII and could thus be generic. Functionality expected for handling 1d data comprises (not complete): normalization of data by any counter configured in the CS, superposition of scans, switching between logarithmic and linear scale, simple mathematical operations like subtraction, multiplication, etc. The program 2d data visualization should allow an easy browsing of file series and simple operations like summing of files, subtraction, switching between linear and logarithmic scale, etc. Both the 1d and the 2d software should allow easy access to all the information associated with a scan or image, such as all motor positions within the beamline, parameters of the sample environments, etc. and they should enable simultaneous access to on-line and off-line data for comparison.

### CHX Specific Software

The main scientific technique covered by the CHX beamline is X-ray photon correlation spectroscopy (XPCS), where the challenges for the data analysis lie in the fast calculation of intensity correlations between data

points/images of a time series. While for sub-microsecond dynamics the data is usually acquired by a point detector (APD) and directly processed by a hardware correlator, slower dynamics will be followed with 2d detectors and the correlations will be calculated by software, ideally in real-time and in parallel to the data acquisition. Contrary to e.g. standard SAXS, XPCS is a relatively new and less wide spread technique and consequently software developments for XPCS analysis are rather local, although one software package (PYXPC, python based correlation and analysis software by C. Caronna et al., ESRF/SLAC) might become available as open source software. However, with the envisioned data rates of up to ~550GB/s it is evident that at least an optimization with respect to data transfer and calculation using parallel computing will be indispensable to cope with the data stream. The development of the PYXPCS code (which could be done in a collaboration between ESRF, SLAC and BNL) would comprise the separation of the GUI from the data processing part (allowing an easier change of the calculation algorithm without affecting the GUI and enable to run the program in batch processing mode), optimization of the algorithm (e.g. for parallel computing, GPU,...), development of an easy to install stand-alone package for external users and the implementation of a direct link to the on-line data (rather than reading the data back from storage). Contrary to the specific software described above, the CHX beamline will also need analysis software for standard SAXS and WAXS data which will be acquired in parallel to the XPCS data as complementary techniques. A survey of existing analysis software is missing at this point, but due to the wide spread of these two techniques, it is expected that solutions exist which could be adapted for the CHX beamline.

## Hutches

An overview of the CHX FOE and EESE is shown in Figure 33. The FOE is a lead hutch which hosts the main optical components of the beamline. The EESE is a steel hutch, accommodating some local beam conditioning elements, the sample stage and detectors. The roofs of both enclosures are accessible and correspondingly secured with railings and toe-kicks in conformity with the relevant safety guidelines. The roofs will be used for air-handlers, labyrinths and electronic racks.

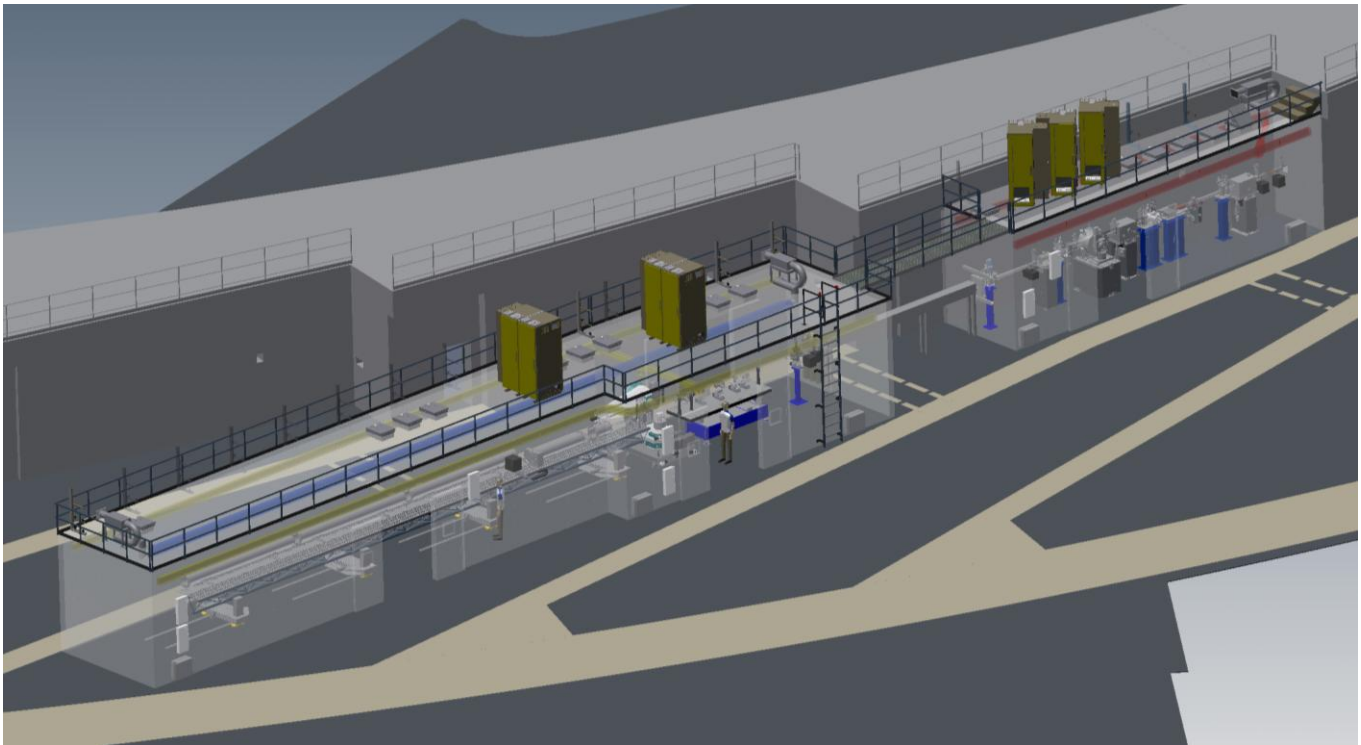


Figure 33. Overview of the CHX FOE and EESE.

### First Optical Enclosure (FOE)

The FOE of the CHX beamline (see Figure 34 a)) contains the main optical elements such as the horizontally deflection mirror, monochromators and focusing optics. Because of the Bremsstrahlung present in the FOE, the hutch will be made of lead lined panels with lead thicknesses of 50mm (downstream), 18mm (outboard wall) and 6mm (roof), respectively. The FOE will be build against the ring tunnel wall, which will be the inboard wall of the enclosure. The hutch will start at 25.5m from the source, just after the ratchet wall, and end at 37m. The height of the hutch is foreseen as 3.5m and the width of the hutch spans from 1.96m at the ratchet wall to 2.78m at its end, increasing at a 4° angle. A 2m wide opening double door will be located 7.57m downstream of the ratchet wall. For cost saving reasons the door will be windowless, so cameras inside the hutch are envisioned for optical inspection. The FOE will have two wall mounted user labyrinths, of which one will be dedicated to the PPS. The roof of the FOE will be accessible from the mezzanine via three steps. Six roof labyrinths for motor and vacuum controls as well as for liquid nitrogen for the DCM, utilities and communication are foreseen. Furthermore, the roof of the FOE will accommodate three water-cooled electronic racks dedicated to motor, vacuum and cryo-cooler control as well as an air handler. The air distribution inside the hutch occurs via an ‘air-sock’ to minimize the disturbance of the air inside the FOE. The cryo-cooler for the DCM will be accommodated on mezzanine. A crane with a 1000kg load capacity will be mounted inside the FOE to facilitate installation and future upgrades of the optical components. The crane rails will be following the hutch profile.

### Experimental Endstation Enclosure (EESE)

Because of the Bremsstrahlung being stopped in the FOE, the EESE (see Figure 34 b) can be made of steel panels, which will be 6mm thick for the walls and 3mm thick on the roof (P.K. Job, Guidelines for NSLS-II Beamlines and Front End Radiation Shielding Design, Doc # LT-ESHDES-08-003-rev001). The EESE starts at 42.5m and ends at 69.5m from the source. The height of the EESE is 3.5m and its width narrows from 4.3m to 3.8m. The hutch features three double doors, one on the inboard side, 3m from the upstream wall and two located on the outboard side, 6m and 17.5m from the upstream wall. While the inboard doors are windowless, the two outboard double doors will feature windows to enable an easy optical inspection of the interior. In addition, this enclosure will also be equipped with several video cameras to conveniently monitor critical equipment. The outboard wall of the EESE will have five wall mounted labyrinths, two next two the upstream door, one at the downstream wall and two just before the end of the enclosure. One user labyrinth next to each double door will be dedicated to the PPS. The inside of the hutch will feature a crane with 1000kg load capacity to facilitate the installation of beamline components and user equipment. The crane rails will be tapered to follow the hutch walls. The roof of the EESE will accommodate two air handlers, four water cooled electronic racks as well as ten roof labyrinths for utilities, communications, motor and vacuum controls. The air distribution inside the enclosure will occur via ‘air-socks’ like in the FOE. In addition, the doors which will be used to access the EESE during an experiment will have air curtains in order to minimize turbulences and temperature instabilities upon opening the door and accessing the enclosure. The roof of the EESE will be accessible from the roof of the FOE via a 44inch wide pylon supported bridge, spanning the 5.4m between the FOE and the EESE. The utilities will run in a roof mounted utility tray which spans between the two enclosures along with the bridge. A safety egress roof ladder will be mounted on the outboard wall of the EESE, approximately at 44m from the source in order to be compliant with the 100 ft safety egress rule.

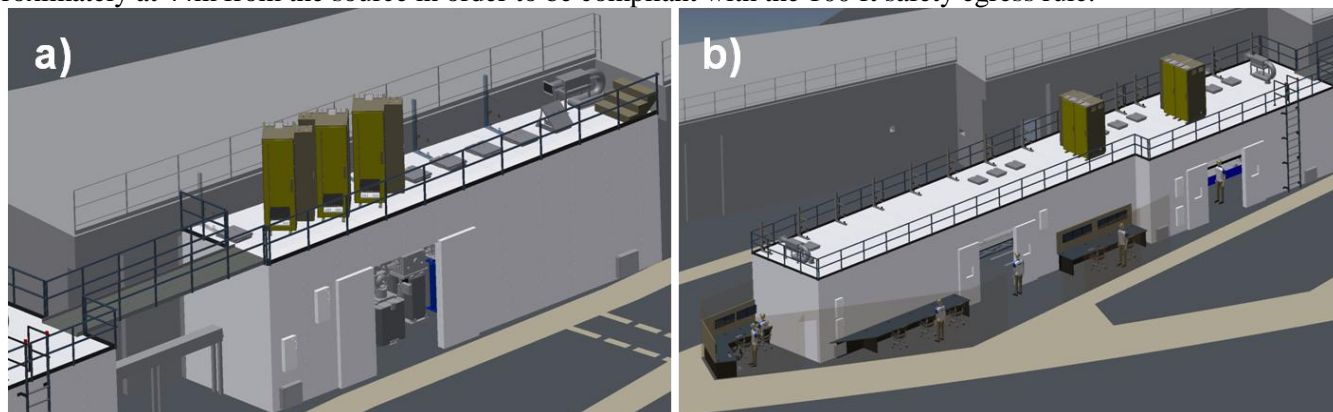


Figure 34. First Optics Enclosure (FOE). b) Experimental Endstation Enclosure (EESE) and user space.

### **Personnel Protection System (PPS)**

The aim of the personnel protection system (PPS) is to exclude the possibility to have persons in the FOE and EESE while the beam is on. The design, specifications and elements of the PPS are described somewhere else. A schematic for the layout of the PPS for the CHX beamline is shown in Figure 48. A stack lamp, showing the interlock state, and a set of ‘emergency stop’, ‘door open’ and ‘search’ buttons will be located next to the double door on the inboard wall of the FOE. Two sets of search and emergency stop buttons will be located inside the enclosure, one on the outboard wall close to the ratchet wall and one on the downstream wall. The optical and acoustical signal (siren and strobe) will be located on the ring wall or the downstream wall of the hutch. The panel for the labyrinth keys will be located in the proximity of the door.

The main entrance of the EESE will be the double door at the downstream outboard side of the enclosure. The touch panel for the PPS and a set of ‘emergency stop’, ‘door open’ and ‘search’ buttons will be located next to this door. A second set of buttons will be next to the upstream door, which serves as an alternative access to the EESE. Contrary, the double door on the inboard side will not be used for hutch access on a regular basis and will thus be locked by Kirk keys like a labyrinth. The stack lamp for the EESE will be located around the middle of the hutch at a height from where it can be seen from both interlockable doors. Three sets of ‘search’ and ‘emergency stop’ buttons will be distributed in the EESE, one next to the upstream door on the outboard site, one at around 52.5m on the outboard wall and one at the corner of back and inboard wall. The stroboscopic light and the siren need to be mounted close to the ceiling on the outboard wall at about 52m, in order to be seen from all positions within the enclosure. The key panel for the labyrinths of the EESE will be located in this area as well.

### **User Space**

The control area of the CHX beamline will take the floor space left on the outboard side of the EESE, starting at 52.5m downstream of the source. Computer workspace for 4-5 users/beamline staff will be created. Cubicle walls will provide some shielding against ambient noise from the experimental floor of the facility and lockable sliding doors would give some level of protection against theft when the beamline is left unattended. Lowest noise level and thus the least tiring working environment could be created by a real control cabin, featuring a closed roof and thus complete shielding from the experimental floor noise. Such cabin might be installed at a later stage as part of the major scope of the CHX beamline. The control area will house the computers/workstations needed to control the beamline as well as to acquire and analyze the data. All equipment installed in racks on the FOE and EESE which needs configuration (e.g. motor controllers, monochromator cryo-cooler, etc.) will be accessible via login from computers in the control area. Due to the limited floor space and in order to keep the noise level low, computer will be moved from the control area to the roof racks wherever practical.

### **Sample Preparation Laboratory**

The CHX beamline is tentatively located in convenient proximity to LOB3 which houses a chemistry wet lab. Nevertheless, a small sample preparation lab will be set up behind the end of the EESE. This lab is not aimed for doing chemistry, but rather for e.g. filling samples in capillaries, cleaning sample environments and beamline equipment, etc. The equipment and chemicals allowed in this space will be subject to a safety review, but currently a hood with controlled air flow, a small storage cabinet for common solvents like ethanol, acetone, etc., a microscope, magnetic stirrer and some glass ware are anticipated.

### **Storage Space**

For storage of beamline equipment, such as vacuum parts, sample environments, spare motors, etc. the floor space between the FOE and the EESE (keeping the duck under clear) could be used. Storage cabinets with roll-up doors would require a minimum of floor space and avoid the problem of a safety egress being blocked by the open door of a cabinet. For rarely used items, storage cabinets could be also set up on the roof of the ES.

## **Environmental**

The temperature and stability in the experimental hall is specified as  $24\pm 1^\circ\text{C}$  and the relative humidity as  $50\%\pm 10\%$  and  $30\%\pm 10\%$  in summer and winter, respectively. It is assumed that with standard air-handlers a temperature stability of  $\pm 0.3^\circ\text{C}$  can be reached in FOE and EESE, which might be sufficient for the CHX beamline. However, the air-handler units will be prepared for an upgrade with an additional cooling-heating unit at the air

intake, which would presumably increase the temperature stability in the enclosures to  $\pm 0.1^\circ\text{C}$ . Every piece of equipment will be specified to work in the temperature range 10-38°C and 20-80% relative humidity. The vibration criteria for the NSLS-II experimental floor is "E" (VC-E) and all equipment will have to comply to this criteria in order not to degrade this low level of vibration. In addition, noise performance criteria will be included in the specifications of all components to ensure a noise level which allows a comfortable prolonged working on the experimental floor.

## Surveying Requirements

Beamline Components at NSLS-II will be surveyed in place using a laser tracker. The NSLS-II facility, including the storage ring tunnel and experimental floor, is fitted with a network of survey monuments referenced to a pair of monuments in the center of the ring. This network will be regularly surveyed with a laser tracker to create a robust and accurate network of arbitrarily positioned monuments. Monuments can be added as required, including inside hutches and on the storage ring wall etc. Positioning a laser tracker on a tripod such that it can view more than three monuments allows it to calculate its position, and the position of any new monuments.

Precision machined holes in components are surveyed prior to installation, relative to the component aperture, crystal, mirror or grating surface etc, fitting a reflector into the precision hole allows the laser tracker to survey the absolute reflector position so that the aperture or optic position can be accurately calculated. This system of surveying is extremely accurate, globally (within the NSLS-II complex) components may be positioned to within 100 microns, and where components are close to one another (within a few meters and without sighting restrictions) the accuracy improves to ~30 microns.

## 4. SPECIAL BEAMLINE REQUIREMENTS

### Special Requirements for Utilities

The CHX beamline will use compressed air in a number of critical components. Most importantly a beamline fast closing valve placed just downstream of the Be CRL Transfocator will protect the beamline optics from the pressure wave cause by an accidental break of the Si3N4 window in the experimental station. The compressed air pressure required to close the valve ranges between 70-110 psi with 70 psi as an absolute minimum. For a better safety margin, a min pressure of 80 psi in the compressed air system is preferred.

### Special Requirements to the Conventional Facilities Division

“Extended” (70 m) floor space due to the need to accommodate a long experimental hutch (up to 25 m) while leaving an opened gap (and creating a “duck under”) between it and the First Optic Enclosure

### Requirements to the Accelerator Systems Division

Since XPCS is based on measuring time autocorrelation of fluctuating speckle intensity coming from the sample, the beamline has special requirements for electron filling modes of the storage ring. Based on previous experience, the proposed NSLS-II baseline mode with has 1/5 of the ring empty as an ion clearing gap, is not expected not offer “optimal” conditions for “classic” fast XPCS measurements. In order to mitigate the effect of artefacts such as “spikes” in the correlation functions associated to the time structure in the ring the CHX beamline will require precise triggers that will allow the synchronization of the detection with individual bunches in the SR train.

The availability of a quasi-uniform filling mode with no ion-clearing gaps is also desirable if post day-1 developments will allow it. Alternatively, uniformly distributed bunches with not more than 100 ns intervals in between will allow studies in the microsecond scale without much interference from the SR time structure.

The electron Beam stability requirements, and indicated in Table-3, Insertion Device requirements.

Table 22 CHX Beamline Electron Beam Stability Requirements

Parameter	Unit	Value
Vertical Position	Centroid $\mu\text{m}$	0.1
	Width $\mu\text{m}$	0.1
Vertical Angle	Centroid $\mu\text{rad}$	0.1
	Width $\mu\text{rad}$	No special requirement.
Horizontal Position	Centroid $\mu\text{m}$	0.2
	Width $\mu\text{m}$	No special requirement.
Horizontal Angle	Centroid $\mu\text{rad}$	0.5
	Width $\mu\text{rad}$	No special requirement.
Frequency or Time Range		100 $\mu\text{sec}$ to ~2 hours

## APPENDIX 1: SCHEDULE

Table 23 CHX Beamline Schedule

<b>Activity</b>	<b>Start</b>	<b>End</b>
Preliminary Design Report		Oct 11, 2010
Approval of long-lead time procurement	Nov 2010	
Work on Final Design Report	Oct. 2010	Feb. 2012
Final design of major components	Oct. 2010	Apr. 2011
Final Design Report		Feb 2012
Long lead time procurement	Jan 2011	Nov 2012
Procurement	Apr 2012	Aug 2013
Beneficial occupancy of the experimental floor	May 2012	
Equipment Installation	June 2012	Jan 2014
Sub-system testing	Aug. 2012	Feb. 2014
Integrated testing	Aug 2013	May 2014
Beamline available for commissioning	June 2014	

## **APPENDIX 2: REFERENCE DRAWINGS**

The following drawings are provided here for reference:





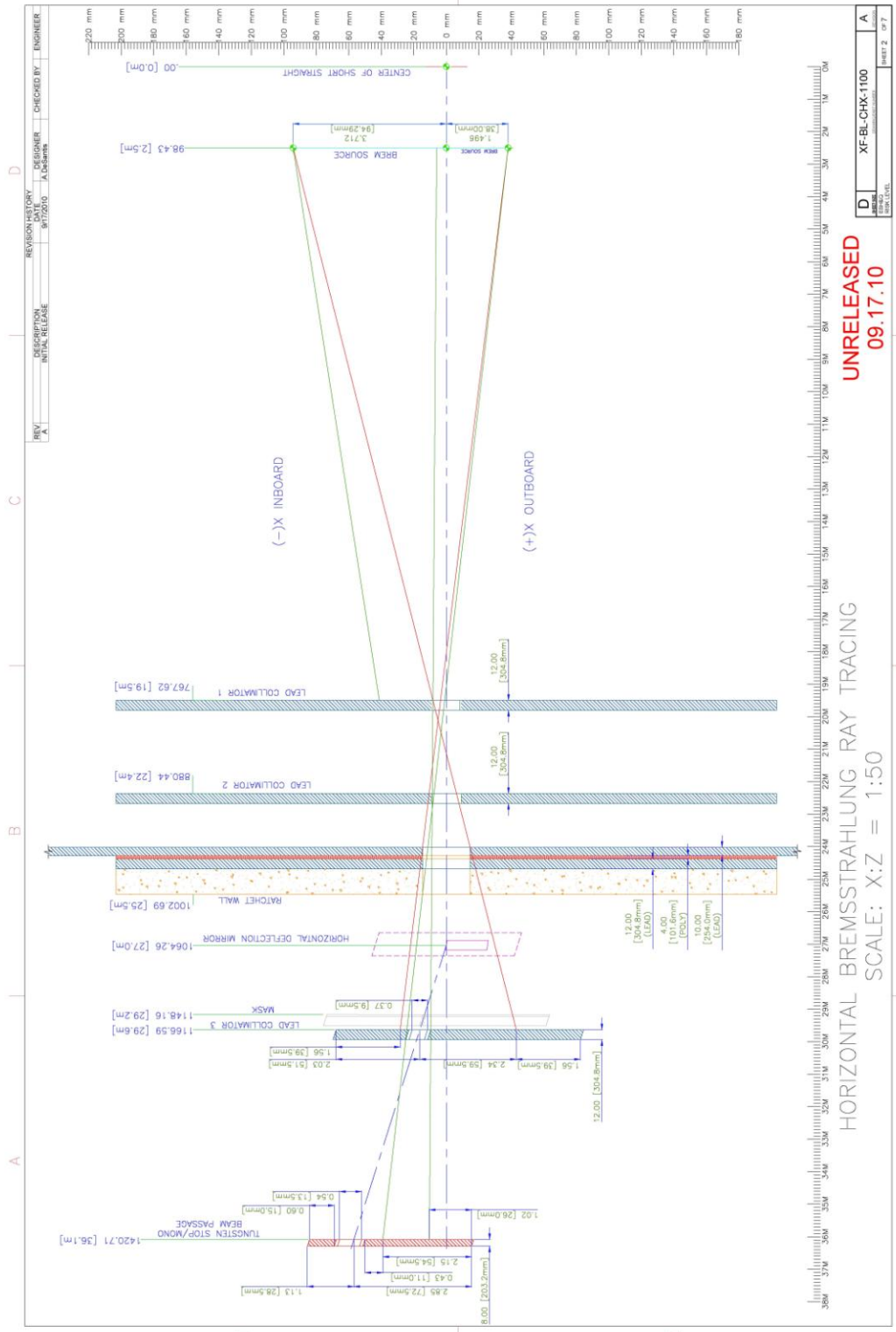


Figure 37 Bremsstrahlung ray tracing – Horizontal

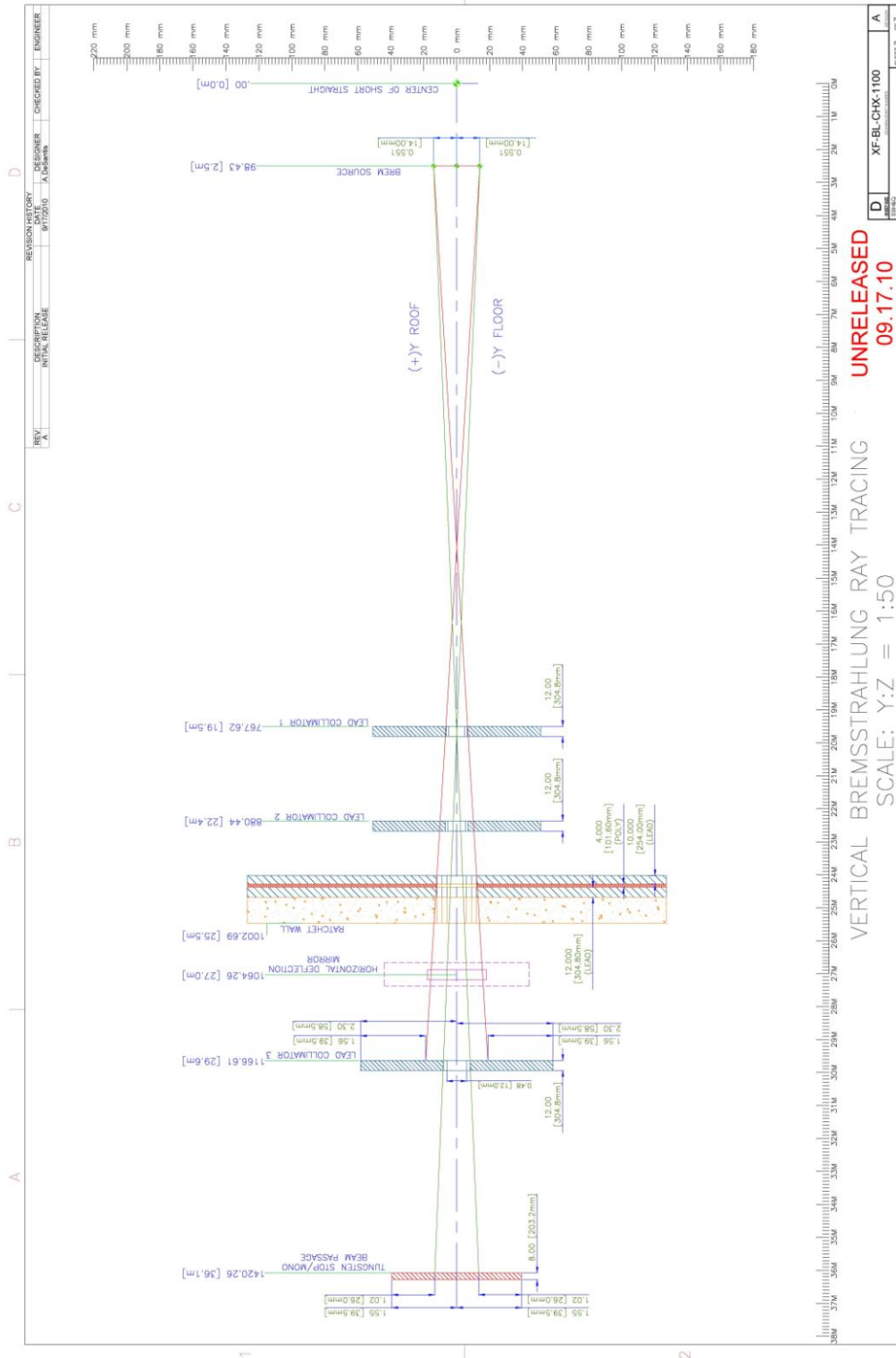


Figure 38 Bremsstrahlung ray tracing – Vertical





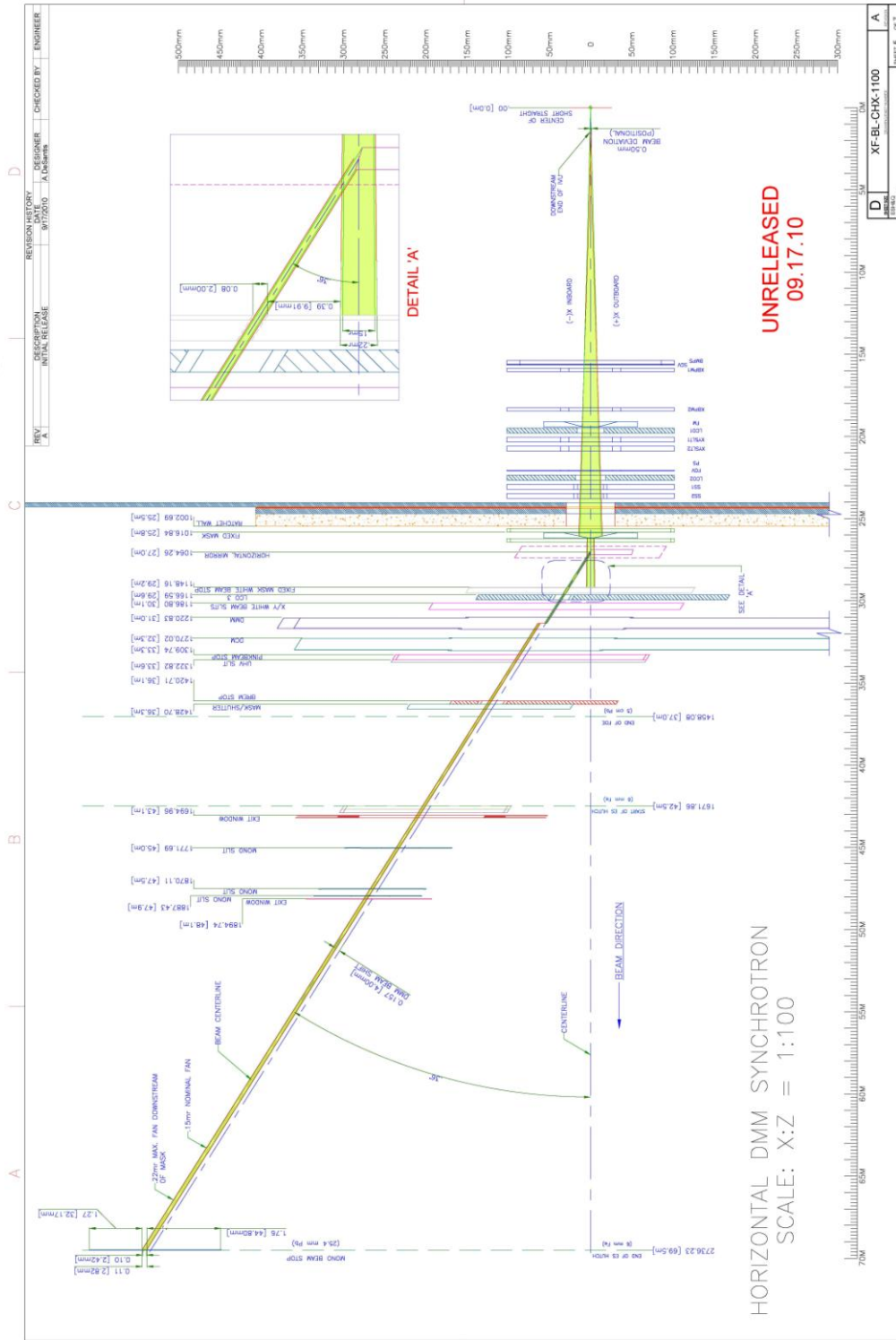


Figure 41 Synchrotron Ray Tracing (with DMM) – Horizontal

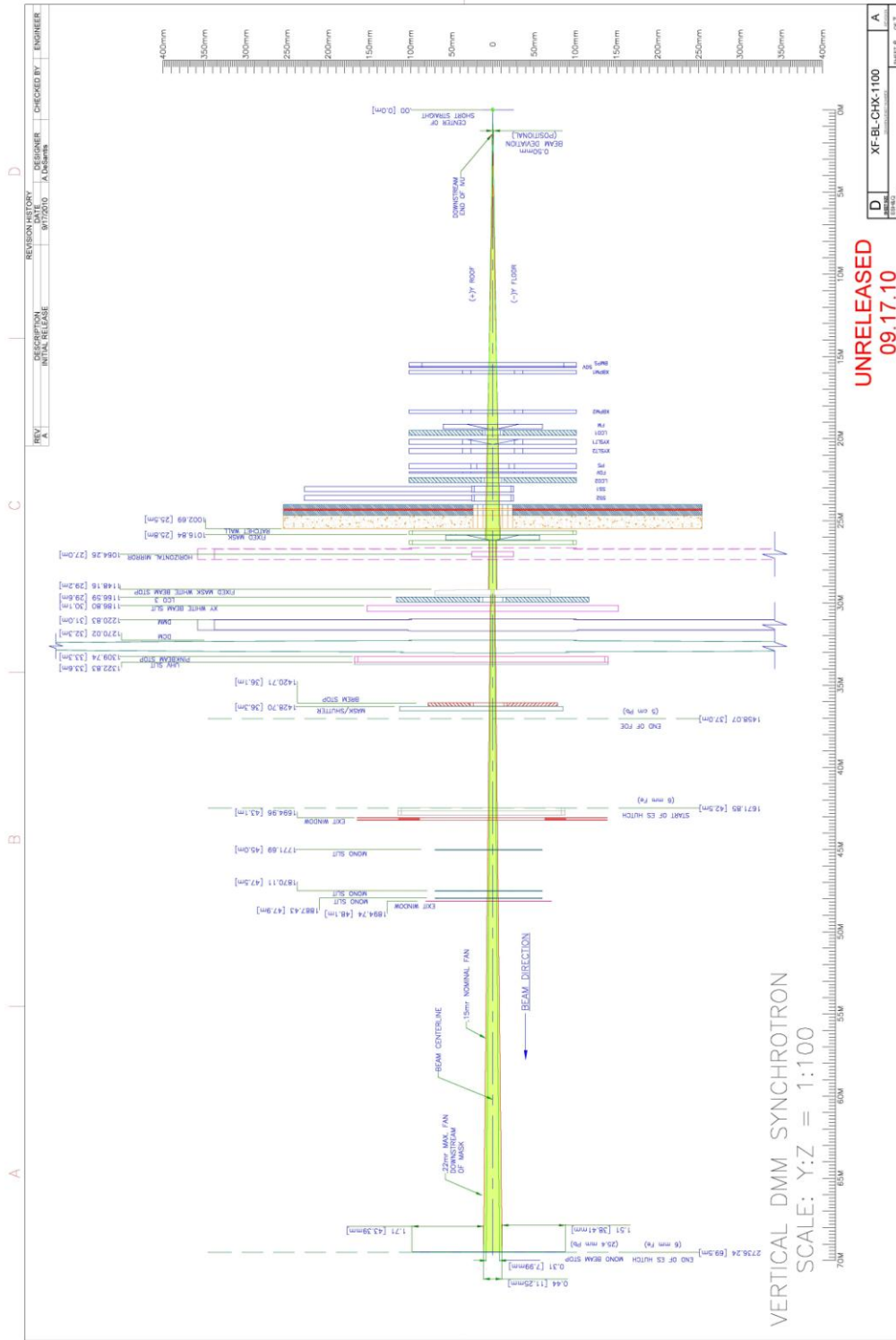


Figure 42 Synchrotron Ray Tracing (with DMM) – Vertical

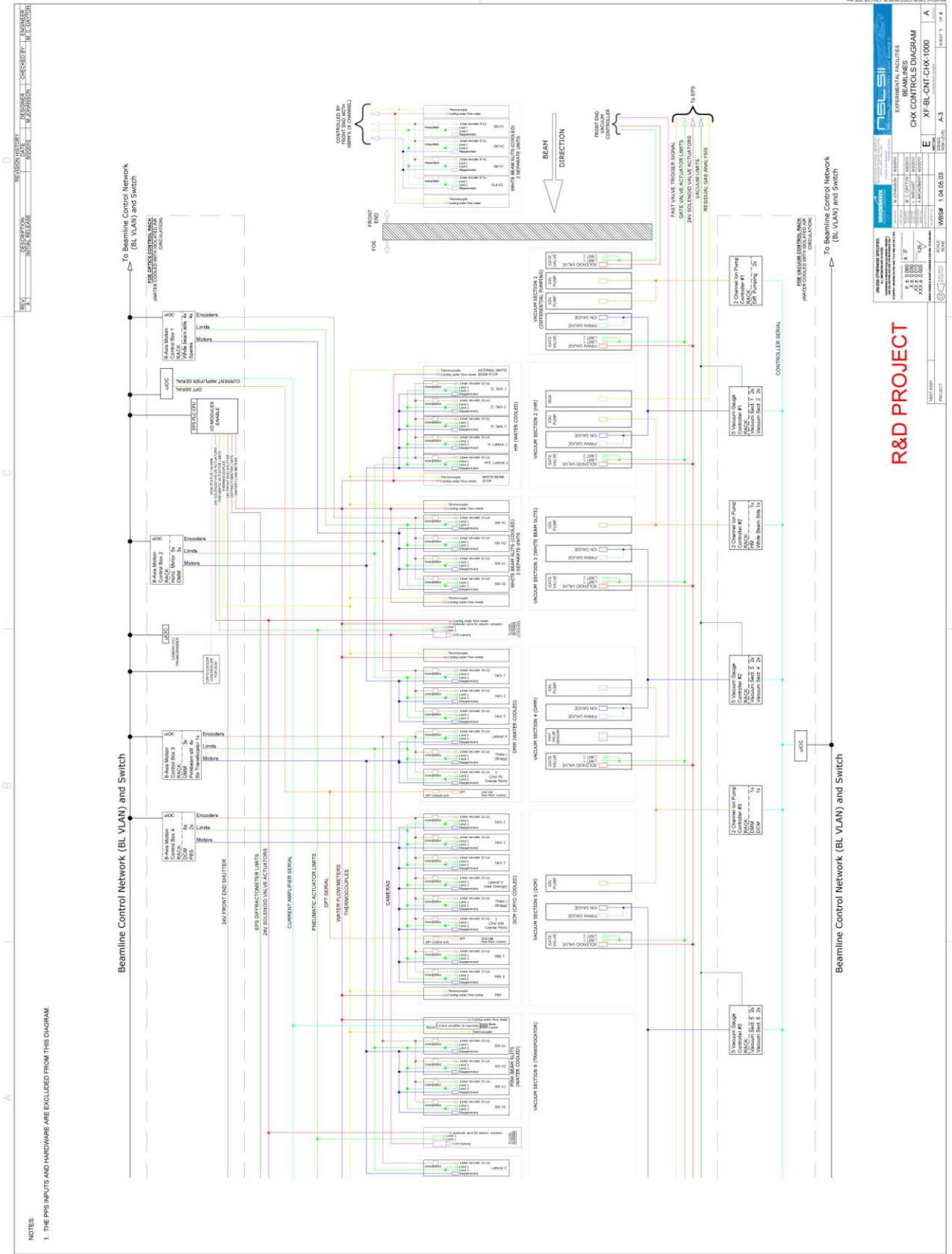


Figure 43 CHX controls diagram (1/4)

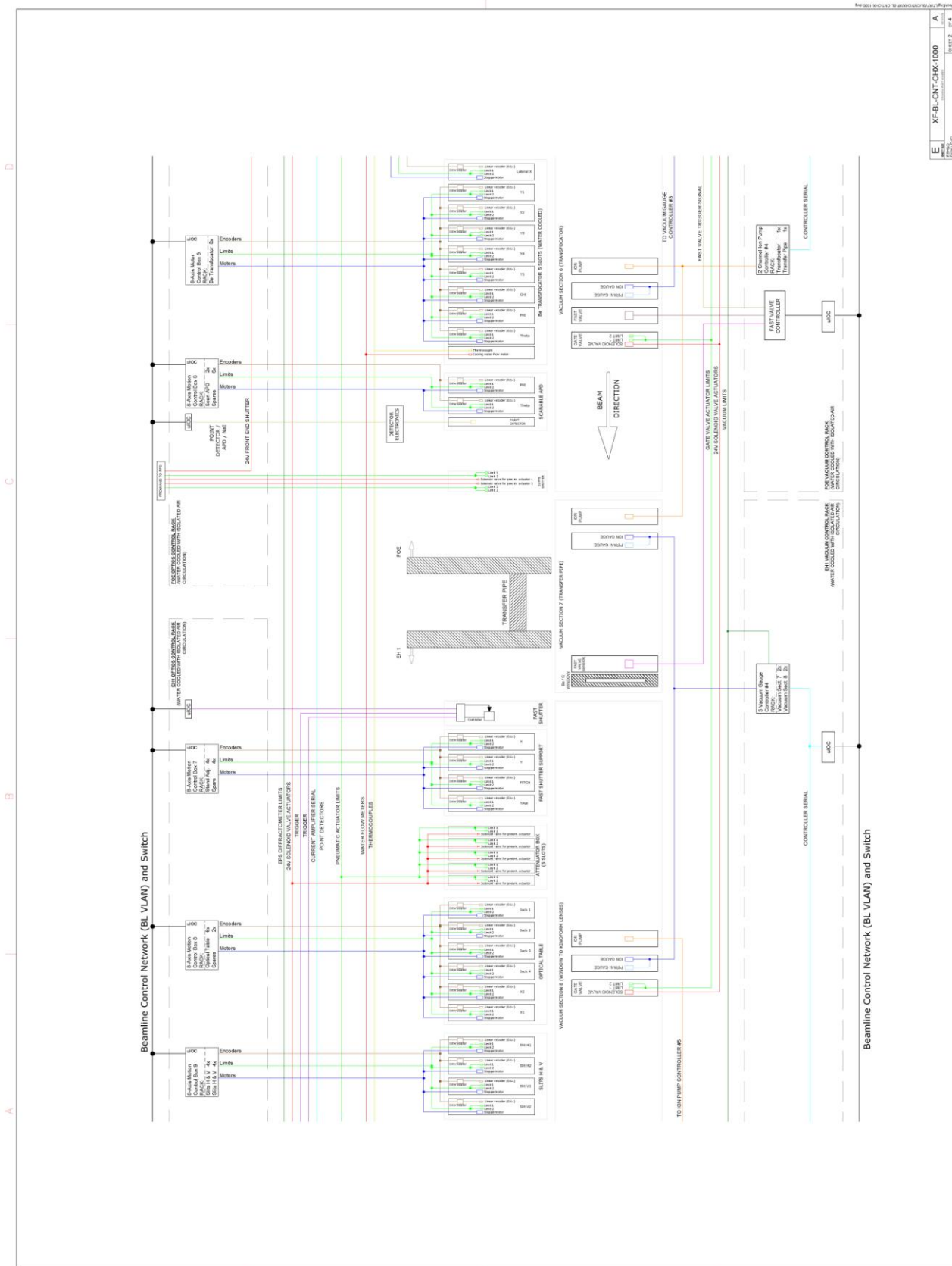


Figure 44 CHX controls diagram (2/4)





Figure 47 CHX beamline utility layouts

